National Library of Canada
Acquisitions and Bibliographic Services Branch
395 Wellington Street
Ottawa, Ontario
K1A 0N4

Bibliothèque nationale du Canada
Direction des acquisitions et des services bibliographiques
395, rue Wellington
Ottawa (Ontario)
K1A 0N4

Your file Votre référence

Our file Notre référence

NOTICE

The quality of this microform is heavily dependent upon the quality of the original thesis submitted for microfilming. Every effort has been made to ensure the highest quality of reproduction possible.

If pages are missing, contact the university which granted the degree.

Some pages may have indistinct print especially if the original pages were typed with a poor typewriter ribbon or if the university sent us an inferior photocopy.

AVIS

La qualité de cette microforme dépend grandement de la qualité de la thèse soumise au microfilmage. Nous avons tout fait pour assurer une qualité supérieure de reproduction.

S'il manque des pages, veuillez communiquer avec l'université qui a conféré le grade.

La qualité d'impression de certaines pages peut laisser à désirer, surtout si les pages originales ont été dactylographiées à l'aide d'un ruban usé ou si l'université nous a fait parvenir une photocopie de qualité inférieure.

Canada

Effects of Electrochemically Incorporated Bismuth on the Reduction and Re-oxidation of Electrolytically Deposited Manganese Dioxide

by Christopher Graham Castledine

A thesis submitted to the School of Graduate Studies
and Research in partial fulfillment of the requirements
for the Degree of
Master of Science in Chemistry

University of Ottawa
Ottawa, Ontario, Canada

ISBN 0-315-93615-0

UNIVERSITÉ D'OTTAWA
UNIVERSITY OF OTTAWA

Abstract

The inclusion of bismuth species in electrolytically produced MnO_2 deposits on porous graphite is reported together with some electrochemical effects of the bismuth species on rechargeability of electrodeposited MnO_2. The optimum conditions for deposition found in the study are:

Temperature:	85 - 90 °C
Bath Composition:	0.5M to 2M H_2SO_4
	0.5M $MnSO_4$
	0.005M to 0.01M Bi^{3+}
Current Density:	5 to 20 mA cm^{-2} (apparent)

The proposed mechanism for the inclusion of bismuth species is by continuous precipitation caused by high local acid strength created at the electrode by the reaction of anodic deposition of MnO_2.

Bismuth species are not "included" in deposits made from nitrate and perchlorate baths but bismuth species may be absorbed into the graphite substrate and then become electrochemically active when the electrode is placed in strong alkali. Bismuth species, no matter how they are introduced into the electrochemical cell, enhance the rechargeability characteristics of MnO_2 when it is subjected to cyclic voltammetry in aqueous 9M KOH.

With respect to the mechanism of reduction and re-oxidation of MnO_2 with bismuth species present in 9M KOH, the role of soluble intermediates is confirmed. It is proposed that bismuth may, among other things, act to stabilise soluble Mn^{3+} species in solution and/or aid in the nucleation and growth process of these species

that must take place in order for them to react further at the electrode.

The rotating-disk cyclic volatammetry of bismuth and manganese metals is also reported. Bismuth shows good cycling behaviour with the formation and reduction of a passive oxide layer several hundred monolayers in thickness. Manganese displays a unique anodic feature on the cathodic sweep. A model for the explanation of this peak is presented.

Acknowledgements

It is traditional and yes, a relief, to sit down at the end of the long task of putting together a thesis and write a few words to thank the people who helped you through it. First of all, to Professor B.E.Conway, who seems to have the knack of guiding you through it all and making it seem like everything is your idea. For not only is he a great researcher and educator but he also happens to be a really nice guy.

The help of S.Y.Qian and L.Bai is gratefully acknowledged. They seem to be around with the experience and knowledge when you just can't find Dr.Conway (must be qut of the country again!). Also, thanks to the rest of the members of our research group and to the staff and students of the Electrochemical Science and Technology Center at the University of Ottawa (ESTCO), particularly Dr. Bill Adams for .interesting and informative discussions.

My thanks also go to the support staff in the chemisty department, particularly Don and John Hopkins who not only do their job but are genuinely interested in giving you a helping hand. Also, special thanks to Ray Doré of ESTCO for helping sort out the dreaded BET apparatus.

Lastly, I would like to thank all of the friends I have made in my stay at the University of Ottawa, especially Mike Tjepkema and Mark Lefebvre, with whom I have established "fast friendships" that I am sure will last a long time.

Table of Contents

List of Figures

List of Tables

List of Abbreviations

a	activity
AAS	Atomic Absorption Spectrometry
A	amperes
aq.	aqueous
BET	method for determining surface area named after the authors: S.Brunauer, P.H.Emmett and E.Teller
C	coulomb
C_{dl}	Capacitance of the double layer
CE	counter-electrode
cm	centimetre
CM	Chemically modified MnO_2 material prepared according to Yao et al [10]
d	diameter or atomic diameter
E	potential of a redox process
E°	standard potential of a redox process
EDX	Energy Dispersive X-Ray (analysis)
e.g.	for example
F	Faraday's constant, normally taken to be 96,500 C per mole of electrons
FW	formula weight
g	gram
i	current
keV	kilo electron volt

l	litre
m	metre
M	molar (moles per litre)
mA	milliampere
mC	millicoulomb
mg	milligram
ml	millilitre
mM	millimolar
min	minute
mol	mole
mV	millivolt
n	nano (10^{-9})
N	normal (equivalents per litre)
N_a	Avagadro's number (taken as 6.023×10^{23} electrons, atoms or molecules per mole)
ρ	density
q	charge (associated with a process)
R	gas constant (normally taken as 8.314 J K^{-1} mol^{-1})
RE	reference-electrode
s	second
SCE	saturated calomel electrode
SEM	Scanning Electron Microscopy
t	time

T	temperature (K unless otherwise specified)
μ	micro (10^{-6})
v	volume
V	volt
viz.	namely
v/v	volume - volume (refering to the dilution of a volume of solute to a volume of solution with water)
WE	working-electrode
XRD	X-Ray Diffraction (analysis)
z	The number of electrons associated with a process

CHAPTER 1 INTRODUCTION

1.1 MnO_2 Batteries - An Overview

The use of manganese dioxide as a battery cathode material dates back to the invention of the Leclanché cell, by Georges Leclanché in 1866 [1]. The cell consisted of an amalgamated zinc bar as the anode, a solution of ammonium chloride as the electrolyte, and a mixture of manganese dioxide and carbon powder packed around a carbon rod as the cell cathode. In 1888, the first "dry cell" was constructed by Dr. Carl Gassner. He also introduced the practice of adding zinc chloride to the electrolyte, which reduces local chemical action and increases shelf life.

Current zinc-MnO_2-carbon batteries are little changed from the original cells of Leclanché and Gassner. Present cells incorporate a zinc anode, a manganese dioxide cathode and an aqueous electrolyte containing ammonium chloride and/or zinc chloride. Although these batteries do not exhibit the performance of some other battery systems that are currently available, they still hold a large fraction of the primary battery market due mostly to their ease of fabrication and corresponding low cost. As of 1985 these batteries had the largest market share with 38% of the world production of portable batteries [2].

Although the use of alkaline electrolyte dates back to almost the same time as the development of the Leclanché cell and working cells were demonstrated in the early part of this century [3], it was not until 1948 that the first commercial alkaline manganese dioxide cell was developed. The capacity of these cells may be as much as

five times or more than that of the equivalent Leclanché cell [1], especially under continuous use, high discharge-rate conditions. In addition, these cells have better shelf life, leakage resistance and low-temperature performance. The main drawback is the higher initial cost of production of these cells which is usually outweighed by their increased performance. The market for these cells is indeed considerable. In 1985, they were second only to Leclanché cells with 27% of the world's total production of portable batteries [2]. By 1988, the total worldwide market for alkaline MnO_2 batteries amounted to over $2 billion (US) [4].

There has been a great deal of interest in the last 30 years in the application of lithium as the anode material for high energy-density batteries [5]. Manganese dioxide is used as the cathode material for one of many variants of the lithium cell, which must, of course, use a non-aqueous electrolyte due to the reactivity of lithium. Unlike the aqueous MnO_2 batteries described above, the discharge reaction at the cathode is not *per se* a chemical reduction but involves the formation of a Li-Mn_2O_4 intercalation species which may be viewed formally as either the intercalation of Li^+ in a host which is reduced to $Mn_2O_4^-$ or the intercalation of Li^0 which has been reduced by electron transfer to the host Mn_2O_4 lattice. The total market for all lithium primary batteries (including Li/MnO_2) was 5% of the portable battery market in 1985 [2].

1.2 The Importance of Battery Rechargeability

There are three main driving forces towards the increased use of rechargeable batteries over primary cells: a) increased power demands for portable equipment, b)

environmental concerns and c) convenience in the use of small electrical appliances and toys.

Devices such as camcorders and battery operated power tools have larger power requirements than "traditional" battery powered devices such as radios and flashlights, making primary batteries impractical. The electric vehicle is perhaps the most extreme example of a system demanding portable power.

Pressure is mounting from environmental concerns regarding the disposal of primary cells, particularly those which contain elements such as mercury, cadmium and lead. The concerns over the presence of mercury in alkaline MnO_2 batteries have prompted manufacturers to reduce the quantity of mercury used to a bare minimum. These advances have been realised from improvements in the purity of the zinc used as the anode material and from the use of additives such as In or Ga [6].

Nickel-Cadmium batteries are also under attack even though they are the current mainstay of the portable rechargeable battery market. Mandatory recycling or perhaps a total ban on these batteries is a possibility [5]. There has long been concern over the disposal of lead-acid batteries and recycling programs for them have been instituted [5].

In addition to concerns over disposal, the energy required to manufacture a primary alkaline cell is several times the energy that it produces [7]. The consumption of power is also indirectly an environmental issue and rechargeable batteries lessen the ratio of energy consumed to energy produced.

As can be seen, there is considerable impetus to develop new technologies for

rechargeable battery systems which have high volume and weight energy-density and are environmentally benign. The rechargeable alkaline MnO_2 battery, using the recently developed bismuth-doped MnO_2 material, looks like a very promising candidate as its energy density is as good as or better than that of the primary alkaline cell. The problem of mercury in these cells is likely to continue but the disposal impact of the mercury in a rechargeable cell is inversely proportional to its useable cycle life. In other words, the disposal of one cell at a hundred cycles takes the place of the disposal of 100 separate primary cells.

1.3 Rechargeability of MnO_2 Battery Systems

Recharging of Leclanché batteries may only be performed under certain specific and essential conditions [8]. They must not be over-charged or fully discharged, the charging rate must be low and the history of the discharge of the cell affects the recharge. Due to these constraints, the recharging of Leclanché cells uses little of the available charge density or "capacity" of the cell and is impractical for a consumer product.

Considerable effort has been put into research on rechargeability of alkaline MnO_2 batteries. There are currently two schools of thought on this subject. Kordesch and co-workers [9] have developed cells in which the depth of discharge of regular MnO_2 cathode material is strictly limited while our research group and others have concentrated on investigations of MnO_2 doped with foreign metal ion species such as Bi^{3+} or Pb^{2+} species. The original work in this area was done by Wroblowa and

coworkers at Ford Scientific Laboratory and is described in publications [10-13] and patents [14,15] issued since 1984.

The discharge mechanism of γ-MnO_2 has been the subject of many investigations [16-27]. While there is not full consensus on the mechanism of the second electron reduction stage, there is general agreement that the first electron reduction involves an homogeneous reaction proceeding by a "proton insertion" mechanism coupled with electron transfer as proposed by Kozawa and coworkers [17]:

$$MnO_2 + H_2O + e^- \rightarrow MnOOH + OH^-$$

Figure 1.1 shows the proton insertion mechanism with protons and electrons jumping through the lattice in opposite directions (reprinted from reference [17]).

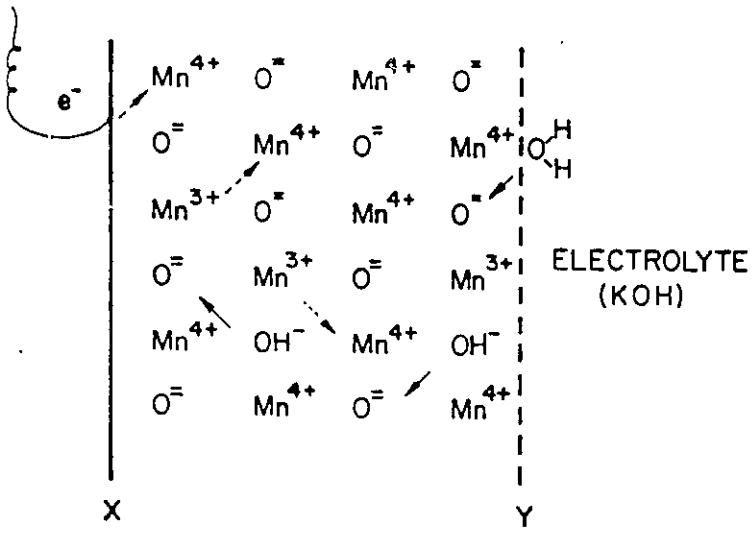

Figure 1.1: Schematic presentation of the solid phase (Mn^{4+} - Mn^{3+} - O^{2-} - OH^-) during the discharge of MnO_2. The arrows show the direction of movement of the electrons and protons: ——— proton movement, ····· electron movement; X, MnO_2 - electronic conductor interface; Y, MnO_2 - solution interface.

The term "homogeneous" refers to a mechanism where no phase changes occur and is evidenced by a continually sloping discharge curve. As outlined by Kozawa and Powers [17], based on the thermodynamic treatment of Vetter [28,29], the sloping discharge curve is due to a Nernst relationship in a homogeneous phase:

$$E = E^{\circ} - \frac{RT}{F} \ln \frac{[Mn^{3+}]_{solid}}{[Mn^{4+}]_{solid}}$$

For conditions where there is conversion of one solid phase to another, the potential during the discharge should remain virtually constant because the activities of the two solid phases do not depend on the quantity present viz.

$$E = E^{\circ} - \frac{RT}{F} \ln \frac{a_{red}}{a_{ox}}$$

with a_{red} and a_{ox} constant throughout the discharge.

According to the proton insertion model, dilation occurs in the host lattice during discharge. So long as there is no irreversible change of the geometry and coordination of the host lattice, then the process should ideally be completely reversible.

The evidence for the proton insertion mechanism comes from x-ray diffraction (XRD) studies. XRD has been used in many investigations on the reaction of discharge of MnO_2 [eg.30-32]. There are, however, difficulties in applying this technique to the study of MnO_2. Burns [33] cites "a score or more of Mn(IV) oxide phases occurring as minerals or products of synthesis". Often, the material may be amorphous, especially when reduced beyond $MnO_{1.5}$, and some of the different manganese oxide materials have very similar XRD patterns. Notwithstanding these

difficulties, some excellent work has been done with XRD in conjunction with electrochemical reduction/re-oxidation of MnO_2. Especially the work of McBreen, published in 1975 [30,34], gives a detailed mechanism for the γ-MnO_2 redox system which fits the experimental observations well. The reaction pathway for the cathodic reduction and anodic oxidation of γ-MnO_2 is based on data obtained in low sweep-rate cyclic voltammetry (25 $\mu V\ s^{-1}$) studied in conjunction with X-ray diffraction examination of the structures of the reaction products at various potentials; the behaviour can be summarized in terms of the following steps:

(i) Protons are incorporated into the γ-MnO_2 lattice causing dilation and the formation of an amorphous phase (α-Mn.O.OH);

(ii) Further reduction, results in conversion of the amorphous phase to $Mn(OH)_2$;

(iii) Oxidation of $Mn(OH)_2$ results in the formation of a mixture of γ-Mn_2O_3, γ-Mn.O.OH and β-Mn.O.OH.;

(iv) Further oxidation yields δ-MnO_2 with reduction of δ-MnO_2 yielding Mn_3O_4;

(v) Mn_3O_4 cannot be electrochemically oxidized but is reducible to $Mn(OH)_2$ which is then re-oxidizable to δ-MnO_2.

Figure 1.2 shows this set of reaction pathways, reprinted from McBreen [30], in schematic form.

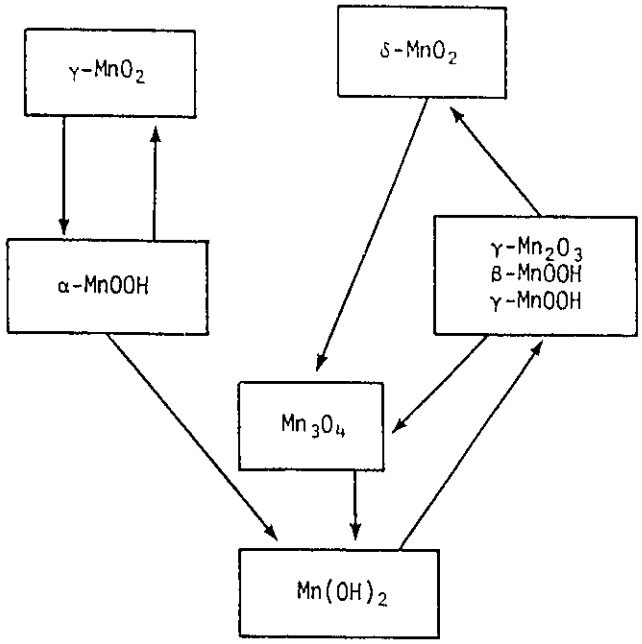

Figure 1.2: Schematic representation of the reaction paths for the reduction and oxidation of manganese oxides in 7M KOH.

In more recent work, some of the exact structural assignments of McBreen [30] have been questioned but the reaction pathways seem sound. Ultimately though, the only reaction step which is mechanistically confirmed by XRD is the proton insertion step near the beginning of the discharge.

Kordesch et al [9] have shown that there is a logarithmic relationship between the depth of discharge and the number of discharge-recharge cycles which may be obtained in the discharge range up to 60% of the one-electron capacity for γ-MnO_2. It is assumed that the deterioration arises from gradual breakdown of the lattice due to repetitive dilation and contraction. There is, therefore, a trade off between the depth of discharge and the number discharge-recharge cycles that may be obtained in their system. In practice, a 40% extent of discharge of the "first electron" (Mn^{4+} to Mn^{3+})

is seldom exceeded. In order to control the extent of discharge, the cells are "anode limited", in other words the amount of zinc in the anode is restricted to that which will "use up" the desired fraction of the MnO_2 capacity.

In contrast, the work of Wroblowa et al [11-15] and the subsequent research by other workers in our laboratory [35] indicates that the so-called chemically modified (CM) MnO_2 is not γ-MnO_2 and behaves in a markedly different way from it under discharge and recharge. Chemically modified material is produced by rendering basic a solution of Mn^{2+} and Bi^{3+} (or Pb^{2+}), then oxidising the precipitated mixture by bubbling with oxygen. Bismuth has been shown to have a substantial effect on rechargeability when present in as little as 2 mole% [13] but it is usually added in the range of 7 to 12 mole%. It does not itself contribute to the charge capacity of the MnO_2 as the reduction potential lies below the point where reduction of MnO_2 occurs.

With the chemically modified material, little deterioration in discharge behaviour is observed even after hundreds of cycles to 80% of the "two electron" capacity and there is strong evidence to suggest that the reaction is at least partly heterogeneous throughout the first and second electron reductions and oxidations [35]. Detailed work on the redox mechanisms of the CM MnO_2 system is the subject of the research of others in this group and is not the main topic of the present thesis.

Finally, a few words about rechargeable lithium batteries using MnO_2 cathodes should be given. The performance of MnO_2 as a rechargeable material for intercalation of lithium as the cathode reaction, using a lithium metal anode, appears to be good [36]. In this type of embodiment, the intercalation of Li^+ ions parallels the

process of insertion of protons in the case of the mechanism of reduction of MnO_2 in alkaline solution, referred to earlier (cf. refs. 16-21). Most of the problems associated with this system are due to processes occurring at the lithium electrode, such as dendrite formation, side reactions with the electrolyte and catastrophic failure under certain conditions [5]. The most serious of these is the issue of safety, as the batteries can explode due to the very high reactivity of lithium re-deposited during re-charging. A so-called "rocking chair" battery in which Li is intercalated in both the anode and the cathode rather than being deposited as metal on recharge is inherently much safer. The use of $LiMn_2O_4$ produced from MnO_2 as a cathode material in a rocking chair cell is described in a recent publication [37]. Although not without its problems, this cell, in combination with carbon as the negative intercalation electrode, shows promise.

1.4 Aims of the Present Research and Scope of the Thesis

Whereas other workers in our research group have been attempting to investigate the properties of CM MnO_2 material prepared in a matrix with graphite powder, as described in the literature [10], it has been the aim of the present research project to produce bismuth-containing MnO_2 in a novel way and study its electrochemical behaviour. The method of preparing the material is to co-deposit bismuth species with electrolytic MnO_2 produced according to accepted methodologies [38-40,16] on porous graphite rods. The observation and characterisation of the rechargeability of this deposited material was the main aim of this research.

In addition to the above, several other areas were investigated, viz. the optimisation of conditions for creating the MnO_2 deposits, solubility studies of manganese and bismuth species, cyclic voltammetry of deposits on materials other than porous graphite and cyclic voltammetry of bismuth and manganese metal electrodes were all performed in an effort to better understand the mechanism of rechargeability of bismuth-containing MnO_2 materials. It is not surprising that full elucidation of that mechanism is beyond the scope of this thesis; even after decades of research, there is not yet even complete agreement on the reduction mechanism of common γ-MnO_2.

1.5 Organisation of the Material Presented in this Thesis

The material in the thesis is broken up into three experimental regimes, each comprising one chapter. There is inevitably some overlap between the subjects and the decision of where to include some material in a certain section might seem arbitrary. It is hoped that the reader sees the logic of the layout of the results.

Chapter 2 is concerned with the properties of the deposits that were prepared during the course of the work. The chemical composition, macroscopic morphology and appearance under high magnification are discussed. Chapter 4 details the electrochemical work that was carried out on the deposits described in Chapter 2, while Chapter 3 refers to several experiments which are in themselves important to material discussed in the thesis, but do not fit into the work of Chapters 2 and 4. In some ways Chapter 3 bridges the gap between the other two main chapters. Each of

these main chapters is self-contained with provision of the usual sections: introduction, experimental, results and discussion and conclusions.

Chapter 5 summarises the conclusions of each chapter, pulling them together into overall conclusions for all of the work described in the thesis.

1.6 Some Conventions Used in the Thesis

Since all of the depositions were carried out using the same reference electrode (saturated calomel electrode) and all of the electrochemical experiments were likewise conducted using a common reference (Hg/HgO in 9M KOH), intercomparison of results from experiment to experiment is simple. No attempt was made to convert potentials to the standard hydrogen electrode scale.

The following table of some important potentials relevant to this work is, however, offered for the convenience of the reader:

Saturated Calomel Electrode (in Sat'd KCl)	+0.24V
Standard Hydrogen Electrode	0.00V
Hg/HgO (in 9M KOH)	-0.04V
Normal Hydrogen Electrode (in 9M KOH)	-0.97V
Zn/ZnO_2^{2-} (in 9M KOH)	-1.42V

These values are taken from the standard reduction potentials [41], corrected for the activity of OH^- and H_2O in 9M KOH, where necessary, according to the Nernst equation. The activity coefficient of OH^- in 9M KOH is given by Conway [42] as 4.86. It is assumed that the activity of water in 9M KOH is about the same as it is in 9M NaOH, for which a value of 0.55 is given [42].

For the purposes of discussion and for graphical presentation, the sign

convention for current is that positive current is anodic and negative current is cathodic. In the display of cyclic voltammograms, current is more positive up the page and potential more positive to the right. This means that in normal voltammograms, the sweep is scribed in a clockwise fashion.

CHAPTER 2 PROPERTIES OF DEPOSITS OF MnO_2

2.1 INTRODUCTION

This chapter is devoted to a series of experiments which were conducted with the prime purpose of determining the chemical composition and physical properties of manganese dioxide electrodeposited on graphite rods.

2.1.1 Choice of Methods

The method of choice for the determination of the chemical compositions of the MnO_2 deposits was Atomic Absorption Spectrometry (AAS). This procedure was chosen for its ease, availability of equipment and sensitivity appropriate to the range of concentrations of manganese and bismuth expected to be found in the deposits. Two pieces of information were generally gained from these analyses. Firstly, the overall weight of Mn in the deposit, which gives an indication of the efficiency of deposition, and secondly the ratio of Mn to Bi in the deposit. Previous workers [13] and those in our own laboratory [43] have studied the effect of this ratio on rechargeability of so-called "chemically modified" (CM) MnO_2 material. Since the aim of the present work was to determine the effect of Bi additions on the rechargeability of electrodeposited MnO_2 electrodes, the ratio is obviously of primary interest.

Unfortunately, AAS does not give any indication of the oxidation state of the elements of interest or about other elements expected to be present in the deposits

such as oxygen. Also, anions from the bath and water of hydration or trapped water, may be present in the deposit. Again, this technique can tell us nothing of these constituents.

The physical properties of some representative deposits were studied by means of Scanning Electron Microscopy (SEM) augmented by visual observations of the deposits. Energy Dispersive X-Ray (EDX) analysis was also performed on some of the electrodes as a matter of interest, and to confirm the inclusion of bismuth in the deposited MnO_2. These techniques were chosen in order to get some indication of the macroscopic properties of the deposits.

One experiment was performed using the X-Ray Diffraction (XRD) facilities at Carleton University. As has been pointed out in the literature [33], electrodeposits of MnO_2 tend to be amorphous or semi-amorphous and require special techniques and equipment. The result of the one experiment yielded no information so no further XRD work was done on these deposits.

2.2 EXPERIMENTAL

In the present work, electrochemical deposition of MnO_2 and co-deposition of Bi species onto porous graphite rods was the basis of preparation of MnO_2 for examination of rechargeability in a thin layer state. This procedure for preparation of MnO_2 was chosen in order to provide comparisons with the behaviour of CM material which is produced by oxidising chemically precipitated $Mn(OH)_2/Bi(OH)_3$ mixtures. The CM material is being studied complementarily in this laboratory.

2.2.1 Materials and Equipment

All electrochemical depositions of MnO_2 were carried out in the cell illustrated in Figure 2.1, the design of which is based on that of Kozawa and Yeager [16]. It consists of a 250 ml beaker with a Teflon lid drilled to accommodate the working electrode assembly and surrounded by four equally spaced counter electrodes. Places are also provided for a thermometer and a reference electrode. The beaker was usually submerged in a thermostated water bath to provide a constant temperature (typically about 85 °C) for deposition of the MnO_2.

The counter electrodes were made from commercially available graphite rods (Johnson Matthey Electronics, Ward Hill,MA) of 99.9995% purity which were machined to the required length with the ends being faced on a lathe. One end was then drilled and tapped to accept a 2-56 brass screw which served to make an electrical connection. For most experiments, the same carbon material was used for the working electrode. A standard 0 to 100 °C thermometer was used to monitor the temperature during the deposition experiments. A commercial saturated calomel electrode (SCE) (Corning Glass Works, Corning, N.Y.) was used as the reference electrode to monitor the electrode potentials at which all depositions were carried out.

The chemicals used for all experiments were of analytical or higher grade and were not subjected to any further purification.

A Hokuto Denko HA-501 Potentiostat/Galvanostat (Tokyo,Japan) was used as a power source for all of the deposition experiments.

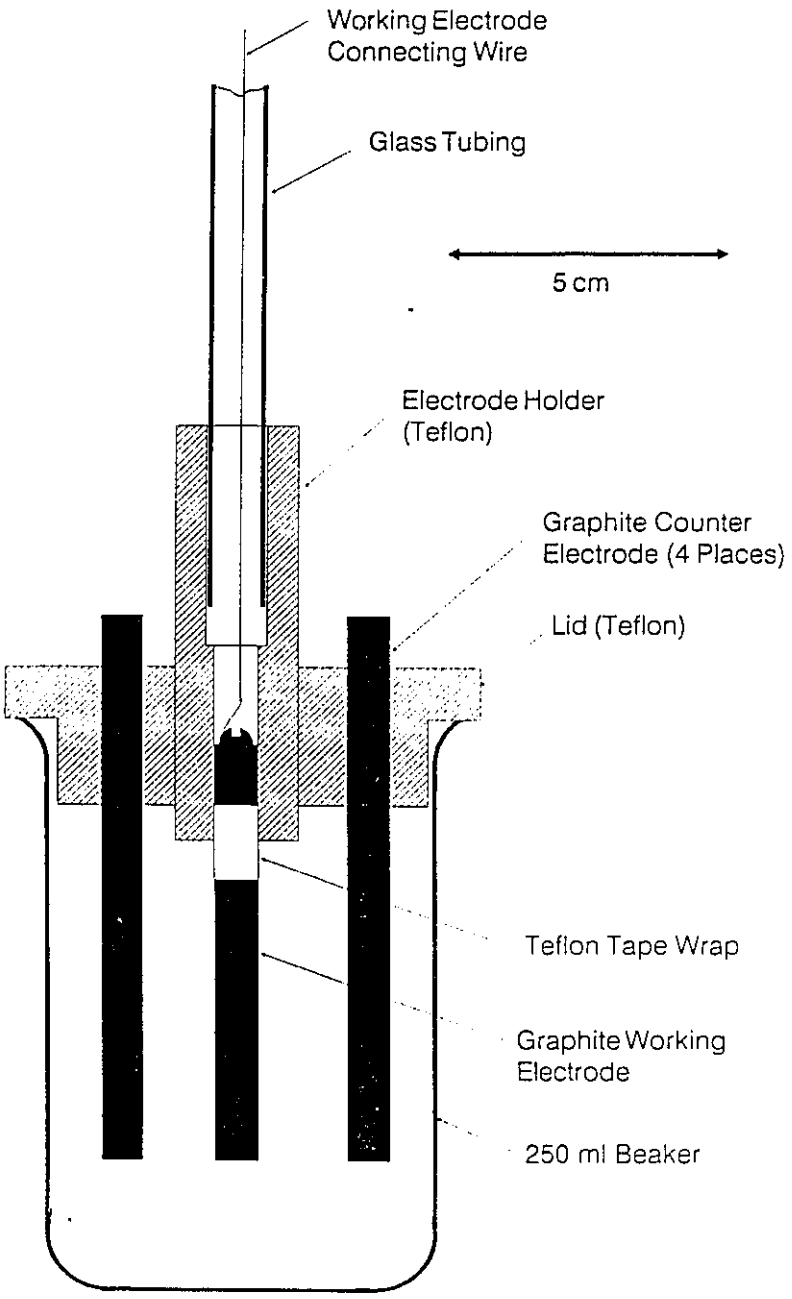

Figure 2.1: Cross-sectional view of the electrochemical cell used for deposition of MnO_2.

Atomic absorption measurements were performed using a Varian Techtron AA-1475 (Mulgrave, Australia) with hollow cathode lamps manufactured by Cathodeon of Cambridge, England.

The SEM and EDX facilities in our own laboratory at the University of Ottawa were used to generate micrograph photos and near-surface analyses. The system consists of a Nanolab 7 SEM operating at 15 or 30 keV with a Kevex EDX detector.

2.2.2 Experimental Procedure

Although many different deposition bath compositions with various anodic and cathodic current densities were tried, the basic deposition experiment was done in the same way. New graphite working electrodes were soaked in sulphuric acid for a short period of time then soaked in distilled water until used. For electrical connection, a copper wire was secured to the electrode using a #2-56 brass screw and nut. The electrode was located in its holder by placing a few wraps of Teflon tape around the electrode and pressing it into the holder. The application of the Teflon tape was done in such a way as to leave 5 cm (or in some cases 1 cm) of electrode length exposed. See Figure 2.1 for details.

Preparation of the deposition baths was straightforward with respect to the manganese content. A salt of a suitable anion was used or, in some cases, manganese metal was dissolved in the appropriate acid. Inclusion of bismuth from a Bi salt was simple for all preparations except those in sulphuric acid. Bismuth metal has a limited

solubility in sulphuric acid and no commercially available bismuth sulphate was found. Bismuth metal was heated vigorously with a small amount of sulphuric acid to dryness. The required amount of acid for the deposition bath was then added to the white residue and heated again before being diluted to the required volume (typically 200 ml in the 250 ml beaker used as the deposition cell). If this procedure was not followed carefully, there would remain either black particles of undissolved bismuth metal or some white precipitate that would never dissolve over a reasonable amount of time. A discussion of insoluble bismuth species in sulphuric acid is given in Section 3.3.1.

Normally the whole cell would be partially immersed in a thermostated bath at 85 to 87 °C and allowed to come to thermal equilibrium before starting the experiment. No attempt was made to exclude atmospheric oxygen from the cell during the deposition experiments. Generally speaking, anodic voltages were applied under galvanostatic control for a fixed period of time. Galvanostatic conditions were preferred so that the total coulombs passed were known and hence the amount of material which would ideally be deposited could be calculated.

During deposition, the temperature of the bath, the working-to-reference electrode potential difference and that between the working and counter electrode were recorded at regular intervals as a system check.

After the deposition, working electodes were removed from the bath and from their holder, then soaked in distilled water for at least overnight before being subjected to any further experimentation.

Samples that were sent for SEM/EDX analysis, were dried in a vacuum oven at about 65 °C for 1 hour. No further preparation was neccessary.

Atomic absorption analyses were conducted using the following instrumental conditions and settings:

Flame: Air-Acetylene
Wavelength and Working Concentration Range:
403.1 nm (Mn), 15-60 $\mu g\ ml^{-1}$
279.5 nm (Mn), 1-4 $\mu g\ ml^{-1}$
223.1 nm (Bi), 10-40 $\mu g\ ml^{-1}$
Spectral Band Width: 0.2 nm
Integration Time: 3 seconds
Readings: 5 per point

Manganese standards were produced from Mn metal (Alfa-Ventron, Danvers,MA) by first removing the outer oxide film with concentrated nitric acid then rinsing and drying. An appropriate amount of the clean metal was dissolved in sufficient HCl to give a final concentration of about 1 g l^{-1} of Mn and 5% v/v aq. HCl. This standard was diluted to the working range in 5% v/v aq. HCl. Bismuth standards were prepared from 99.99% Bi_2O_3 (Aldrich Chemical, Milwaukee,WI) by dissolution and subsequent dilution in 5% v/v aq. HCl. Freedom from sensitivity changes due to HCl in the standards was confirmed by analysing working standards in 1% aq. HCl and in 10% aq. HCl. No difference in analytical response was found.

Solution samples for AAS analysis were simply diluted in 5% v/v aq. HCl. MnO_2 deposits for analysis were first dissolved in the appropriate amount of aq. HCl to give a final concentration of 5% v/v. The solution was then transferred to a volumetric flask with a few washings of distilled water and boiled to expel Cl_2 before

dilution to the required volume. This solution (typically 25 or 50 ml) was usually further diluted in 5% v/v aq. HCl to the working range for the element of interest.

2.3 RESULTS AND DISCUSSION

Many different deposition bath compositions were tried over the course of this work. The physical observations of the resultant deposits are most conveniently presented and summarised in a table (Table 2.1). The first attempts were in buffered solutions under slightly acidic conditions in order to attempt to co-reduce manganese and bismuth metals from their respective salts in the deposition bath. As can be seen from the first three entries in Table 2.1, these attempts were largely unsuccessful. Deposits were poor in appearance or invisible. The reduction to manganese metal in acid media is impeded by the fact that it is unstable and will tend to dissolve spontaneously. The Pourbaix diagram [44] for manganese metal is shown in Figure 2.2. Note that the stability field for manganese metal lies well below that of water and that the potential difference between the Mn/Mn^{2+} couple and the H_2/H^+ corresponding to spontaneous corrosion reaction increases with decreasing pH.

The remainder of the MnO_2 deposition experiments were carried out under anodic polarisation in acid solutions at about 1N in H^+ ion. The accepted method for depositing MnO_2 is from a bath containing manganous sulphate at 0.5M and sulphuric acid, also at 0.5M, at a temperature of 85 to 90 °C [38-40]. This composition was used as a baseline for experimentation. All of the depositions from acidic solutions were carried out at elevated temperature. Other acidic baths in which nitric,

Table 2.1 Observations of Deposits on Graphite Rods

Bath Composition	Temp (°C)	Galvanostatic Conditions [1] (mA/apparent cm^2)	WE vs RE Voltage (vs.SCE)	Observations: Colour	Texture	Adherent(?) (Yes or No)	Other Work
0.1M Mn 0.2M Acetic Acid ph 4	RT	Cathodic Polarisation Curve	-	Brownish (thin) deposit	- CE's have adherent black		
0.001M Bi 0.2M Acetic Acid pH 4	RT	Cathodic Polarisation Curve	-	No visible deposit			
0.5M Mn 1.4M $(NH_4)_2SO_4$ pH 2.3	RT	Cathodic Polarisation Curve	-	No visible deposit			
0.5M Mn 0.015M Bi 1M HNO_3	90	-1, 2 min +1, 8 min	0.75 1.3	Black	Smooth	Y	CV
0.5M Mn 0.02M Bi 1M HNO_3	91	+.5, 5 min	1.0	Not much visible black deposit, few white specks			CV
0.5M Mn 1M $HClO_4$	85	+2, 5 min	1.15	No visible deposit			CV
0.005M Bi 0.5M H_2SO_4	RT	Cathodic Polarisation	-	Black	Powdery	N	-
0.5M Mn 0.005M Bi 0.5M H_2SO_4	86	Square Wave, 10 min +10, 1 sec -1, 1 sec	0.58,0.29	Black	Smooth	Y	CV

Bath Composition	Temp (°C)	Galvanostatic Conditions [1] (mA/apparent cm^2)	WE vs RE Voltage (vs.SCE)	Observations: Colour	Texture	Adherent(?) (Yes or No)	Other Work
0.5M Mn 0.1M Bi 1M $HClO_4$	85	Square Wave, 10 min +10,0.1 sec -1, 0.1sec	0.70,0.65 rising to 0.97,0.81	Black with superimposed colours	Rough	N	CV
0.5M Mn 0.5M H_2SO_4	86	+10, 3 min	1.14	Black	Rough	Y	CV
0.5M Mn 0.005M Bi 0.5M H_2SO_4	85	+10, 10 min	1.17	Black	Smooth	Y	AAS
0.5M Mn 0.005M Bi 0.5M H_2SO_4	86	+10, 5 min	1.14	Black	Sl.rough	Y	AAS
0.5M Mn 0.005M Bi 0.5M H_2SO_4	86	+1, 50 min	1.16 rising to 1.40	Black	Smooth	Y	AAS
0.5M Mn 0.005M Bi 0.5M H_2SO_4	86	+1, 100 min	1.03	Brownish black (Thin)	Rough	Y	AAS
	86	+5, 20 min	1.05	Black	Rough	Y	AAS
	85	+10, 10 min	1.09	Black	Rough	Y	AAS,SEM
	85	+20, 5 min	1.15	Greyish Black	Smooth	Y	AAS
0.5M Mn 0.1M Bi 0.6M HCl	86	+10, 10 min	1.10	Black	Rough		AAS

Bath Composition	Temp (°C)	Galvanostatic Conditions [1] (mA/apparent cm^2)	WE vs RE Voltage (vs.SCE)	Observations: Colour	Texture	Adherent(?) (Yes or No)	Other Work
0.5M Mn 2M H_2SO_4	86	+10, 10 min	1.18	Grey with brown spots	Smooth	Y	AAS,SEM
0.5M Mn 0.01M Bi 2M H_2SO_4	85	+10, 10 min	1.18 rising to 1.26	Dark grey	Smooth	Y	AAS,SEM
	86	+10, 30 min	1.18 rising to 1.40	Dark grey	Smooth	Y	AAS,SEM
0.5M Mn 0.5M H_2SO_4	86	+11, 11 min	1.06	Grey	Smooth	Y	CV
0.5M Mn 0.005M Bi 0.5M H_2SO_4	86	-11, 2 min	-0.95	Grey coating	Rough	N	CV
	86	+11, 10 min	1.25	Black	Sl.Rough	Y	CV

Notes on Table 1:

WE = Working Electrode
RE = Reference Electrode (Saturated Calomel Electrode)
SW = Square-wave current pattern produced by function generator
RT = Room Temperature

[1] -ve indicates cathodic current, +ve indicates anodic current

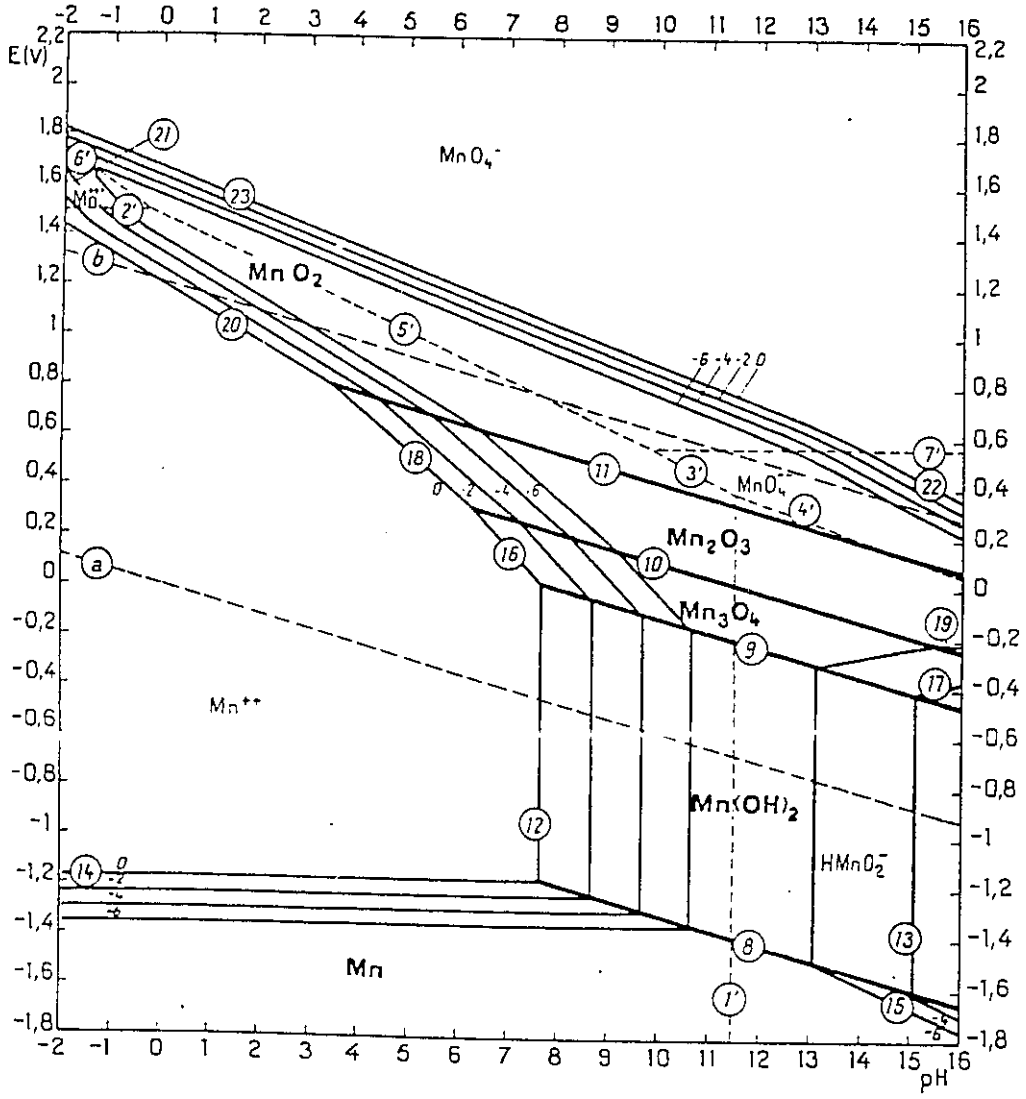

Figure 2.2: Potential-pH equilibrium diagram for the system manganese-water at 25°C (reprinted from ref. 44).

perchloric and hydrochloric acids were substituted for sulphuric acid, were tried in an attempt to increase the extent of co-depostion of bismuth in the deposits. Scanning Table 2.1 reveals that these other acids did not provide good smooth adherent deposits of manganese dioxide.

The results of the atomic absorption analyses are presented in Table 2.2, in which several of the recorded observations are to be noted. In one experiment, the electrode was simply soaked in the deposition bath without the passage of current. This "blank" experiment showed that the inclusion of bismuth from sulphuric acid baths is not simply from absorbed electrolyte. Further to this point, the last entry in the table shows that the Mn/Bi ratio is about the same for depositions of 10 and 30 minutes duration at the same current density. Therefore, the bismuth is included into the deposit on a continuous basis.

There were only two experiments in which MnO_2 deposits from baths other than sulphuric acid were analysed by AAS. The analysis of the deposit from a mixed bath of sulphuric and nitric acids, and the deposits from hydrochloric acid gave a rather low current-efficiency of deposition of MnO_2, consistent with the physical observation of poor deposits. The Mn/Bi ratio in these deposits was also erratic and usually very high.

Table 2.2 Results of Atomic Absorption Spectrometry Experiments

Bath Composition	Temp (°C)	Galvanostatic Conditions [1] (mA/apparent cm^2)	WE vs RE Voltage (vs.SCE)	Manganese Deposited (μMoles/ apparent cm^2)	Coulombic Efficiency (%)	Bismuth Deposited (μMoles/ apparent cm^2)	Mole Ratio Mn/Bi
0.5M Mn 0.005M Bi 0.5M H_2SO_4	85	+10, 10 min	1.17	31	100	1.4	22
	85	SW +10,1s; +0.2,0.2s;0,0.2s	-	38	57	1.6	24
	85	SW +10,1s;-10,0.6s	-	13	85	0.91	14
0.5M Mn 0.005M Bi 0.5M H_2SO_4	86	+10, 5 min	1.14	14	90	0.46	31
	85	soak 50 min (no current)	-	0.09	-	0.009	10
	86	+10, 50 min	1.16-1.40	127	82	3.5	36
0.5M Mn 0.005M Bi 0.5M H_2SO_4	86	+1, 100 min	1.03	23	73	1.8	13
	86	+5, 20 min	1.05	29	93	1.1	26 (20) [2]
	85	+10, 10 min	1.09	30	96	1.2	25 (23) [2]
	85	+20, 5 min	1.15	30	98	0.52	59 (30) [2]
0.5M Mn 0.005M Bi 0.5M H_2SO_4	86	+10, 10 min	1.06-1.15	25	81	1.1	22

Bath Composition	Temp (°C)	Galvanostatic Conditions [1] (mA/apparent cm^2)	WE vs RE Voltage (vs.SCE)	Manganese Deposited (μMoles/ apparent cm^2)	Coulombic Efficiency (%)	Bismuth Deposited (μMoles/ apparent cm^2)	Mole Ratio Mn/Bi
0.5M Mn 0.02M Bi [3] 0.5M H_2SO_4 .1M HNO_3	85	+10, 10 min	1.09-1.38	21	67	2.1	10
0.5M Mn 0.01M Bi 0.6M HCl	86	+10, 10 min	1.09	27	87	0.06	470
0.5M Mn 0.1M Bi 0.6M HCl	86	+10, 10 min	1.10	27	88	0.4	68
0.5M Mn 0.01M Bi 1M HCl	86	+10, 10 min	1.12	0.6	2	0.03	20
0.5M Mn 0.1M Bi 1M HCl	85	+10, 10 min	1.13	14	46	0.3	46
0.5M Mn 2M H_2SO_4	86	+10, 10 min	1.18	28	89	-	-
0.5M Mn 0.01M Bi 2M H_2SO_4	85	+10, 10 min	1.18-1.26	27	87	1.2	23
	86	+10, 30 min	1.18-1.40	59	63	2.7	22

Notes on table 2:

WE = Working Electrode
RE = Reference Electrode (Saturated Calomel Electrode)
SW = Square-wave current pattern produced by function generator

[1] -ve indicates cathodic current, +ve indicates anodic current
[2] Values in parentheses have been scaled for the reduction of Bi concentration during the experiment.
[3] Supersaturation - precipitation occurred in the bath

Owing to the problems associated with deposition from other acids, most of the work was eventually carried out using sulphuric acid baths. The optimal conditions for deposition of bismuth-containing MnO_2 deposits, as found in this study, are as follows:

Temperature: 85 - 90 °C
Bath Composition: 0.5M to 2M H_2SO_4
0.5M $MnSO_4$
0.005M to 0.01M Bi^{3+}
Current Density: 5 to 20 mA cm^{-2} (apparent)

A discussion of the mode of inclusion of bismuth species in deposited MnO_2 is reserved for Chapter 3 where the solubilities of bismuth species with respect to sulphuric acid strength are considered.

The colours of the deposits from 0.5M H_2SO_4 ranged from grey to black when current densities of 5 to 20 mA cm^{-2} were used. They also had a rough or smooth appearance for relatively short deposition times but were usually smooth for longer depositions. All deposits were adherent and the inclusion of bismuth had no apparent effect on the morphology of the deposit.

Figure 2.3 shows SEM micrographs of the face of a graphite rod, with and without electrodeposited MnO_2. The blank graphite surface is quite rough in appearance, showing many cracks and pores. The deposited surface which has a smooth black morphology shows a dried "mud pack" like appearance. The cracks which are seen throughout the surface of the deposit are likely caused by either an expansion or contraction of the surface when it is dried or by thermal contraction

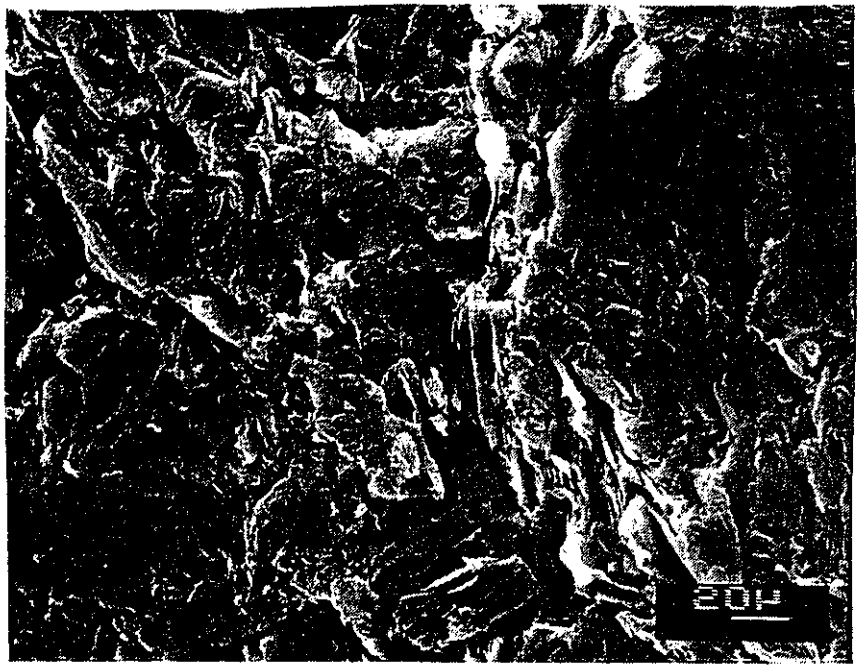

(a)

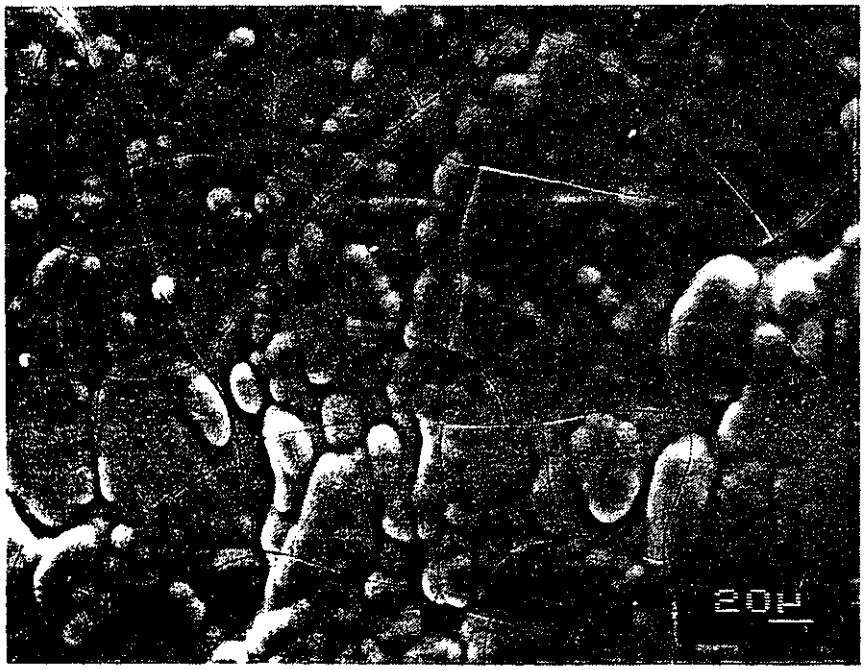

(b)

Figure 2.3: SEM micrographs of the surface of a graphite rod: a) without any deposit, b) with deposited MnO_2 together with included bismuth species.

when the electrode is rinsed with room temperature distilled water after being deposited at 85 to 90°C.

Higher magnifications of deposits are shown in Figure 2.4. These micrographs show the differences in morphology of two areas of the same MnO_2 deposit prepared without bismuth. The lower micrograph is of a smooth grey area of the deposit and the upper micrograph is of a rough black area. Note that the rough deposit has a cluster, or cauliflower-like, appearance and the roughness of the underlying graphite is still visible.

In order to examine the interface between the deposit and the graphite substrate, deposited graphite rods were snapped into pieces and micrographs were taken across the edge of the broken piece. Figure 2.5 shows "edge" shots for two deposits, The upper shows the smooth black morphology of an MnO_2 deposit containing bismuth. The deposit shows up on the left of the micrograph as a coherent layer. The cracks in the deposit are clearly visible. The deposit appears to be amorphous in nature with no apparent crystal structure. This deposit was made with a current density of 10 mA cm^{-2} for 10 minutes or 6 C cm^{-2}. For the two-electron process, the number of moles per cm^2 is given by q/2F where q is the charge passed, 2 is the number of electrons in the process and F is Faraday's constant. This yields a value of 31 μmole cm^{-2} which translates to 2.7 mg of MnO_2 per cm^2. Given a density of about 5 g cm^{-3} [41] for MnO_2, the weight of MnO_2 translates to a volume of 5.4×10^{-4} cm^3 per cm^2, or, in other words, a layer 5.4 microns thick. Inspection of the micrograph shows the layer to be between 5 and 6 microns thick, in agreement

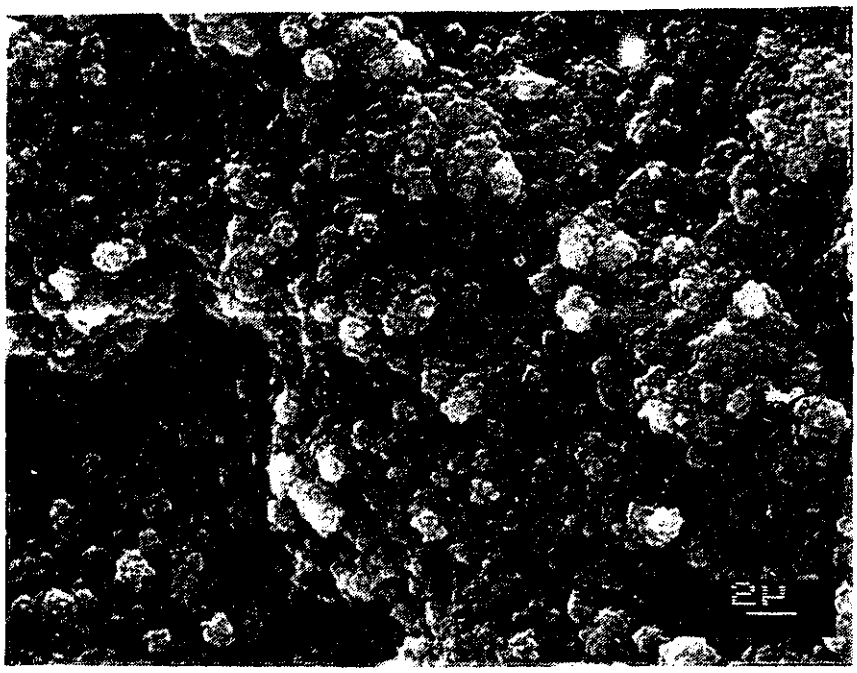

(a)

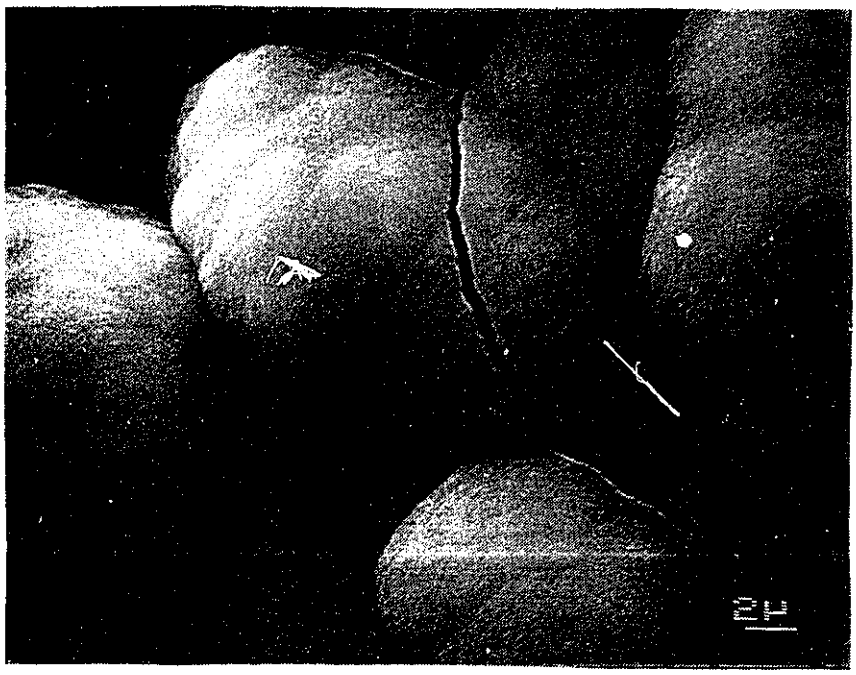

(b)

Figure 2.4: Higher magnification micrographs of an MnO_2 deposit: a) an area with a rough black morphology, b) an area with a smooth grey morphology.

(a)

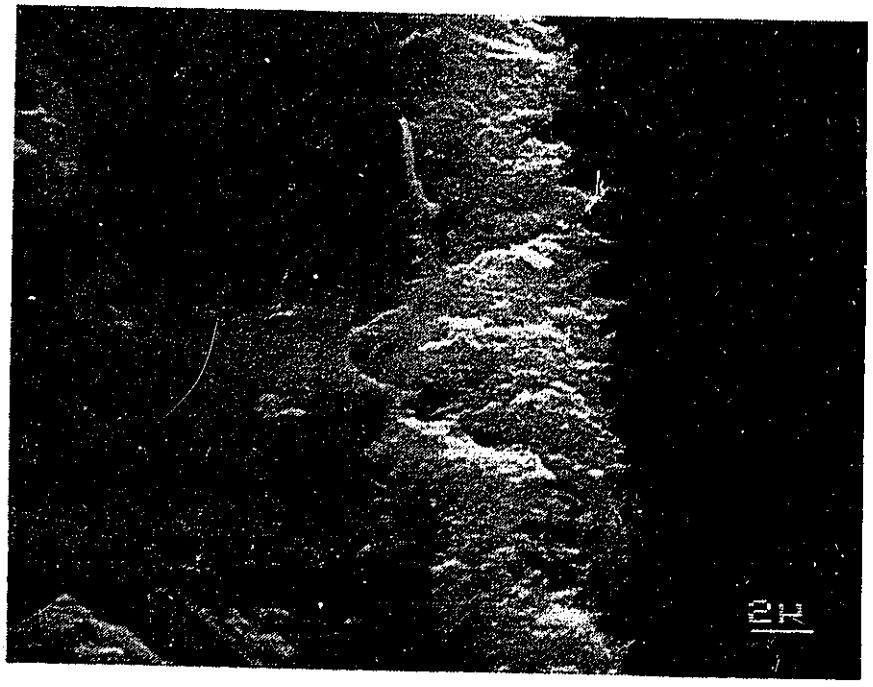

(b)

Figure 2.5: Micrographs of the edges of two deposits: a) smooth black MnO_2 deposit containing bismuth species, b) rough black deposit of MnO_2 only.

with the calculated thickness.

The lower micrograph of Figure 2.5 shows the edge of the rough black deposit. Note that the surface appears fibrous, leading to the macroscopic appearance.

In order to further investigate the mode of inclusion of bismuth in MnO_2 deposits, attempts were made to form bismuth deposits anodically in a bath that contained 0.005M bismuth in 0.5M H_2SO_4 with no manganese present. Under galvanostatic conditions of +11 mA cm^{-2}, the expected reaction at the working electrode would be the evolution of oxygen. During the 10 minutes of passage of current, the working electrode-reference electrode potential difference dropped slowly from 1.59V to 1.46V against the saturated calomel electrode. Gas evolution was observed throughout the experiment. When inspected by SEM, the electrode thus produced showed growth of clusters of crystals. A micrograph photo of one cluster is shown in Figure 2.6. The approximate density of these clusters is about 40 per mm^2. EDX analysis of the cluster portrayed in Figure 2.6 indicates a high bismuth concentration and evidence of sulphur consistent with the crystals being a sulphate of bismuth. The EDX results must be taken with some skepticism due to the overlap of the peaks from bismuth and sulphur but it is apparent that bismuth *is* deposited under these conditions.

Because the working electrode-reference electrode potential difference in the above experiment was close to the potential at which Bi^{3+} could become oxidised to Bi^{5+}, especially in the early part of the experiment (see Pourbaix diagram, Figure 2.7), the procedure was repeated under potentiostatic conditions. A potential of

Figure 2.6: SEM micrograph of a cluster of crystals of a bismuth compound on the surface of a graphite rod.

1.4V against saturated calomel was used tc keep the potential well under that for oxidation of Bi^{3+}. Current was passed for 20 minutes in this experiment and ranged from 12mA at the beginning to 35 mA at the end.

This time, the SEM micrograph did not show clusters and, in fact, the surface looked clean. However, EDX analysis showed that there was still a buildup of bismuth species on the surface of the electrode.

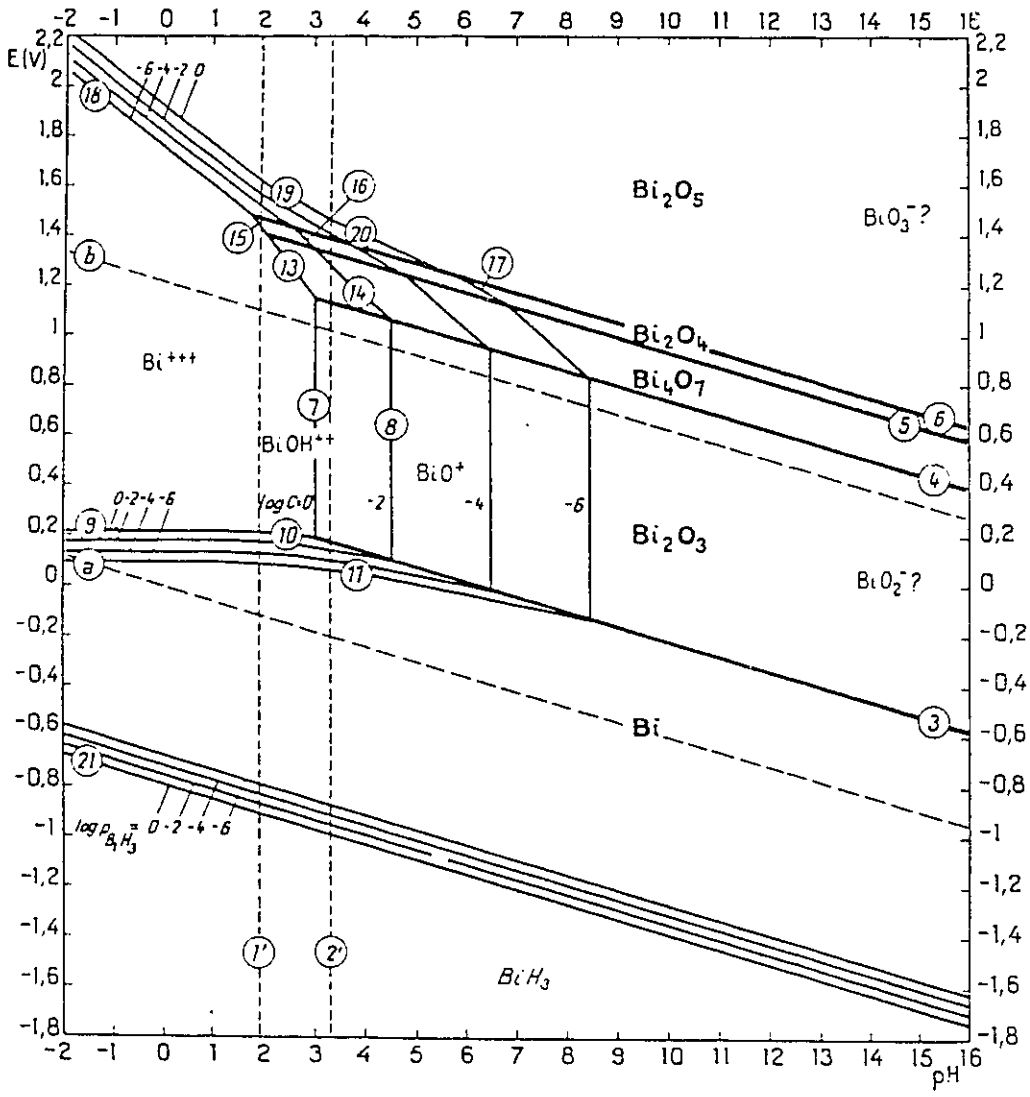

Figure 2.7: Potential-pH equilibrium diagram for the system bismuth-water at 25°C (reprinted from ref. 44).

2.4 CONCLUSIONS

The following conclusions are to be drawn from the work that is outlined in this Chapter:

i) Bismuth species are included in deposits of MnO_2 prepared from sulphuric acid baths, not by a soak and precipitation mechanism but by continuous inclusion as the deposit grows.

ii) The macroscopic morphologies of the deposits do not depend on the inclusion of bismuth species.

iii) Good smooth adherent deposits of MnO_2 can be produced on graphite rods using the optimal deposition conditions, as outlined above.

iv) Bismuth species may be deposited on a graphite surface under conditions similar to those for deposition of MnO_2 but without manganese species being present in the deposition bath.

CHAPTER 3 NON-ELECTROCHEMICAL EXPERIMENTS

3.1 INTRODUCTION

The experiments reported in this chapter are of two types which do not fall into either of the categories of the other two experimental approaches described in Chapters 2 and 4. The first type is concerned with the solubilities of the constituents of the baths used to make MnO_2 deposits and in the 9M KOH solution used as the electrolyte for electrochemical experimentation. The second type involved a simple observation of what happens when $Mn(OH)_2$ in 9M KOH is allowed to become oxidised in air. These few experiments, while they may be quite simple, assist the understanding of the processes involved in the co-deposition of bismuth species in MnO_2 and of the influence of bismuth species on the rechargeability of the resulting MnO_2 deposits.

3.1.1 Choice of Methods

The experiments reported on in this section rely, for the most part, on physical observations. Where measurement of solubilities was required, Atomic Absorption Spectrometry (AAS) was, as in the work reported in Chapter 2, the method of choice as it has the appropriate sensitivity and is relatively easy to use. One drawback, as pointed out in Chapter 2, is that no information is gained about the oxidation state of the analyte.

3.2 EXPERIMENTAL

3.2.1 Materials and Equipment

Atomic absorption analyses were performed using a Varian Techtron AA-1475 (Mulgrave, Australia) with hollow cathode lamps manufactured by Cathodeon (Cambridge, England). Chemicals used for all experiments were of analytical or higher grade and were not subjected to any further purification.

3.2.2 Experimental Procedure

3.2.2.1 Solubility studies

A full description of the technique used for Atomic Absorption measurements was given already in Chapter 2. Acidic solutions to be analysed were diluted to the appropriate analyte concentration range in 5% aqueous HCl. Basic solutions to be analysed were rendered approximately neutral by addition of aqueous HCl, then diluted in 5% aqueous HCl.

3.2.2.2 Air oxidation experiment

Two vials were set up, each containing 5 ml of 9M KOH ;one solution was saturated with Bi_2O_3. Each vial was bubbled with N_2 for about 10 minutes. To each vial, 5 drops of a 25 g l^{-1} solution of $MnSO_4.4H_2O$ was added. After thorough mixing, the N_2 gas was shut off and the vials were allowed to stand open to the air overnight. Observations of the colour of the solutions and the nature of the precipitation were taken during the initial period and after standing overnight.

3.3 RESULTS AND DISCUSSION

3.3.1 Solubility Studies

Not surprisingly, the solubility of Mn was not a problem in any of the acidic baths used for MnO_2 deposition. It is well in excess of the value of 0.5M usually used in the baths that have acid concentrations of 1N. The bismuth solubility , however, varies considerably depending on the acid used. Before the AAS analysis was undertaken, an estimate of the solubility was obtained by physical observation of the prepared baths. Table 3.1 summarises these observations.

Table 3.1 Solubility of Bismuth Species in Deposition Baths Having Various Compositions

Composition	Bismuth Concentration	Observations
0.5M Mn 1N HNO_3	0.1M	Very slight precipitate at 85°C which redissolves on cooling to room temperature
	0.03M	No precipitation at 85°C or at room temperature
1N $HClO_4$	0.5M	No precipitation at 90°C or at room temperature
0.5M Mn 1N HCl	0.1M	No precipitation at 90°C or at room temperature
0.5M Mn 2M H_2SO_4	0.02M	No precipitate at room temperature; heavy precipitation at 90°C
0.5M Mn 0.5M H_2SO_4	0.005M	No precipitation at 90°C or at room temperature

It is interesting to note that the solubility of bismuth is lower at higher temperatures, at least for nitric and sulphuric acids over the 1 to 4N range. Since the solubility of bismuth appeared to be marginal in H_2SO_4, more work was done on this system in the form of AAS analyses. The solubility of both bismuth and

manganese was measured over a large range of H_2SO_4 concentrations both at room temperature and at 85°C, the temperature typically used for MnO_2 deposition. The results of these analyses are summarised in Table 3.2.

Table 3.2 Solubility of Bismuth and Manganese Species in Relation to Sulphuric Acid Strength

H_2SO_4 Concentration (M)	Bismuth (mM) Room Temp	85°C	Manganese (M) Room Temp	85°C
0.05	1.2	0.3	>0.5	>0.5
0.15	2.1	1.1	>0.5	>0.5
0.5	8.9	5.9	>0.5	>0.5
1.5	16	11	>0.5	>0.5
5	>20	>20	>0.5	>0.5
15	<2.2	8.7	0.023	0.072

These data confirm the fact that bismuth species are less soluble at higher temperatures than low, in moderately strong sulphuric acid. The other interesting point illustrated by this set of data is that the solublity reaches a peak and declines somewhere in the range 1.5 to 15M H_2SO_4. At 15M, the solubility of bismuth species has the more normal behaviour with respect to temperature, i.e. it is greater at higher temperature. This indicates that the bismuth species, both solid and soluble, are not the same in highly concentrated H_2SO_4 as in solutions of moderate H_2SO_4 strength.

During the anodic deposition, the overall reaction at the electrode produces protons:

$$Mn^{++} + 2H_2O \rightarrow MnO_2 + 4H^+ + 2e^-$$

The build-up of protons at the surface can be expected to cause a drop in the local pH, dependent on anodic current density. It is this drop in pH which is presumed to cause the chemical precipitation of bismuth species into the growing MnO_2 deposit.

According to the work of Allan [45] and more recently that of Skramovsky and Vondrasek [46], the species of bismuth sulphate that is precipitated from a sulphuric acid solution changes from a basic BiO^+ salt at low sulphuric acid concentration through to a BiH^{4+} species in almost pure sulphuric acid. In 0.5M H_2SO_4 the expected solubility equilibrium is:

$$2BiO^+ + HSO_4^- \rightleftarrows (BiO)_2SO_4 + H^+$$

It would not be expected that this equilibrium would be affected greatly by increases in sulphuric acid strength as the HSO_4^- and H^+ concentrations would both increase, keeping the equilibrium in balance. However, in this acid concentration range, the following protonation equilibrium is expected to exist:

$$BiO^+ + H^+ \rightleftarrows BiOH^{2+}$$

This would explain the increase in solubility of bismuth species with acid concentration at moderate sulphuric acid strengths, if we consider that the salt of the $BiOH^{2+}$ species is more soluble than the salt of the BiO^+ species. As indicated by Allan [45], at about 14N H_2SO_4 the dominant species changes again and we now have Bi^{3+} species or possibly BiH^{4+} species. If it is assumed that Bi^{3+} species are dominant, then we have some thermodynamic data to predict the K for the reaction:

	$2Bi^{3+}$ +	$3HSO_4^-$	K ⇄	$Bi_2(SO_4)_3$ +	$3H^+$	log K
ΔG_f° (kCal mole^{-1}) (Harrington [47])	20.27	-180.7		-525.8	0	14.8
ΔG_f° (kCal mole^{-1}) (Karapet'yants [48])	19.8	-180.7		-617.7	0	70.2

The ΔG_f° values given above for $Bi_2(SO_4)_3$ were estimates derived from data for equilibria of other reactions and indicate the problems that can arise when using estimated values. Also, these values apply to dilute solutions, not the concentrated acid solutions found in this work. At the high acid concentrations found in the system under study, virtually no free H_2O exists, and it might be regarded as a different solvent system. However, this calculation is included to illustrate that $Bi_2(SO_4)_3$ should be very insoluble. This being the case, it can be seen that in the region of 14N H_2SO_4 a very insoluble bismuth species might be expected to form. Of course, when the reaction to produce protons at the electrode is occurring, the sulphate concentration would not be affected but the influence of acid strength on the protonation reaction might be expected to be the important step in the formation of the insoluble bismuth species. It is hard to predict the exact influence on the local acid strength due to the protons produced at the electrode surface but it does not seem unreasonable that a strength of 14N in H^+ might be attained locally. Of course, the process of concentration of protons is opposed by their diffusion away from the boundary layer.

In summary, the generation of protons by the process of deposition of MnO_2 can cause an increase in the acid strength near the electrode which may cause the

protonation reaction to occur and subsequent precipitation of bismuth species, most probably as $Bi_2(SO_4)_3$ or $BiH(SO_4)_2$.

Solubility of manganese species is also an important factor in the study of the electrochemical behaviour of the MnO_2 deposits in 9M KOH and in operational aspects of the alkaline MnO_2 battery. Kozawa et al [49] have determined the solublility of Mn^{2+} and Mn^{3+} species by a polarographic technique over a range of KOH and NaOH concentrations. In 9M KOH, these were reported as 35 mg l^{-1} (6.4×10^{-4}M) and 240 mg l^{-1} (4.4×10^{-3}M), respectively.

Lott and Symons [50] have proposed that the Mn^{3+} would exist as $Mn(OH)_6^{3-}$ in concentrated potassium hydroxide solution. Work conducted in our own laboratory [35] indicates that soluble Mn^{3+} species are important when considering the overall reaction mechanism of the reduction of MnO_2, particularly when attempting to make and evaluate the performance of a practical rechargeable MnO_2 battery.

In another part of this work, the solubility of Bi^{3+} species in 9M KOH was determined. After allowing 9 days for equilibrium to be established in a saturated solution of Bi_2O_3 in 9M KOH, the concentration of Bi was measured in the supernatant by means of AAS and found to be 65 mg l^{-1} or 3×10^{-4}M. This value is in quite good agreement with the value of 5.02×10^{-4}M reported by Wroblowa [11]. As indicated with Mn species, this solubility is to be regarded as significant. However, since the bismuth species are generally not by any means in large enough quantities to contribute significantly to the charge capacity (typically 7 - 12 mole% Bi was used in the studies by Wroblowa [10] and in our laboratory [35]), the solubility of bismuth is

of interest more because it may give some clues about whether the action of the bismuth is related to solid-solid reactions, liquid-liquid reactions or solid-liquid reactions involving Mn species.

Knowledge of the solubility of the various Mn and Bi species leads to at least one conclusion: that the design of any practical MnO_2 electrode system should provide for the absolute minimum of liquid electrolyte so that soluble intermediates and products will be unable to migrate away from or out of the electrode matrix. The ramifications of the solubility of Mn species on interpretation of results of electrochemical experiments conducted with relatively large amounts of free electrolyte will be discussed further in Chapter 4.

3.3.2 Air Oxidation Experiment

Upon addition of the $MnSO_4$ to the KOH solution, a precipitate is formed, rendering the solution very turbid and slightly pink. The insoluble product is, in all likelihood, $Mn(OH)_2$. As the N_2 bubbling was continued, some dark residue formed at the surface. This was the product of reaction of the $Mn(OH)_2$ with traces of atmospheric oxygen reaching the solution to form MnO_2. When the bubbling was discontinued, the oxidation at the surface became more rapid and flakes of MnO_2 formed overnight. The precipitates in each of the solutions, with and without Bi, were initially white in colour but, after sitting overnight the precipitate in the vial with no bismuth species present had a layer on the top which was reddish-brown in colour. Although this material was not characterised, its physical appearance indicated that it

was probably Hausmannite, having the chemical formula Mn_3O_4. Yao et al [10] made the observation in their paper regarding the production of "chemically modified" MnO_2 that the precipitation of $Mn(OH)_2$ and subsequent oxidation with O_2 at room temperature, led to the formation of Hausmannite. They suppressed the formation of Hausmannite by carrying out the oxidation below room temperature. However, in the presence of Bi^{3+} or Pb^{2+}, it was found that the oxidation step could be carried out at room temperature *without* the formation of Hausmannite. The experiment performed here confirms that observation.

McBreen [30] and others [51] have concluded that Hausmannite is not electrochemically rechargeable. Its formation would therefore inhibit or prevent rechargeability of the MnO_2 electrode. It is clear that Bi species interfere with the formation of Hausmannite under these conditions. If we consider only the solids $Mn(OH)_2$, MnOOH, Mn_2O_3, MnO_2 and a soluble intermediate, designated as $Mn^{3+}_{(aq)}$, without knowing the exact species in solution, the Hausmannite could be formed via a number of chemical pathways, as follows:

i) By direct oxidation of $Mn(OH)_2$:

$$6Mn(OH)_2 + O_2 \rightarrow 2Mn_3O_4 + 6H_2O$$

ii) Alternatively, $Mn(OH)_2$ could undergo an oxidation reaction to an Mn^{3+} species followed by disproportionation to produce Hausmannite and MnO_2:

$$4Mn(OH)_2 + O_2 \rightarrow 2Mn_2O_3 + 4H_2O$$

$$2Mn_2O_3 \rightarrow MnO_2 + Mn_3O_4$$

or

$$4Mn(OH)_2 + O_2 \rightarrow 4MnOOH + 2H_2O$$

$$4MnOOH \rightarrow MnO_2 + Mn_3O_4 + 2H_2O$$

and alternatively

$$4Mn(OH)_2 + O_2 + 2H_2O \rightarrow 4Mn^{3+}_{(aq)} + 12OH^-$$

$$4Mn^{3+}_{(aq)} + 12OH^- \rightarrow MnO_2 + Mn_3O_4 + 6H_2O$$

iii) Lastly, oxidation to Mn_2O_3, MnOOH, $Mn^{3+}_{(aq)}$ or MnO_2 might occur, followed by reaction of the oxidised product with $Mn(OH)_2$ to form Hausmannite, as follows:

$$4Mn(OH)_2 + O_2 \rightarrow 2Mn_2O_3 + 4H_2O$$

$$Mn_2O_3 + Mn(OH)_2 \rightarrow Mn_3O_4 + H_2O$$

or

$$4Mn(OH)_2 + O_2 \rightarrow 4MnOOH + 2H_2O$$

$$2MnOOH + Mn(OH)_2 \rightarrow Mn_3O_4 + 2H_2O$$

or

$$4Mn(OH)_2 + O_2 + 2H_2O \rightarrow 4Mn^{3+}_{(aq)} + 12OH^-$$

$$2Mn^{3+}_{(aq)} + Mn(OH)_2 + 6OH^- \rightarrow Mn_3O_4 + 4H_2O$$

or

$$2Mn(OH)_2 + O_2 \rightarrow 2MnO_2 + 2H_2O$$

$$MnO_2 + 2Mn(OH)_2 \rightarrow Mn_3O_4 + 2H_2O$$

It is hard to imagine how the presence of Bi species could influence the

reaction in process i) above as the reaction with O_2 would appear to be a simple process and the presence of Bi species should not impede the oxidation to MnO_2 as evidenced by the formation of the latter material already early in the experiment.

For the reactions in scheme ii), again it is hard to see how Bi species could influence the first oxidation step. Since the second steps are reactions of the type where one product forms two, even though in the solid state this may only involve the rearrangement of a few bonds, the most reasonable role of Bi species in this case would be the stabilisation of the intermediate species. This would allow the product to eventually be further oxidised in a subsequent reaction rather than having a chance to disproportionate.

Much the same argument can be proposed for the reactions of scheme iii). No interference would be expected in the first step while interference with the second step implies that, for the reactions involving the Mn^{3+} intermediate, the Bi might be stabilising that intermediate. In the case of solid-solid reactions, this would mean that the Bi species would have to exist in the solid in a rather large proportion to influence the stability of intermediates. In previous work [13], it was shown that the presence of Bi could influence rechargeability even when very small, virtually "catalytic", amounts were present, down to < 2 mole%. This tends to dismiss stabilisation of solid intermediates as the basis for its effect(s).

Even though the schemes outlined here apply to the oxidation of $Mn(OH)_2$ by oxygen, the arguments could be extended to electrochemical oxidation. It has been shown in other complimentary work in our laboratory [35] that soluble Mn^{3+} species

play a very important role in the rechargeability of "chemically modified" MnO_2. It is therefore suggested that one effect of added Bi species to the MnO_2 electrode is to discourage the chemical conversion to Hausmannite while not interfering with, or perhaps encouraging or catalysing, electrochemical oxidation or reduction. The formation of a soluble complex between Mn^{3+} and Bi species is one possibility, although the existence of such a species has not been proven.

This effect of Bi species has been indirectly observed in the course of performing cyclic voltammetry experiments during the present work. Even when O_2 is excluded from the electrochemical cell by bubbling with N_2, during long experiments some O_2 may eventually diffuse into the system. In such experiments, the electrolyte becomes quite coloured with what is now presumed to be soluble Mn^{3+} which probably exists as $Mn(OH)_6^{3-}$. When oxidation or disproportionation of this material can occur, MnO_2 is deposited, for example on the cell walls or at the N_2 outlet holes. It has been observed that these deposits occur in different areas of the cell depending on whether Bi is present or not. In a specific cyclic voltammetry experiment in 9M KOH with Bi present, the deposits arose in the holes leading to the counter-electrode compartment while when Bi was absent the deposition was between the layers of the separator material. This implies that the Mn^{3+} species is more stable with bismuth present, as it travels farther in the cell before being oxidised. This is a subtle difference, of course, but it is probably significant and it does illustrate that there is some different behaviour of the soluble Mn species with respect to their chemical reactions, with and without Bi species being present.

3.4 CONCLUSIONS

The work reported in this chapter leads to the following conclusions:

i) It is possible to present a feasible mechanism for the inclusion of bismuth species in electrodeposited MnO_2. The bismuth is probably precipitated as either $Bi_2(SO_4)_3$ or $BiH(SO_4)_2$ by the local increase in acidity at the electrode, produced by the MnO_2 electrodeposition reaction.

ii) Bismuth species in solution impede the formation of Mn_3O_4 from the oxidation of $Mn(OH)_2$ in strong alkali. The possibility was suggested that one mode of enhancement of rechargeability of MnO_2 by bismuth might be the formation of a soluble complex between Mn^{3+} and Bi^{3+} species in solution.

CHAPTER 4 ELECTROCHEMICAL EXPERIMENTS

4.1 INTRODUCTION

For the most part, this chapter describes those experiments which employed conventional electrochemical techniques to gain information about the deposits that were generated using the method described in Chapter 2. Several experiments were also conducted on surfaces other than those of such types of deposits. The preparation of such surfaces will be described in this chapter.

4.1.1 Choice of Methods

The main body of the electrochemical experiments involved cyclic voltammetry, a technique which is also known as linear sweep voltammetry especially when used in a non-repetitive, single-sweep mode. In this type of experiment, the potential of the working electrode vs. the reference electrode is varied linearly with time between preset voltage limits using a potentiostat (operating as a "potentiodyne") as the controlling instrument. The voltage is swept back and forth with anodic processes generally occurring as the voltage increases positively and cathodic processes occurring as the voltage decreases. When the current is plotted against the voltage, a closed loop is formed giving a current-response representation of the behaviour of the electrode over that voltage range.

This technique can yield much useful information. It is possible to determine which cathodic and anodic processes are conjugate to one another, or in other words

which one is the opposite of the other. Information about the reversibility of processes may also be obtained from the voltage offset between the anodic peak and the corresponding cathodic peak of such conjugate processes. By varying the sweep rate, information may be gained about the kinetics of a particular process, i.e., is the process diffusion controlled? Perhaps most importantly for battery research, the retention of capacity with continued cycling may be easily assessed, giving information about the rechargeability of that electrode/electrolyte system at a given discharge and recharge rate. Finally, the charges passed, corresponding to the various anodic or cathodic peaks can be quite accurately derived by integration of the i(V) or V(t) profiles, and compared with one another, after allowance has been made for the so-called double-layer capacitance (C_{dl}) charging effect which is always a background current, $i_{dl} = C_{dl}(dV/dt)$. This procedure for charge evaluation is particularly useful for assessment of battery materials, e.g. here MnO_2 or CM MnO_2.

4.2 EXPERIMENTAL

4.2.1 Materials and Equipment

During the course of this work, three different electrochemical cells were constructed and used. All of these cells were of the standard three-compartment layout. Most of the experiments were carried out in 9M KOH and the reader should assume that this is the electrolyte, unless otherwise noted. The first of these, the "large" cell, is depicted in Figure 4.1. It is constructed of PTFE (Teflon). The volume of electrolyte in the working compartment was about 70 ml with the reference and counter-electrode

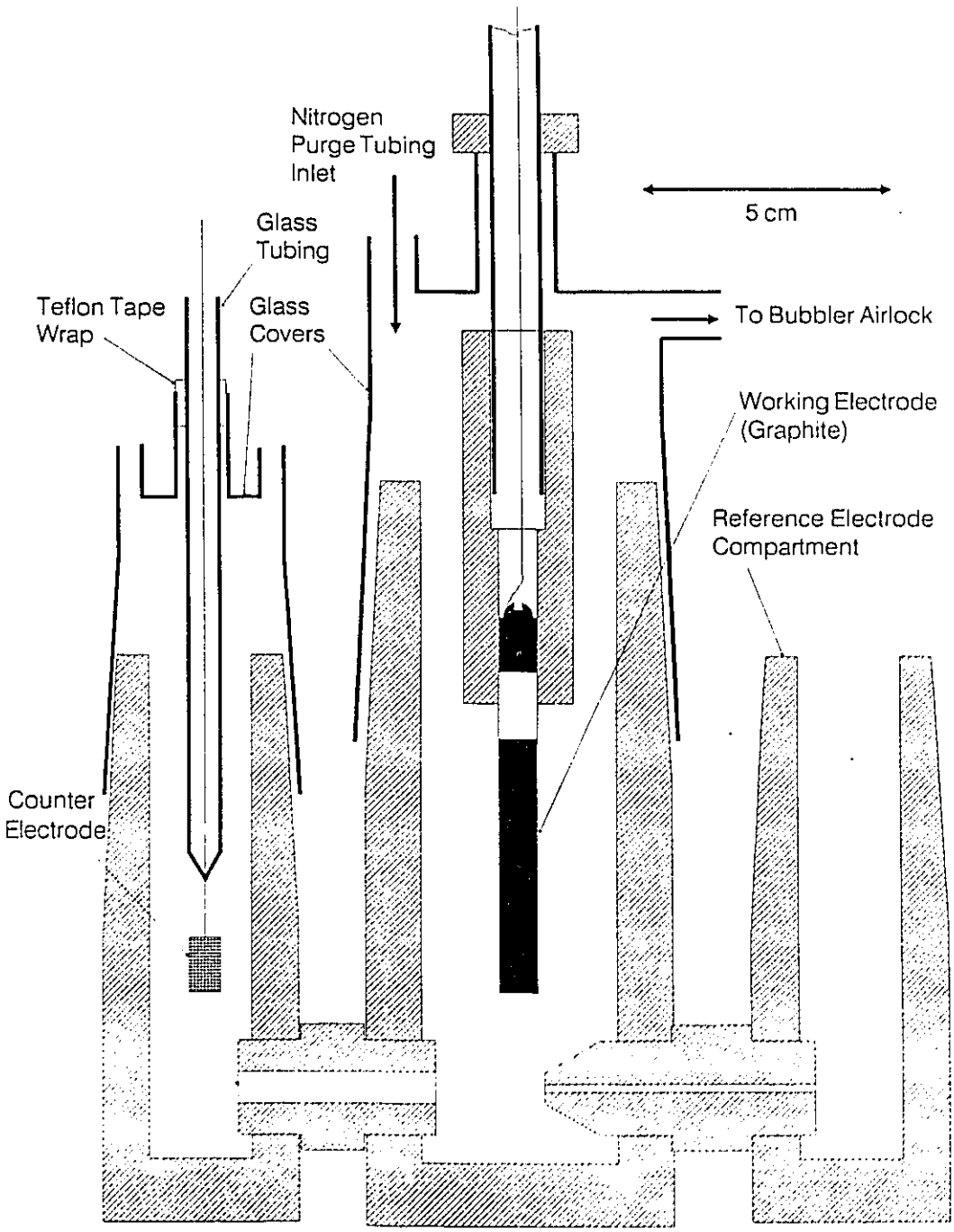

Figure 4.1: The "Large" cell used for electrochemical experiments.

compartments containing each about 15 ml. The working and counter-electrode compartments were joined by a large tubular passage while the reference was joined by a small diameter passage which acts as a Luggin capillary. The counter electrode was a platinum mesh about 6 cm^2 in area. The capillary end of the reference electrode, shown in Figure 4.2, was dipped into the reference electrode compartment during experiments.

The reference electrode for all experiments was Hg/HgO in 9M KOH and was constructed of glass. A pool of mercury sat in the rounded bulb portion of the bottom of

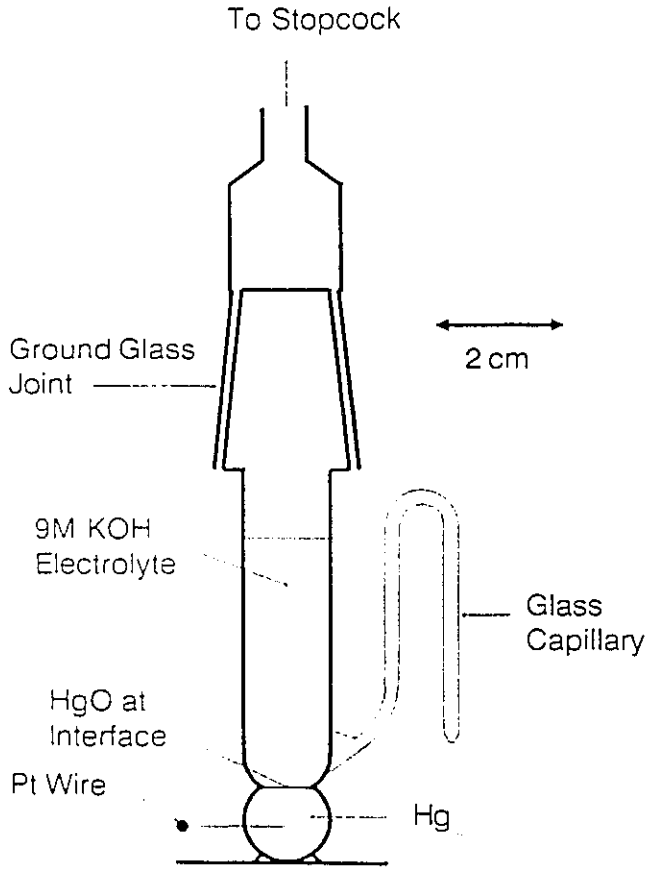

Figure 4.2: The Hg/HgO reference electrode with 9M KOH electrolyte.

this apparatus. The electrical connection to the Hg electrode was made through a Pt wire that protruded through the bulb. After filling the electrode vessel with 9M KOH, a small amount of HgO was dropped into the solution and allowed to settle at the interface of the mercury and the electrolyte. A valve was included on the top of the assembly to facilitate filling the capillary with electrolyte.

The second cell used for electrochemical experiments is shown in cross sectional view in Figure 4.3 and will be referred to here as the "rotating disk" cell as it was used

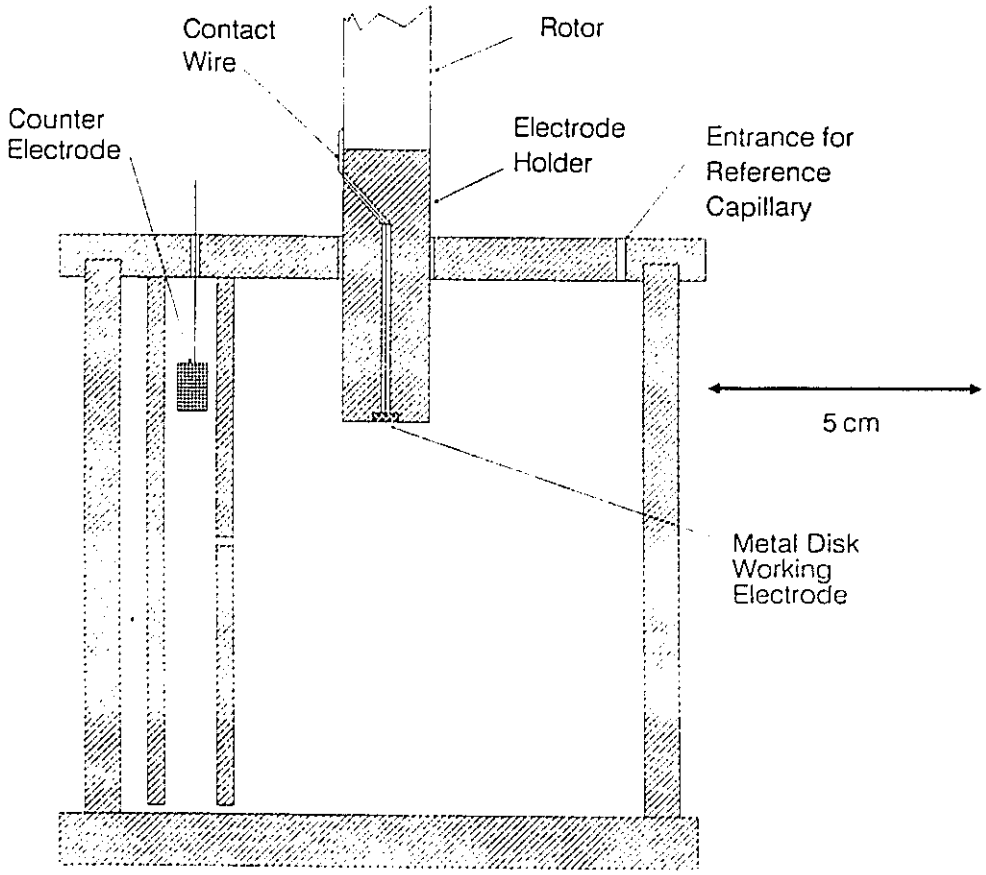

Figure 4.3: The "Rotating Disk" cell used for electrochemical experiments.

exclusively for rotating-disk cyclic voltammetry experiments. This cell was constructed of acrylic plastic. The main compartment was tubular in shape and was welded to the base plate by using CH_2Cl_2 to soften the material, then pressing the pieces together. This compartment held about 700 ml of electrolyte with the counter electrode compartment consisting of a tube welded to the lid and projecting down to near the bottom of the main compartment. A drill hole was also provided about half way up the counter electrode tube to provide connection to the main compartment. The same platinum mesh counter-electrode as for the "large" cell was used in this cell. The reference electrode capillary dipped down into the main compartment through a small hole in the lid. A facility for purging the main compartment with a stream of N_2 was provided by a small hole in the lid of the cell (not shown).

Figure 4.3 also shows the rotating-disk electrode as used for electrode rotation experiments. The sheath material was acrylic plastic and metal disks of 6.4 mm in diameter were recessed into the end. For the manganese electrode, the metal (Alfa-Ventron, Danvers,MA) was cleaned in HNO_3 and rinsed, then shaped into a round disk. A copper wire for electrical connection was soldered to the back face of the disk and led through the center hole in the holder to exit from the diagonal passage to be connected to the rotating shaft. The disk was epoxyed in place using Epofix HQ (Struers, Copenhagen,Denmark) and, after curing, the face of the electrode was finished with successively finer silicon carbide papers up to 2400 grit.

The bismuth rotating electrode was prepared from a bismuth rod (Johnson Matthey, Ward Hill,MA) in the same manner except that the back of the rod was drilled

and tapped, and the contact wire was held in place with a brass screw.

The third electrochemical cell, dubbed the "rod end" cell, shown in cross section in Figure 4.4, was designed to do experiments on the flat end of a test electrode. The upper and lower acrylic blocks are held together by four screws (not shown) at the corners of the upper block. The volume of the working-electrode compartment of this cell was of the order of only one or two drops. The working electrode was lowered into the compartment until it contacted the separator material. The only electrolyte that then

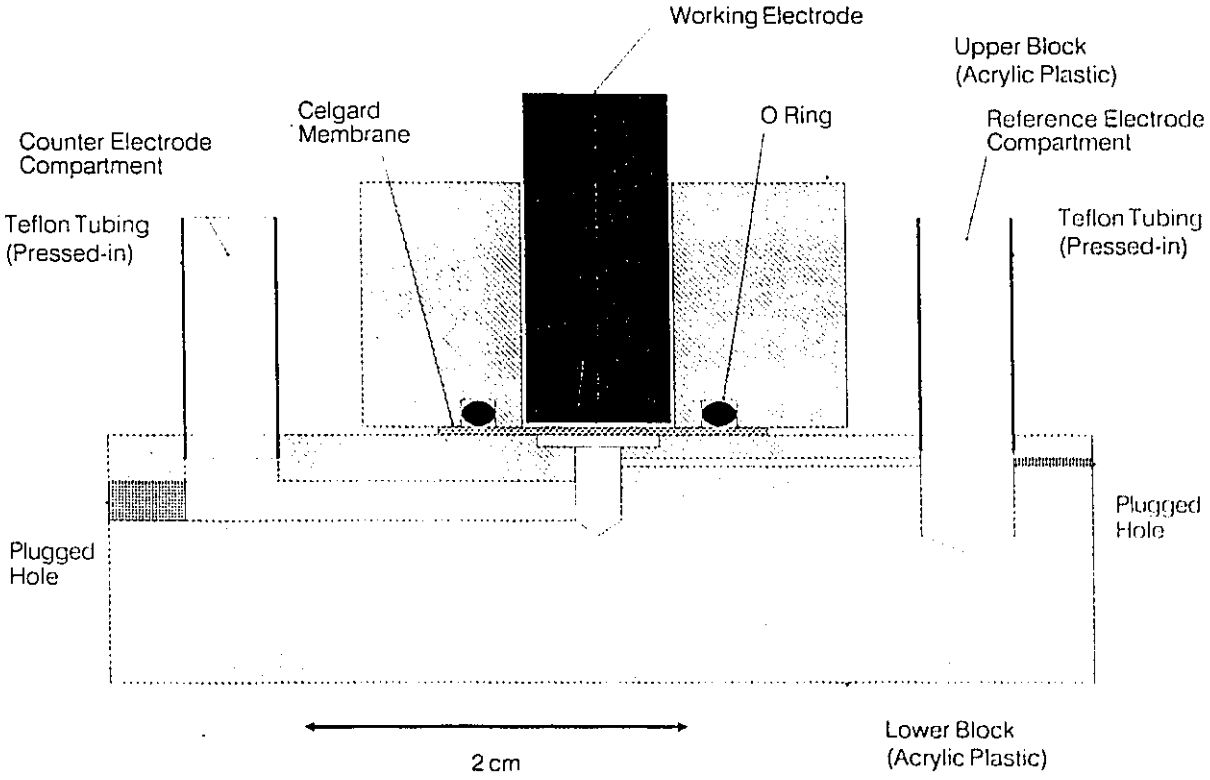

Figure 4.4: The "Rod-End" cell used for electrochemical experiments.

remained in the compartment was that which was not squeezed out during this procedure. The capillary from the reference electrode (shown in Figure 4.2) was dipped into the "reference electrode compartment" and a nickel mesh was usually used as the counter electrode, dipped into the "counter electrode compartment". No allowance was made for nitrogen purging in this cell.

When N_2 gas was used for purging the electrochemical cells, UHP grade was utilised after further purification by passage through a series of traps containing magnesium perchlorate, 4A molecular sieves and lastly copper turnings heated to about 350 °C to remove any residual traces of O_2.

The electrochemical instrumentation used was as follows. A Hokuto Denko HA-501 Potentiostsat/Galvanostat (Tokyo,Japan) was employed in conjunction with an HB-104 Function Generator from the same manufacturer. Data were collected digitally on a Nicolet 2090 Digital Oscilloscope (Madison,WI) and transferred to an HP 9000 series 216 computer (Hewlett Packard Co.,Fort Collins, CO) via an IEEE interface. The data were processed and plotted on an HP 7470A plotter using Basic software developed in this laboratory.

4.2.2 Experimental Procedure

All experiments were conducted in 9M aqueous KOH. When desired, the cell was purged with N_2 for at least 1 hour before beginning the experiment. Most cyclic voltammetry experiments were conducted at a sweep rate of 10 mV s^{-1} and the reader can assume that this was the sweep rate used in all experiments unless otherwise stated. Since

the deposits were expected to be fully anodically charged, sweeps were usually started in the "cathodic" direction at the anodic potential limit.

4.3 RESULTS AND DISCUSSION

4.3.1 Cyclic Voltammetry of Bismuth Deposited on a Graphite Rod

In order to provide some orientation concerning how Bi itself may behave under conditions of cyclic voltammetry in alkaline solution, a series of preliminary experiments were conducted as described below.

Bismuth was electrodeposited from a bath containing 0.02M Bi as nitrate in a 1M HNO_3 solution. The cathodic deposition was performed for 10 minutes galvanostatically at 10 mA. The total charge used to form the deposit was therefore 6 coulombs. The apparent surface area of the working electrode was calculated as follows:

diameter of rod = d = 0.615 cm

exposed length of rod = h = 5 cm

area of the end of the rod = $\pi(d/2)^2$ = 0.30 cm^2

area of the side of the rod = πdh = 9.7 cm^2;

$\therefore$ total area = 10 cm^2.

The amount of charge applied to the electrode was therefore 0.6 C cm^{-2}. A cyclic voltammogram for this deposit at a sweep rate of 100 mV s^{-1} is shown in Figure 4.5. This voltammetry experiment was conducted in the "large" cell.

The system appears to be quite rechargeable with two anodic peaks having a total charge of 2.6 mC cm^{-2} and two cathodic peaks corresponding to a total reduction charge

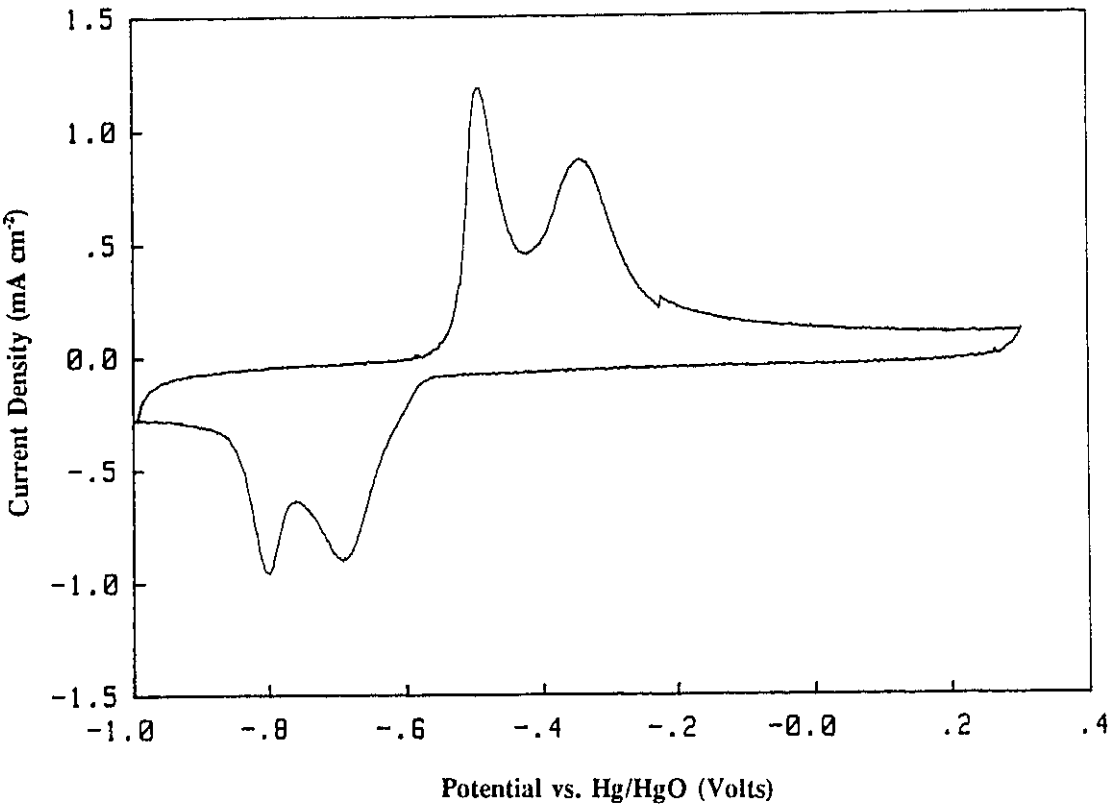

Figure 4.5: Cyclic voltammetry of bismuth deposited on a graphite rod. Sweep rate 100 mV s^{-1}.

of 2.8 mC cm^{-2}. It should be pointed out that the term rechargeable refers to the fact that the anodic and cathodic charges are equal. The system cannot be said to be reversible in the kinetic sense unless the anodic and cathodic peaks arise over the same potential, as they do in some supercapacitor oxides, e.g. RuO_2 or IrO_2. Note that the charge passed during this cycling experiment is much less than that used to apply the deposit. Therefore, either the efficiency of cathodic deposition of bismuth is relatively poor or the bismuth is somehow lost and cannot be cycled properly.

The peaks on the voltammogram shown in Figure 4.5 are centered around -0.55V. According to the Pourbaix diagram for bismuth (Chapter 2, Figure 2.7), the transition which occurs at this potential is between Bi^0 and Bi^{3+} in the form of either solid Bi_2O_3

or bismuthate ion, BiO_2^-, in solution.

The charge q, required to form a monolayer of bismuth per cm^2 may be calculated as $zF / N_A d^2$ where q is the charge per cm^2, z is the number of electrons per atom involved in the process (3 in this case), F Faraday's constant, N_A Avogadro's number and d is the atomic diameter. The value of d used for this calculation may be obtained from reference texts or may be calculated from the bulk density. The volume v occupied by each atom will be given by: $FW / \rho N_A$ where FW is the formula weight and ρ the density. The effective dimension d is simply the cube root of this quantity. In order for this to be the real diameter, cubic packing of the atoms would have to be assumed. The literature value for the atomic diameter of bismuth in the metallic form is 0.309 nm. This yields a charge of 0.50 mC cm^{-2} for formation of a monolayer. Using the bulk density method, the diameter is found to be 0.328 nm which gives a charge of 0.45 mC cm^{-2}. The benefit of using the latter calculation procedure arises when dealing with molecules or molecular structures rather than atoms. For example, the charge for a monolayer of MnO_2 can be quickly calculated without any reference being required to the bond lengths or molecular structure of the material. For the sake of consistency and simplicity, the values calculated from bulk density will be used in this thesis.

The roughness factor, or ratio of actual to apparent surface area for the graphite rod used in this experiment has been measured by the BET method. The factor was found to be 950. Using this roughness factor, the charge required to form a monolayer of bismuth would be 430 mC cm^{-2}. This charge is some 150 times the charge associated with the cyclic voltammetry experiment. While the BET surface area is a good indicator

of the effective surface area, not all of the surface may be electrochemically accessible [52,53]. Notwithstanding this effect, it is apparent that what is seen in this experiment is a reaction involving much less than a monolayer.

Bismuth species may also be deposited on the graphite rod electrodes simply by being precipitated in place on the surface and in the pores The amount of bismuth thus deposited is then related to the bismuth concentration in the bath. It is very hard to control the conditions for this kind of precipitation but it can be seen from the data in Table 4.1 that such a correlation exists. All electrodes were allowed to stand in water overnight after the soaking experiment and before cyclic voltammetry or AAS analysis was carried out.

Table 4.1 Deposition of Bismuth Species by Soaking

Bath	Soaking Conditions	CV Capacity ($mC\ cm^{-2}$)	Equivalent Bi ($\mu moles\ cm^{-2}$)	Bi by AAS ($\mu moles\ cm^{-2}$)
0.005M Bi 0.5M Mn 0.5M H_2SO_4	85°,50 min	-	-	0.009
0.01M Bi 1M HNO_3	90°,40 min	8	0.028	
0.1M Bi 1M HNO_3	90°,4 min	40	0.14	
0.1M Bi 1M HNO_3	RT,40 min	50	0.17	
0.1M Bi 1M HNO_3	90°,40 min	160	0.55	

It is not entirely clear whether the precipitation occurs during the water soak or when the electrode is placed in the KOH. Considering the mode of deposition, it is

remarkable that the precipitate has electrical contact with the surface and hence good electrochemical properties.

It was shown in Chapter 2 that the amount of bismuth species deposited by soaking in H_2SO_4 baths was not large enough to account for the resultant quantity of bismuth actually in the deposits. The total amount of included bismuth increases with deposition time for deposits from H_2SO_4 but the same cannot be said for deposits from other acid baths. For this reason, the mechanism for inclusion of bismuth species in deposits from H_2SO_4 is considered to be unique, due to the limited solubility of bismuth in this medium (see Chapter 3).

4.3.2 Rechargeability of Bismuth-Containing Deposits

As detailed in Chapter 2, deposition of MnO_2 from acid baths containing bismuth leads to inclusion of the bismuth in the deposits. It is found that the bismuth enhances the electrochemical rechargeability of the deposits when subjected to cyclic voltammetry, a technique which simulates the repetitive discharge and recharge of an active battery material, but under potential rather than current control.

Figure 4.6 shows the early cycling behaviour of MnO_2 deposits from 2M H_2SO_4 with 0.5M $MnSO_4$. For this experiment, all cycling was done at a sweep rate of 10 mV s^{-1}. The upper voltammogram is for a deposit with *no* bismuth. The charge capacity, both anodic and cathodic, is seen to decrease continuously as the electrode is cycled. The lower voltammogram is for a deposit made in the same bath but saturated *with* Bi^{3+}. The exact concentration of bismuth in the bath is not known in this case. The

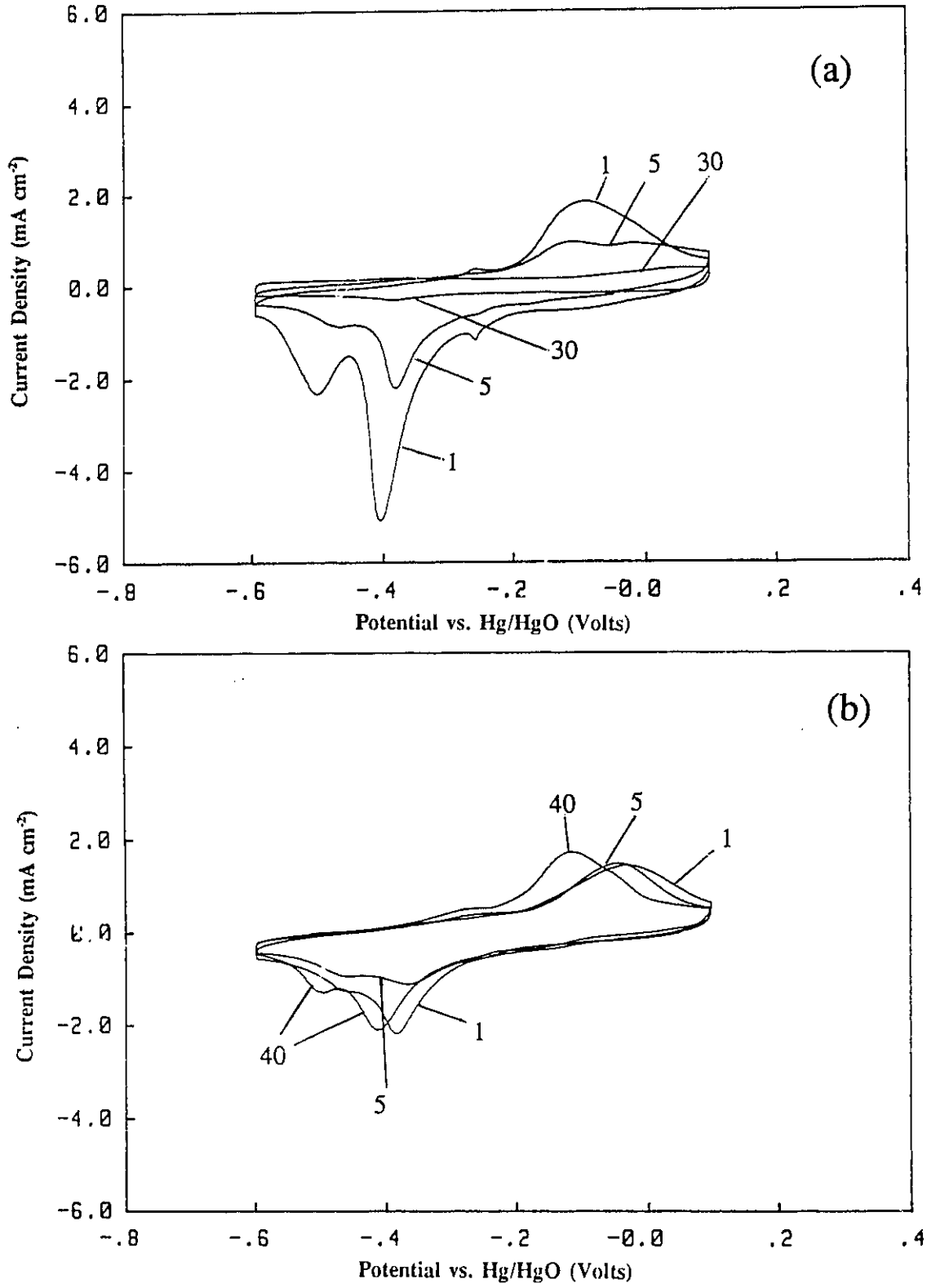

Figure 4.6: The early cycling behaviour of deposits of MnO_2: a) no bismuth present in the deposit , the 1st, 5th and 30th cycles are shown; b) with bismuth species in the deposit, the 1st, 5th and 40th cycles are shown.

initial concentration was 0.02M but precipitation occurred as the bath was heated to 85 °C. Based on the solubilities reported in Chapter 3, the concentration of bismuth should be between 0.01 and 0.02 M. The charge capacity for this deposit decreases for the first few cycles then increases back to about the original level and stays there for many cycles. Figure 4.7 shows the substantial longevity of the rechargeability of the deposit with bismuth present in the material. The 40th and 640th cycles of this deposit are shown.

The anodic and cathodic capacities of the two deposits with respect to cycle number are summarised in Table 4.2. Note that, with bismuth, the deposit has retained virtually *all* of its capacity during the 640 cycles whereas, without bismuth, the anodic capacity becomes reduced to 30% after only 30 cycles.

Table 4.2 **Cycling behaviour with and without bismuth**

Cycle #	Charge - With Bismuth (mC cm^{-2})		Charge - No Bismuth (mC cm^{-2})	
	Anodic	Cathodic	Anodic	Cathodic
1	37	48	39	88
5	35	37	30	34
30			12	14
40	41	45		
640	40	42		

The charge for formation of a monolayer of MnO_2 is calculated according to the formulae given in section 4.3.1 as 0.334 mC cm^{-2} given a density of 4.85 g cm^{-3} [54] and a two-electron process. Using the BET roughness factor of 950, this indicates that a

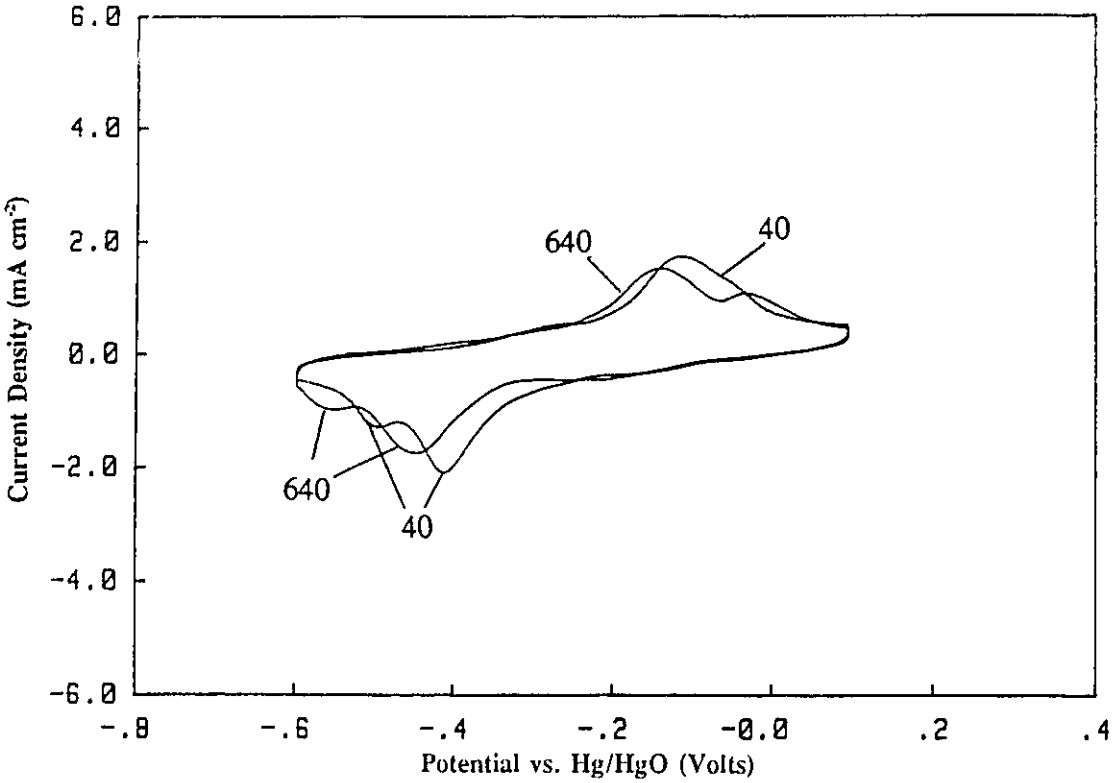

Figure 4.7: Extended cycling of an MnO_2 deposit with bismuth species included. The 40th and 640th cycles are shown.

charge of 317 mC cm^{-2} would be required. As stated above, all of this surface area may not be electrochemically accessible, but it does appear that the anodic and cathodic charges are related to the reaction of less than a monolayer.

The cathodic charge is always larger than the anodic charge in the experiments for which data are given in Table 4.2. This is therefore a measure of the non-rechargeability of this system. This is particularly marked for the first cycle of the deposit with no bismuth: the cathodic charge is more than double that of the anodic re-charge. Some of the large imbalance during the first cycle might be due to reduction of O_2 trapped or adsorbed in the deposit. The bulk of the charge imbalance could be due to loss of material during the cathodic portion of the cycle through dissolution into the bulk electrolyte. This material would then be unavailable for re-oxidation in the subsequent anodic sweep. After a few cycles, this imbalance is reduced but still persists

and the ratio of cathodic to anodic charge is always higher for the deposit with no bismuth.

Both deposits were made by passing 150 mC cm^{-2}. It was seen in Chapter 2 that the efficiency of deposition under these conditions is of the order of 90%. This would mean that the capacity during cycling would theoretically be 135 mC cm^{-2}. Without bismuth, the cathodic capacity on the first cycle is 65% of this figure and becomes reduced rapidly to 25% after only 5 cycles. For the deposit with bismuth, the cathodic capacity stays within the range 30 to 35% of the theoretical 2 electron charge for the full 640 cycles of the test.

It is clear that not all of the deposit is available for undergoing electrochemical processes under these conditions. In fact, after cycling any of these deposits for an extended period, the electrolyte becomes coloured and solid particles are found to be floating in the electrochemical cell. This behaviour tends to support the existence of a soluble intermediate being formed in the charge - discharge %wgime which can diffuse away from the electrode. Indeed, other workers [16] have postulated a soluble intermediate and in another study in this laboratory [35] the production of this colour in the solution has been directly related to the formation of soluble Mn^{3+} species. Ruetschi [24] has observed the transition through a soluble species under a microscope, using ultrathin MnO_2 electrodes. The formation of the soluble intermediate would also undermine the deposit on the electrode and cause pieces to simply fall off during cycling [30].

It seems likely that only that part of the deposit which is resident in the pores of

the graphite material can avoid this diffusion process and be available for further cycling. Wroblowa and coworkers [12], and workers in our own laboratory [35], have had the greatest success in achieving good cycling behaviour when the "chemically modified" material used in those studies is diluted with a large ratio of graphite and/or the electrode material is cycled in a "starved electrolyte" cell, i.e. containing the absolute minimum of free electrolyte. This evidence suggests that enhancement of rechargeability may be attained by keeping soluble manganese intermediates in contact with the graphite long enough for the required further reactions to occur or by reducing electrolyte volume so that the intermediates saturate the electrolyte and/or are adsorbed on the solid particles and cannot further diffuse away from the electrode.

4.3.3 Cyclic Voltammetry of MnO_2 Deposited from Perchlorate and Nitrate Baths

It was mentioned earlier that the majority of MnO_2 deposits were made from sulphuric acid baths. There were, however, several attempts to make deposits from other baths.

Figure 4.8 shows the voltammogram of a deposit made from a bath of 0.5M $Mn(ClO_4)_2$ in 1M $HClO_4$. The deposition was carried out for 5 minutes at 20 mA on a 10 cm^2 electrode. The deposit was not visible, although the voltammogram showed a cathodic capacity of 0.137 C cm^{-2} on the 3rd cycle. This is about 23% of the capacity corresponding to the quantity that was deposited. As was seen for other MnO_2 deposits without bismuth, the capacity becomes reduced with cycling. At the 44th cycle, the cathodic capacity becomes reduced to 0.032 C cm^{-2}, or less than 25% of the capacity at

the 3rd cycle.

The voltammograms shown in Figure 4.9 were also generated by study of a deposit made in perchloric acid medium. In this case the deposition solution contained 0.5M Mn, 0.1M Bi and 1M $HClO_4$. The deposition was done by means of a repetitive square-wave current pattern consisting of 0.1 sec at +100 mA and 0.1 sec at -10 mA. The deposition time was 10 min. Therefore, the total anodic charge for this scheme is 27 C or 2.7 C cm^{-2} for the 10 cm^2 electrode. The current pattern was intended to provide for reduction of Bi into the deposit during the cathodic portion of the cycle and deposition of MnO_2 during the anodic current portion. It was, however, found later that it was not neccessary to cycle in this manner to have some Bi included in the deposit.

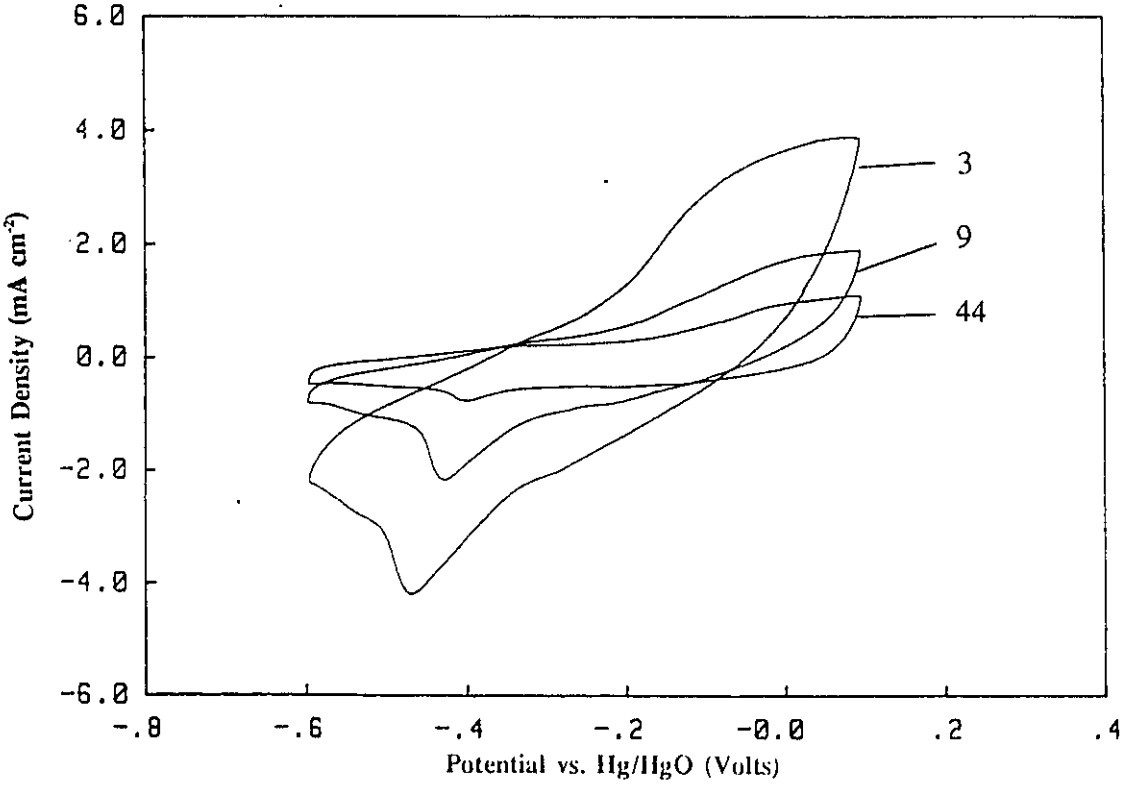

Figure 4.8: The early cycling behaviour of an MnO_2 deposit made from a perchloric acid bath. The 3rd, 9th and 44th cycles are shown.

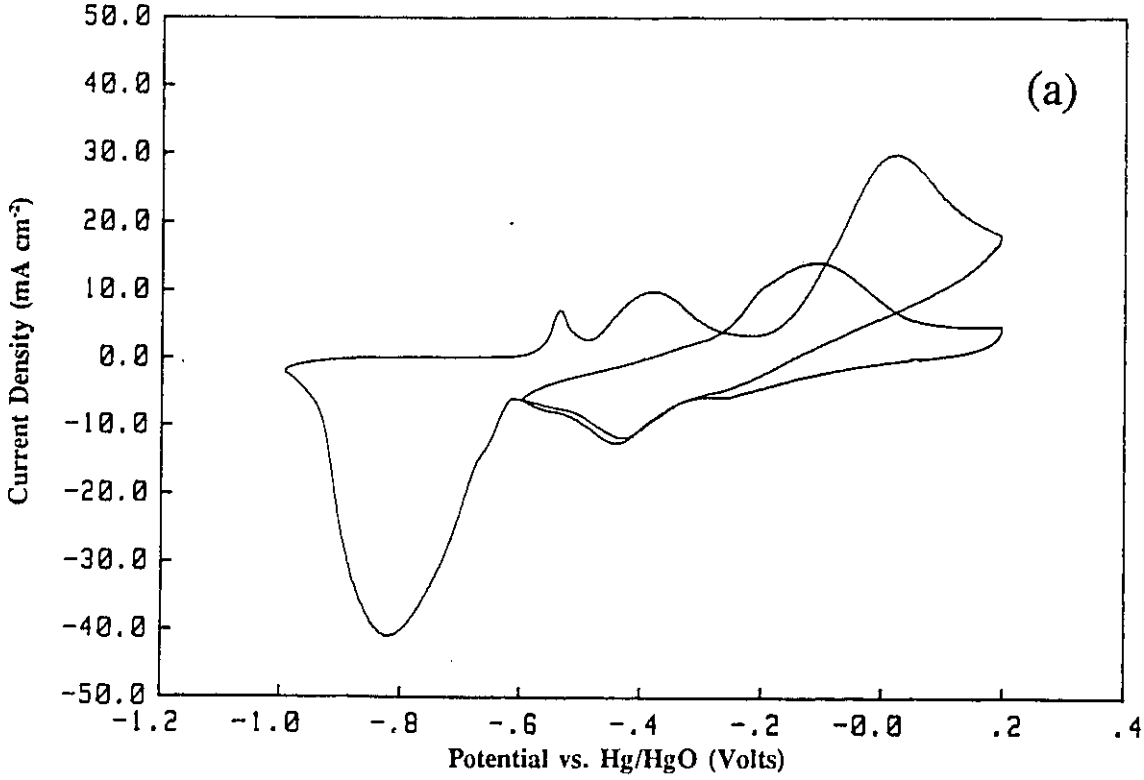

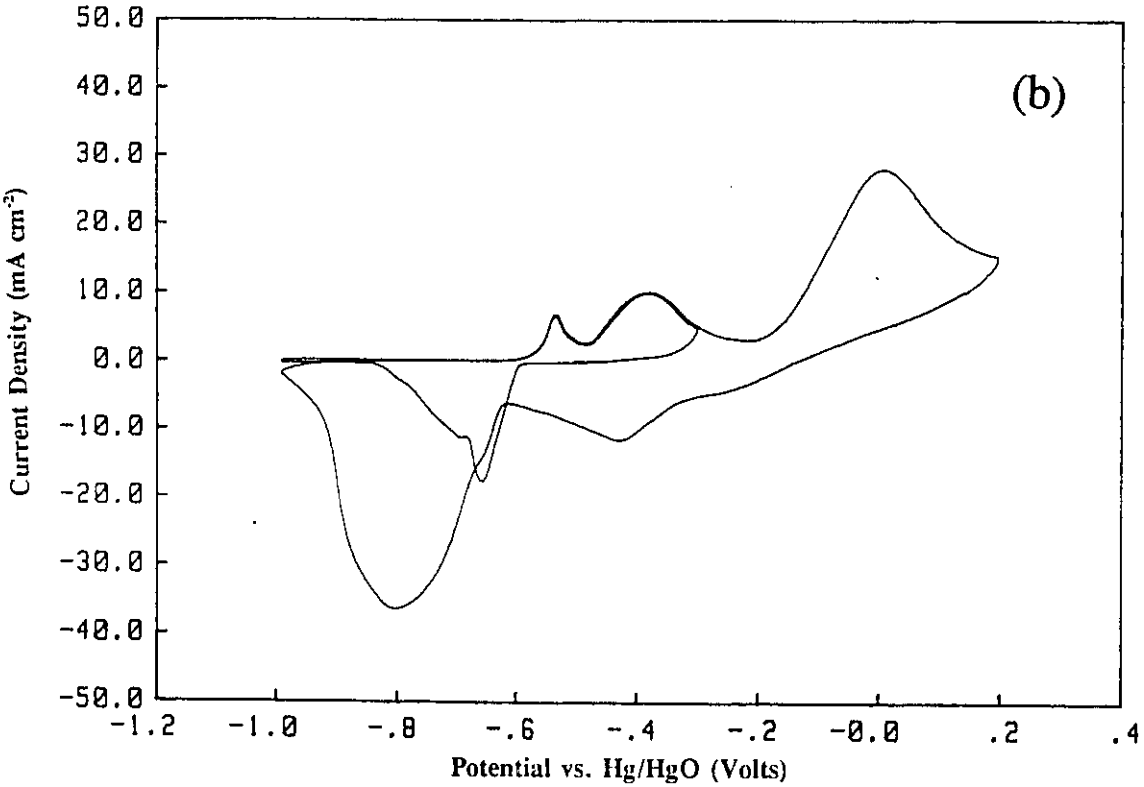

Figure 4.9: Cycling of deposits of MnO_2 with bismuth species: a) a comparison of a cathodic limit of -0.6V with -1.0V; b) a comparison of an anodic limit of -0.3V with +0.2V.

From inspection of the voltammograms in Figure 4.9 a number of observations can be made as follows. When the sweep is limited to the range -0.6V to +0.2V, which is similar to the range of the voltammograms reported so far, the "normal" manganese pattern is seen. The capacity is quite poor, however, with a total cathodic charge of only 0.43 C cm^{-2} (16% of the deposited capacity). When the cathodic sweep is extended to -1V, a large feature appears at about -0.8V. Two anodic features appear at about -0.6 and -0.4V which can be attributed to the oxidation of bismuth in the deposit. However, a new anodic feature is now seen to dominate the upper end of the voltammogram and it is conjugate to the new large cathodic feature. Interestingly, the normal anodic peak is diminished or shifted to a higher potential. The lower voltammogram on the page shows what happens when the anodic sweep limit is set at -0.3V. Under these conditions, only the bismuth appears to undergo redox cycling. A full discussion of the peak assignments is reserved for presentation in a later section (4.3.9).

When the total charge is measured for the full sweep range, the cathodic charge adds up to about 1.2 C cm^{-2} corresponding to a 2-electron efficiency of 44%. This number is high in comparison with the recoveries stated above (Section 4.3.2) but the capacity is of little practical use for a battery system. The bulk of the discharge occurring at -0.8V is only 0.6V above the potential for zinc, the material which is normally used for the anode in the practical battery system. Also, there is an irreversibility corresponding to about 1 volt between the reduction peak and the re-oxidation peak! This huge irreversibility would mean extremely large energy losses in the recharging of such a system.

Before moving on, it is worth pointing out that the deposits made in perchloric acid did not appear smooth and adherent. It is therefore doubtful that such a solution could be useful for the bulk production of electrolytic MnO_2. Deposits containing bismuth would also be hard to control since the mode of inclusion is assumed to be precipitation of Bi which is soaked into the pores of the substrate material.

Some deposits used for cyclic voltammetry experiments were also produced from nitric acid baths. As shown above (Section 4.3.1), the amount of bismuth that becomes included in these deposits depends largely on the concentration in the deposition solution, as may be expected. Figure 4.10 shows a cyclic voltammogram for a deposit from

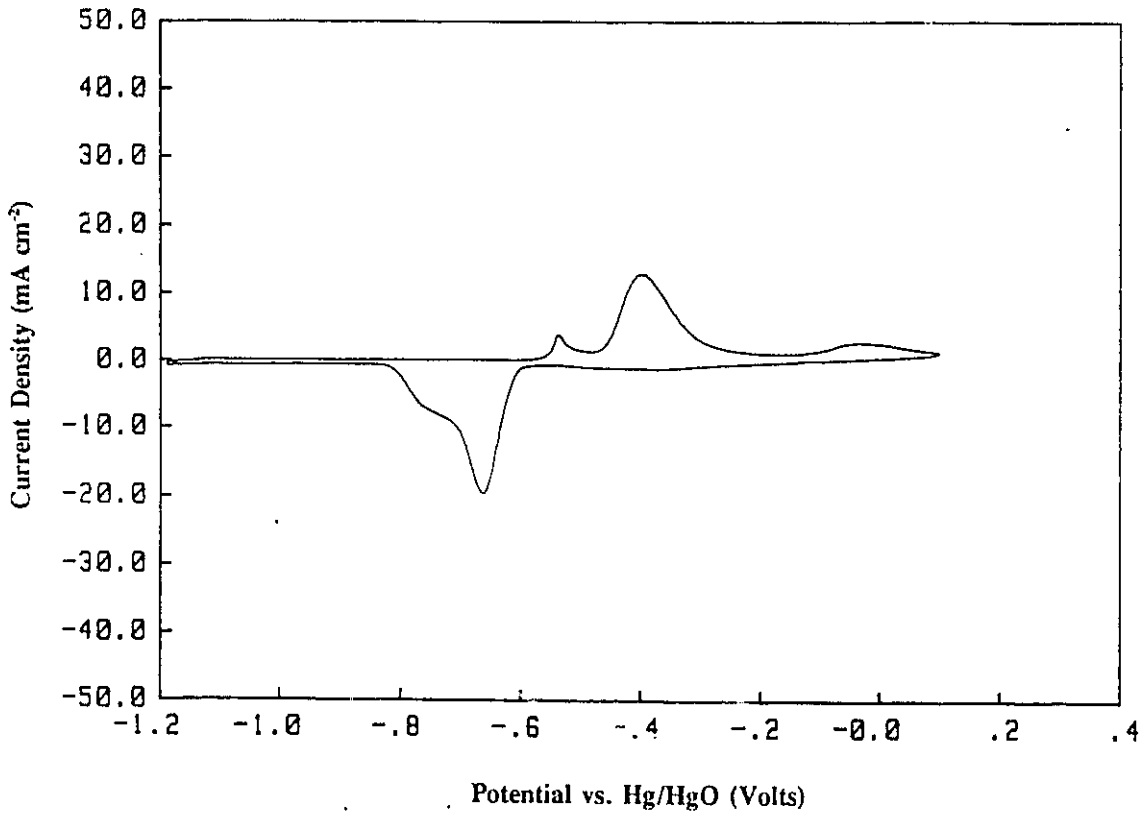

Figure 4.10: Cyclic voltammetry of an MnO_2 deposit from a nitric acid bath with bismuth species present.

0.1M Bi and 0.5M Mn in 1M HNO_3. Note the very large bismuth peaks in the cathodic range -0.6 to -0.8V, and in the anodic range -0.6 to -0.3V. In fact, the capacity of these peaks exceeds the 1.5C used to make this deposit so that most of this bismuth must have been precipitated in place and not deposited electrochemically. On the scale of this figure, the manganese peaks are barely visible.

Figure 4.11 shows the potential range over which manganese current response arises for deposits with and without bismuth. Both deposits were made by passing a current of 5 mA for 5 minutes for a total charge of 1.5 C or 150 mC cm^{-2}. The upper figure shows the 5th and 15th cyclic voltammograms for a deposit *without* bismuth. The total cathodic capacity decreases from 36 mC cm^{-2} to 24 mC cm^{-2} during this period, i.e. by 33%. For the deposit *with* bismuth, the 5th and 40th cycles are shown. The cathodic capacity has decreased from 41 mC cm^{-2} to 35 mC cm^{-2}, i.e. by only 12.2%. Clearly the rechargeability of this system has become enhanced due to the presence of Bi in the structure.

4.3.4 The Effect of Additions of Bi_2O_3 During Cyclic Voltammetry Experiments

In order to see what effect bismuth oxide *in solution* might have on the cycling behaviour of MnO_2 deposits, two types of experiment were conducted. In the first type, a small amount of MnO_2 was deposited on a bare graphite electrode by cycling in a saturated solution of $KMnO_4$ in 9M KOH. Figure 4.12(a) shows a cycle in this solution and a cycle after Bi_2O_3 was added to the cell sufficient to saturate the solution. Note that the manganese capacity is not initially affected very much by this addition but an anodic

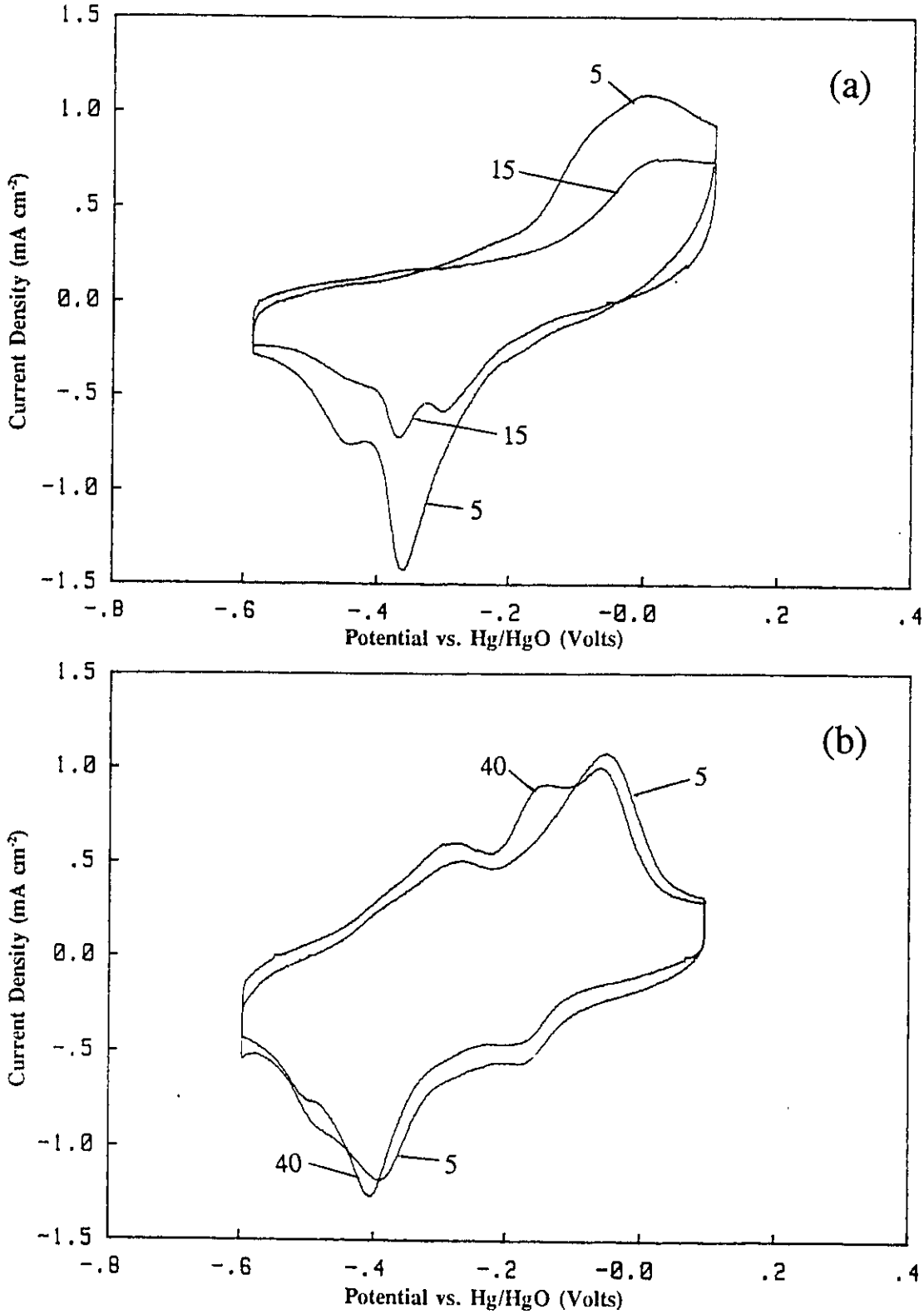

Figure 4.11: Cycling behaviour for MnO_2 deposits from a nitric acid bath: a) cycles 5 and 15 for a deposit without bismuth species; b) cycles 5 and 40 for a deposit with bismuth included.

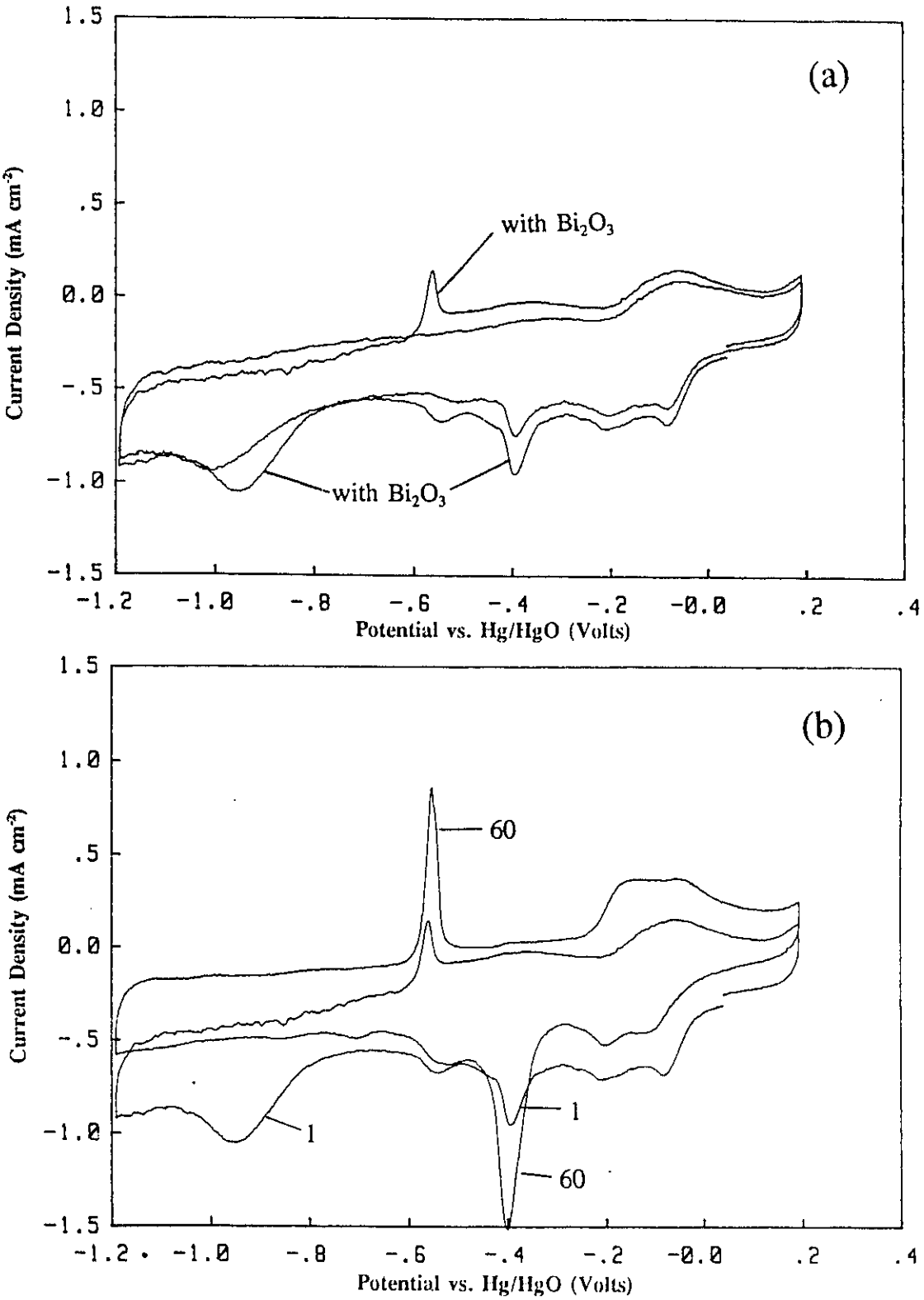

Figure 4.12: Cyclic voltammetry of a bare graphite rod in a saturated solution of $KMnO_4$ in 9M KOH: a) before and after the addition of Bi_2O_3 to the cell; b) the 1st and 60th cycles after the addition of Bi_2O_3 to the cell.

peak from bismuth appears. Figure 4.12(b) shows, however, the effect of continued cycling in this solution viz., cycles 1 and 60 after the addition of Bi_2O_3: both the manganese and bismuth capacities are seen to have become increased dramatically.

Figure 4.13 shows what happens when the electrode is removed from the $KMnO_4/Bi_2O_3$ solution and placed in a clean (i.e. Bi and Mn free) 9M KOH solution; the 2nd and 15th cycles are shown. In the "clean" solution, the bismuth peak almost completely disappears. This could mean one of two things: the bismuth oxidation peak corresponds to a reaction between the electrode and bismuth in solution or, if the bismuth exists as a solid on the electrode, it is almost immediately dissolved out of the matrix.

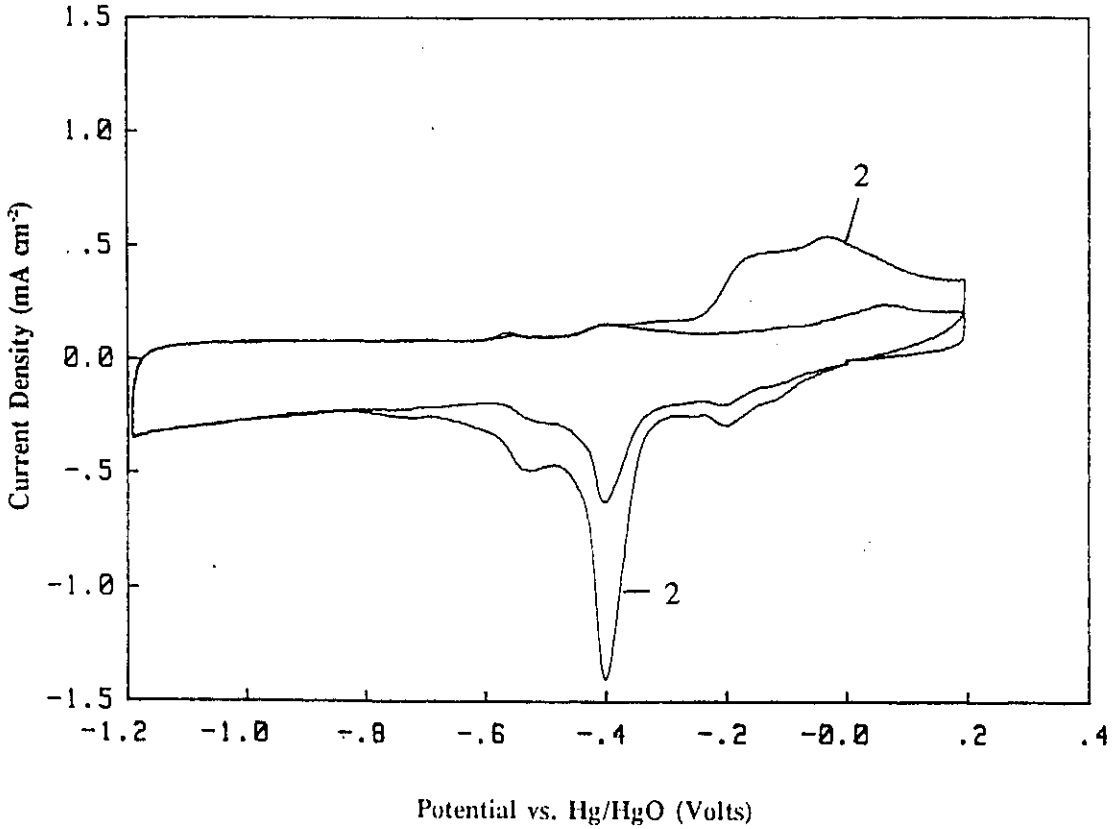

Figure 4.13: Further cycling of the electrode following the experiment illustrated in Figure 4.12 after draining the electrolyte and refilling with pure 9M KOH. The 2nd and 15th cycles are shown.

In either case, it is apparent that the role of dissolved bismuth is important to the rechargeability process. The other observation to be made from Figure 4.13 is that the rechargeability becomes diminished: the capacity at the 15th cycle is much less than at cycle 2.

The second type of experiment was designed to see the effect of Bi_2O_3 in solution on the behaviour of a deposit of MnO_2. For this experiment the cyclic voltammetry was conducted at a sweep rate of 5 mV s^{-1}. Figure 4.14(a) shows one cycle before and one cycle after addition of Bi_2O_3 to the cell. Again, there is initially little difference except for the (expected) appearance of a bismuth anodic peak at about -0.6V. Figure 4.14(b) shows the 2nd and 20th cycles after addition of the Bi_2O_3: the bismuth peak has become intensified somewhat but the capacity at the ends of the voltage range has become reduced considerably. The cathodic capacity in the region of -0.5V has also decreased, but not so dramatically. The bismuth, in this case, appears to be aiding the rechargeability but not as dramatically as in the experiments where it had been co-deposited. Finally, Figure 4.15 shows two cycles, 2 and 30, after the electrode had been transferred into a "clean" KOH solution. Unlike the cycling of the bare electrode, a small bismuth peak remains, indicating that some bismuth was incorporated into the deposit during the previous step. Unlike the results in the previous experiment, the bismuth seems to help the rechargeability slightly as there is some retention of capacity after 30 cycles.

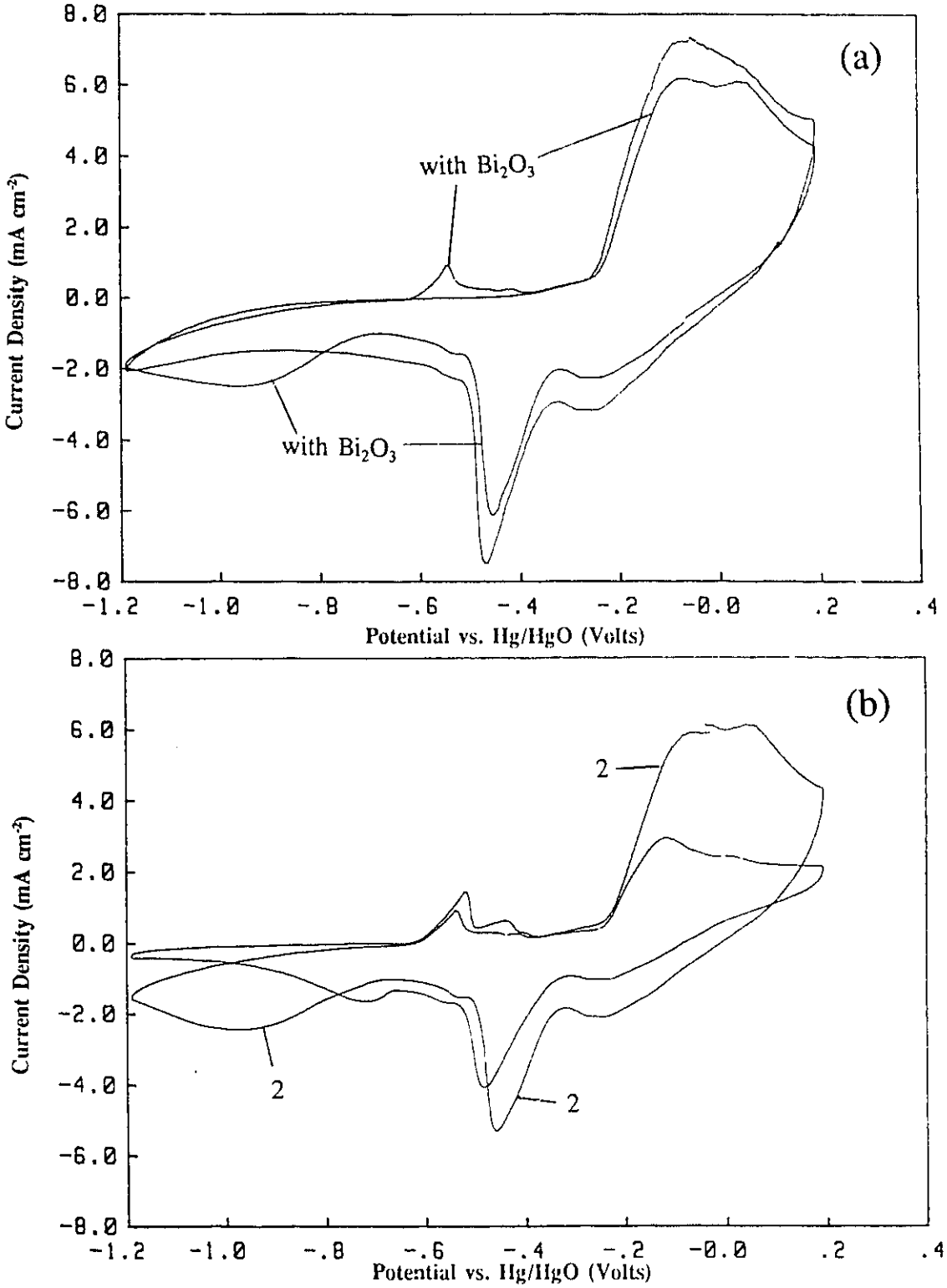

Figure 4.14: Cyclic voltammetry of an MnO_2 deposit in 9M KOH: a) before and after the addition of Bi_2O_3 to the cell; b) the 2nd and 20th cycles after addition of Bi_2O_3 to the cell.

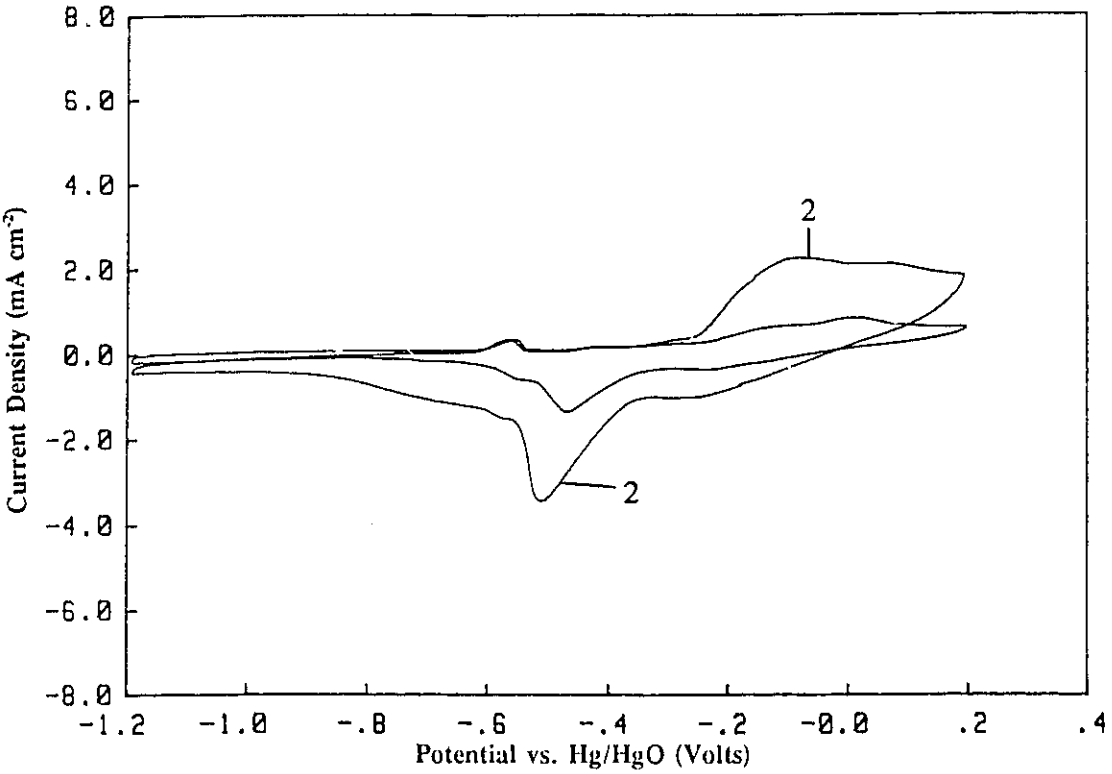

Figure 4.15: Further cycling of the electrode following the experiment illustrated in Figure 4.14 after draining the electrolyte and refilling with pure 9M KOH. The 2nd and 30th cycles are shown.

From these two types of experiments, the following conclusions can be drawn:

i) That bismuth can aid in the deposition of MnO_2 from solutions of $KMnO_4$ in 9M KOH.

ii) That Bi_2O_3 in 9M KOH aids in the rechargeability of MnO_2 deposits.

iii) That some bismuth may be incorporated into MnO_2 deposits by cycling in the presence of Bi_2O_3, provided the MnO_2 films are thick enough.

iv) That this method of introducing bismuth into MnO_2 is not optimal for enhancing rechargeability and is not suitable for thicker films; however, simply introducing solid Bi_2O_3 into an alkaline-MnO_2 electrode should improve rechargeability somewhat by dissolution of Bi_2O_3 in the electrolyte with subsequent incorporation into the MnO_2.

4.3.5 Experiments on Glassy Carbon

In order to investigate the effect of the porosity and roughness of graphite on cycling behaviour of deposited MnO_2, several comparative experiments were conducted on glassy carbon. This material is effectively non-porous and relatively smooth in comparison with regular graphite.

For these experiments, MnO_2 was deposited only on the end of a 7 mm diameter rod and then cycled in the "rod end" cell. The apparent surface area for these experiments was then 0.4 cm^2. Deposits on the glassy carbon generally had good appearance but were not well adherent. Cyclic voltammetry was conducted at a sweep rate of 5 mV s^{-1}.

Figure 4.16 shows a comparison between the third cycles of deposits made with and without bismuth. The deposition baths contained 0.5M Mn and 0.5M H_2SO_4 and the bath containing bismuth was 0.005M in Bi. Voltammetry was done in the "rod end" cell as described earlier. The first thing that is apparent about Figure 4.16 is that the cycling capacity is much larger with bismuth in the deposit. Also, a single anodic bismuth peak is observable at about -0.5V.

Figure 4.17 shows that the capacity of the deposit with bismuth increases with cycling, the 1st and 12th cycles being shown. After the 12th cycle, however, the capacity declined slowly. The charge associated with the anodic manganese peak is 0.066 C cm^{-2}. This is still relatively small when compared with the 0.6 C cm^{-2} used to make the deposit. This shows how important is the available contact area of the carbon in affecting the cycling behaviour.

In order to illustrate this point further, the experiment was repeated but with about 10 mg of Lonza graphite in the form of a paste with 9M KOH being added to the cell. This material was sandwiched between the end of the electrode and the Celgard separator. This left the graphite in intimate contact with the deposit. Figure 4.18 shows a comparison between cycling of MnO_2 deposits (including bismuth species) with and without the Lonza graphite. Note that these voltammograms are plotted on a 5 times larger current scale than the previous two figures. The charge capacity of the deposit cycled *with* Lonza graphite quickly increases with cycling such that the capacity by the third cycle, as shown, is markedly higher than cycling *without* Lonza graphite. The

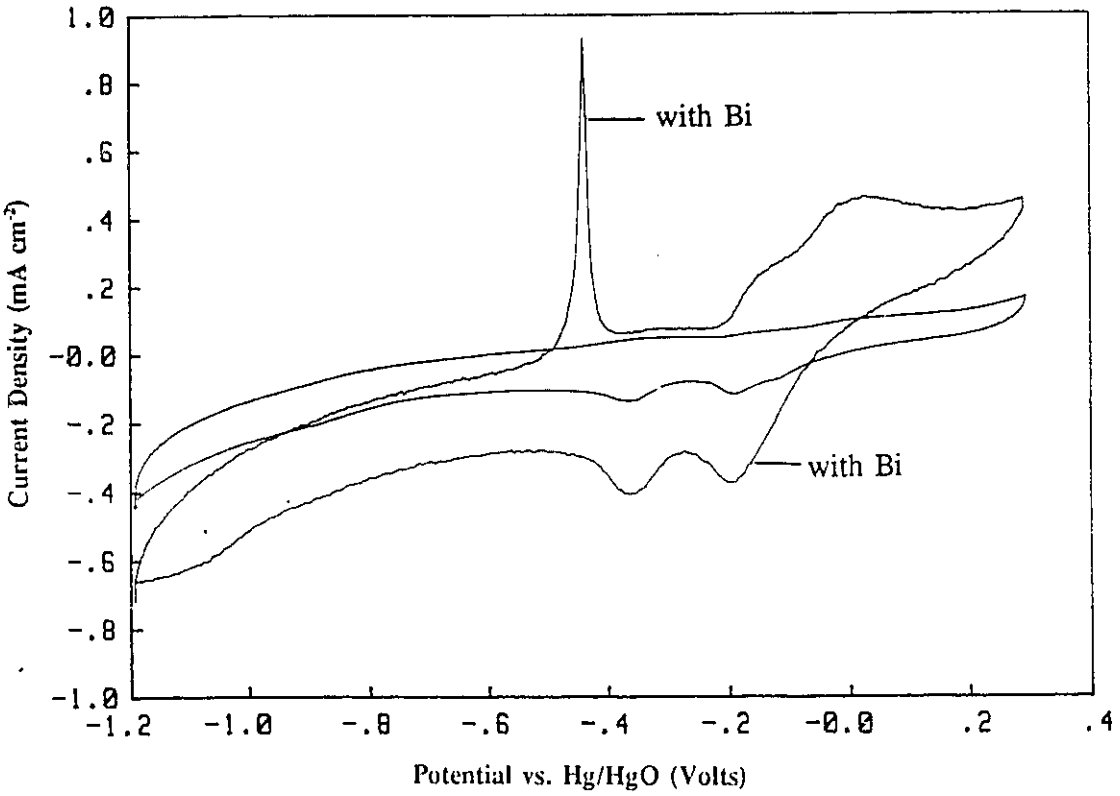

Figure 4.16: Cyclic voltammetry of MnO_2 deposits on glassy carbon with and without bismuth species in the deposit.

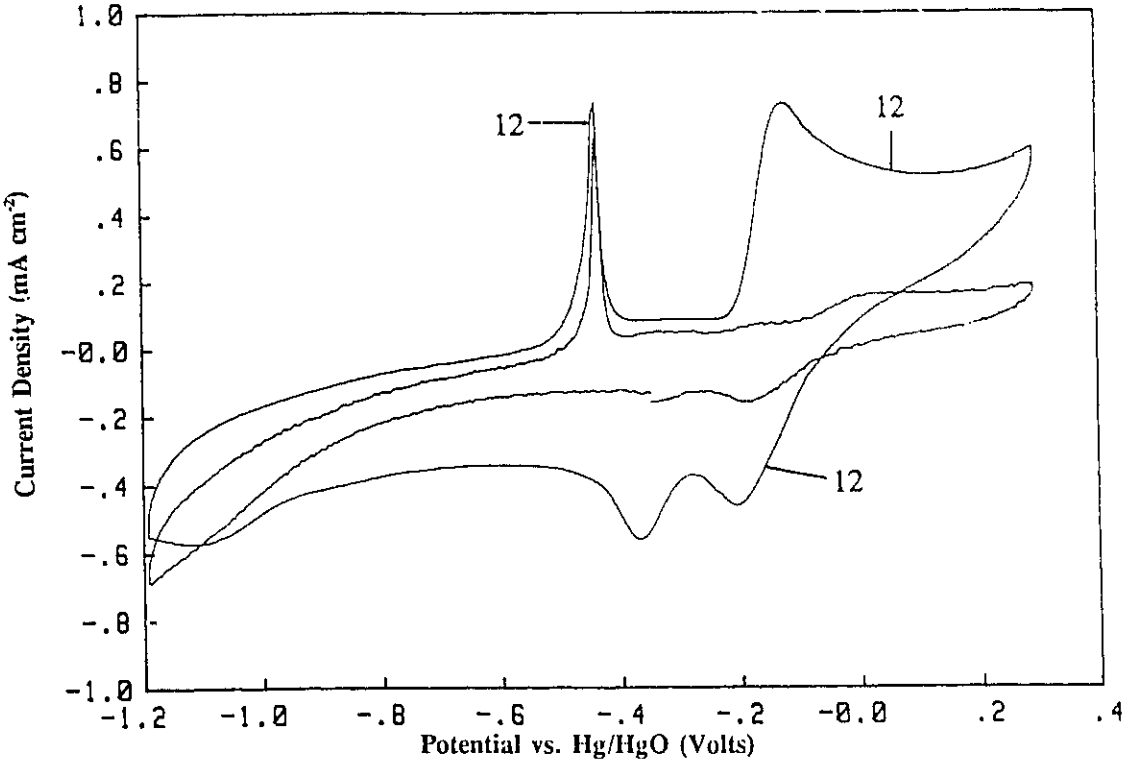

Figure 4.17: Cyclic voltammetry of an MnO_2 deposit with bismuth species on glassy carbon. The 1st and 12th cycles are shown.

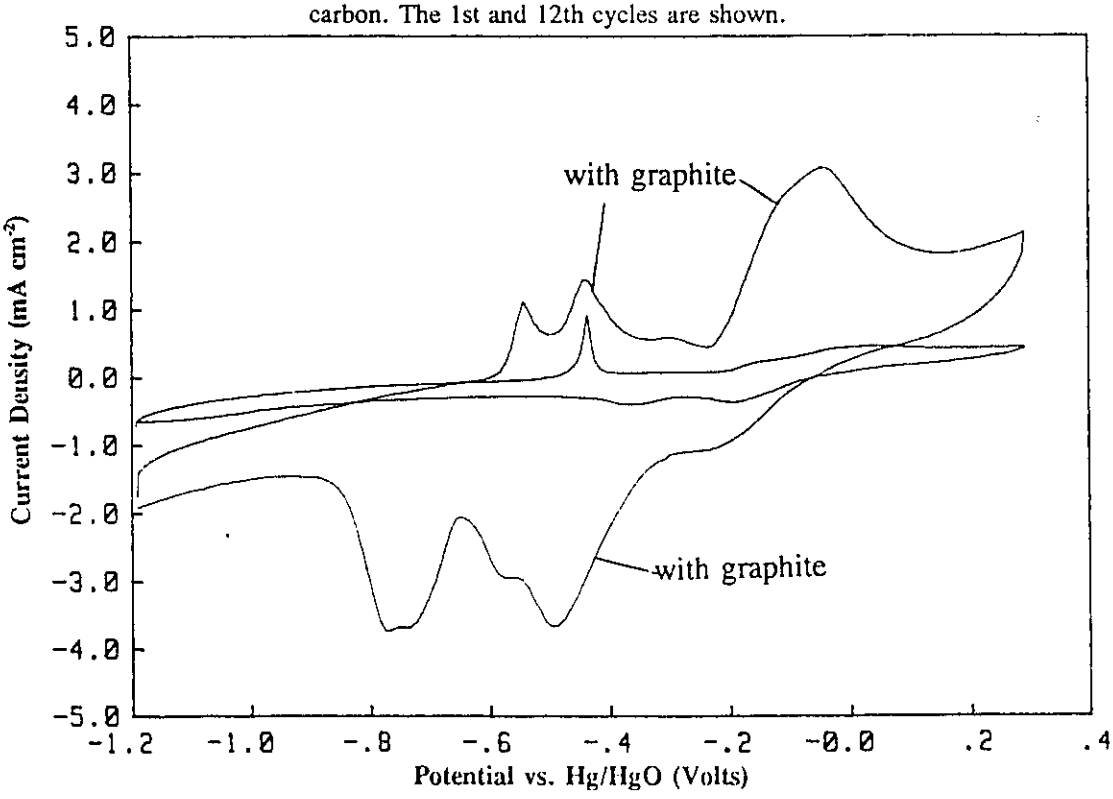

Figure 4.18: Cyclic voltammetry of MnO_2 deposits (including bismuth species) with and without Lonza graphite added to the working-electrode compartment. The 3rd cycle of each is shown.

charge of the anodic manganese peak with Lonza graphite is 0.27 C cm^{-2}, a value which is now much closer to the charge which was used to perform the deposition. This experiment highlights the fact that a large surface area of graphite is required to support good rechargeability but it also provides support for the soluble intermediate pathway for the charge-discharge mechanism as the manganese must become soluble at some point in order to become transferred to the Lonza graphite and become electroactive, presumably at its surface.

4.3.6 Deposits on Carbon Felt

Several attempts were made to perform MnO_2 deposition directly on carbon felt material. This experiment was considered to be of some practical importance as it might be a convenient way to produce a flat battery cathode for direct use in say, a button cell.

Two types of material were used, both from Alupower Inc. (Warren N.J.). These are designated as woven and non-woven material. An SEM micrograph of the woven material is shown in Figure 4.19(a). Note that the material consists of strands of graphite which are microscopically very smooth when compared with the surface of the graphite rods shown in Chapter 2. On the other hand, the non-woven material shown in Figure 4.19(b) has a mud-pack like appearance with strands running through it.

Using similar current densities and temperatures as for the graphite rod experiments, the cyclic voltammetry in all cases showed very poor charge capacity. However, the reasons for such performance are different for the two materials. Deposition occurs on the woven material as evidenced by the colour difference between

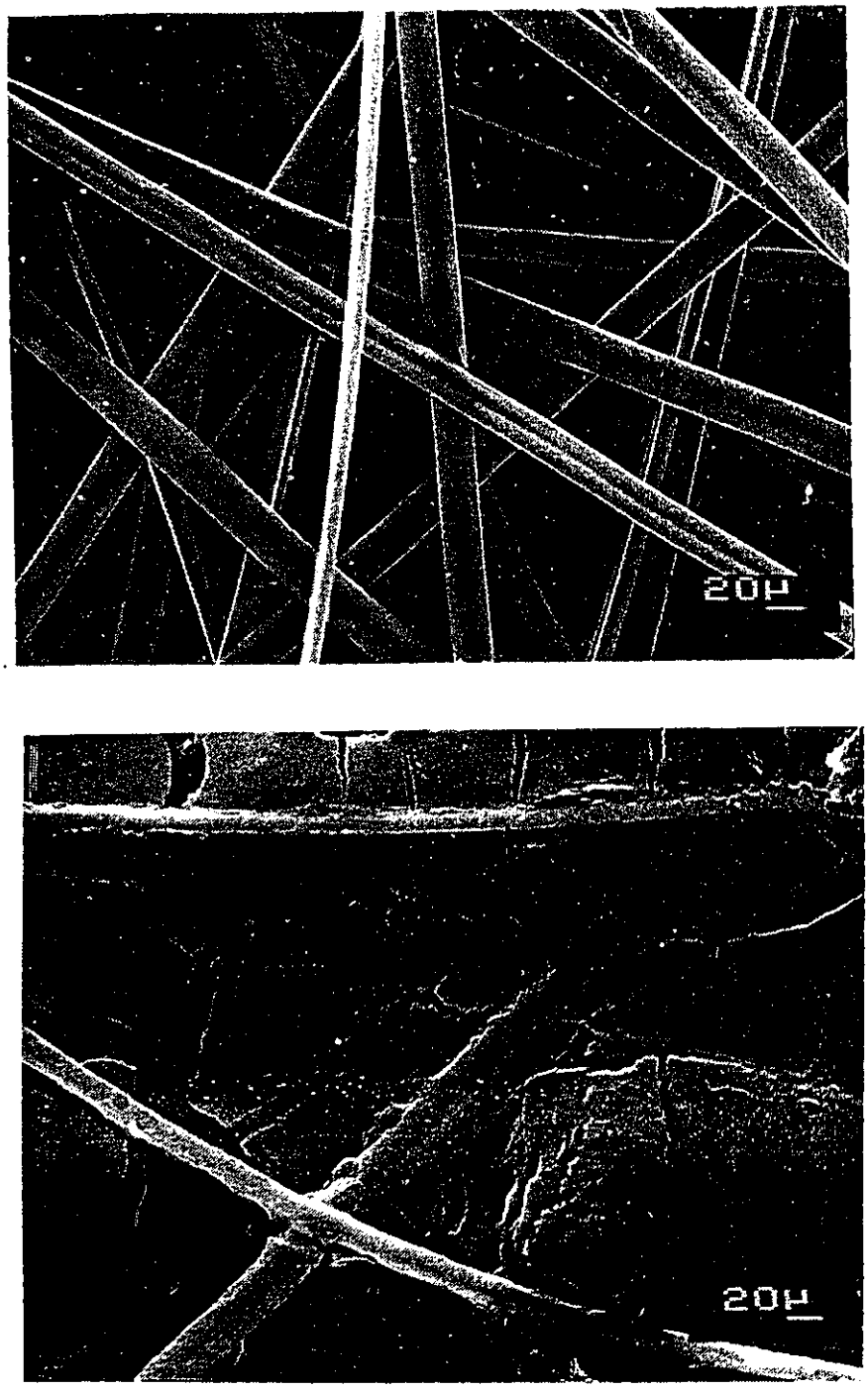

Figure 4.19: SEM micrographs of the carbon felt materials used for attempts at MnO_2 deposition and cyclic voltammetry: a) "woven material", b) "non-woven material".

the MnO_2 deposit and the substrate material which is a dark grey colour. However, when the deposit is cycled in 9M KOH, the charge capacity is very poor.

The surface area of this material using the BET method was found to be 0.60 $m^2\ g^{-1}$. This is quite close to the figure obtained for the graphite rod material. However, rough calculation of the theoretical surface area of the woven material assuming that the strands are uniformly round, estimating the average diameter of the strands as 20 μm (from the SEM micrograph) and given a density of 2.25 g cm^{-2} [41] yields a value of 0.09 $m^2\ g^{-1}$. When calculated in this manner, the roughness factor for the strands is only 6.7, confirming the visual observation on the SEM micrograph that the strands are very smooth and not apparently porous. The poor cycling behaviour is attributed to the microscopic smoothness of the material and is analogous to the observations of deposits on glassy carbon. It is assumed that without the highly porous structure, the intermediates of the reduction and oxidation lose contact with the surface and are unavailable for further reaction.

The situation with the non-woven material is quite different. Deposition never takes place at all with this material. Deposits would not, however, be visible on this material as its colouration is about the same as the MnO_2 deposits. The lack of deposition was confirmed by AAS analysis of the material following a deposition attempt. Virtually no Mn was found. The reasons for the lack of deposition are not immediately obvious although some possiblities are:

i) poor conductivity of the material;

ii) the possibility that it had been treated to make it hydrophobic;

and iii) the possibility that it contains some species which are electroactive in the potential region used for deposition.

If the surface area of the material is a major criterion for good cycling behaviour as is suspected, then the non-woven material would probably perform well as its specific surface area as measured by BET was 61 $m^2 g^{-1}$, some hundred times higher than the woven material. However, the attempts to deposit on the non-woven material were unsuccessful.

The failure of these deposition and cycling experiments does not indicate that the concept of depositing directly on carbon felt is unviable, just that it was not possible using the materials at hand. The deposition and subsequent use as a battery cathode may be possible given the right substrate material.

4.3.7 Rotating Disk Cyclic Voltammetry Behaviour of Bismuth Metal

Rotating disk experiments were conducted with bismuth metal in an attempt to further understand the electrode processes involving bismuth-containing MnO_2 deposits. While the observations were interesting, the relevance of an exhaustive investigation to this thesis is questionable. Therefore, the description of these results will be brief.

The voltammetry was performed in the "rotating-disk cell" as described earlier, with 9M KOH as the electrolyte. The exposed surface area of metal was 6.4 mm in diameter yielding an apparent surface area of 0.32 cm^2. The metal was finished with 2400 grit silicon carbide paper which normally gives a smooth mirror finish to metal surfaces. However, bismuth metal is quite soft and no amount of polishing would give

an extremely smooth surface with this polishing technique.

Voltammograms produced by sweeping the full range between -0.2V and -0.9V can show up to 6 peaks. No other electroactivity was seen between -1.2V and +0.2V, the region of interest for cycling of MnO_2. Peak assignments are shown in Figure 4.20. The A1 (first anodic) peak is small and the A2 peak may appear as a leading shoulder or be merged with the A3 peak at the sweep rate of 5 mV s^{-1} used for most of the experiments. The combined charge of the A2-A3 peaks is about 100 times the A1 charge. For full sweeps the C1 peak is usually obscured and the C2 peak may be a leading shoulder on C3 or may be completely merged with it.

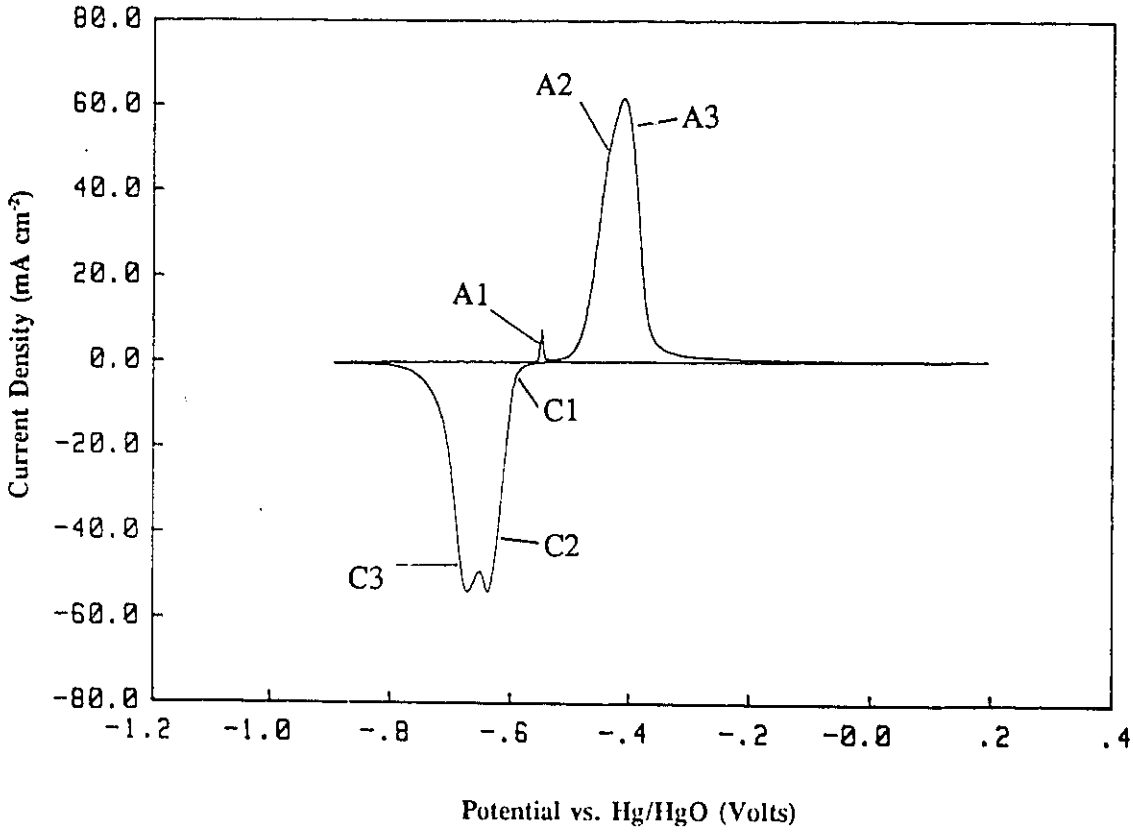

Figure 4.20: Cyclic voltammetry of bismuth metal in 9M KOH.

No reference was found in the literature to cyclic voltammetry of bismuth in concentrated KOH. Williams and Wright [55] reported similar work in solutions of pH 5-14. The major difference between the reported voltammograms and those in this work is that their anodic peaks tailed off to high potential without reaching the baseline indicating that the film growth process was incomplete.

Under the conditions of the present work, if full reduction is allowed during cycling but the anodic sweep is reversed just after the A1 peak (shown in Figure 4.21) the A1-C1 pair appear distinct and almost reversible. (Note that the current scale has been expanded on this figure for clarity.) The charge associated with these peaks is

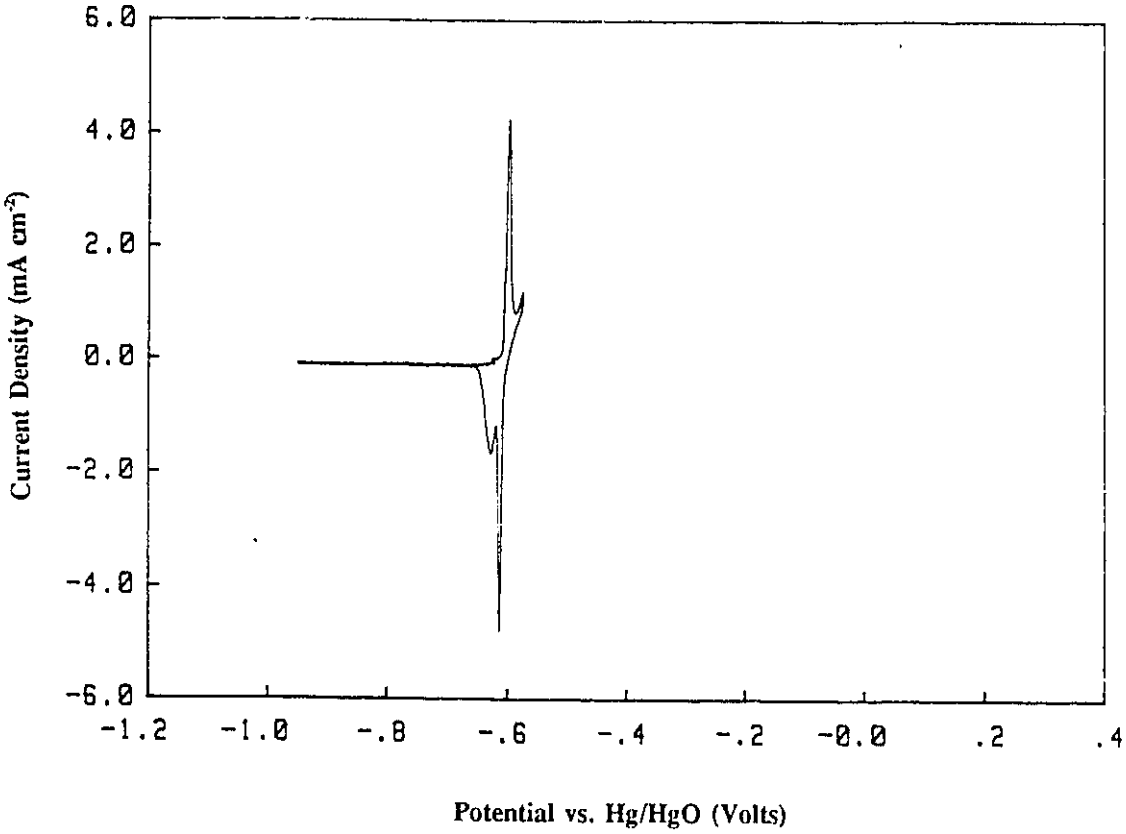

Figure 4.21: Isolation of the A1-C1 peaks of bismuth by limiting the anodic sweep to -0.52V.

typically 4 to 12 mC cm^{-2}. In section 4.3.1, the charge for the reduction of a monolayer of bismuth onto a surface was calculated as 0.45 mC cm^{-2} for the three-electron process. Considering the reversibility of the peaks and the fact that the charge for these peaks is not affected by rotation at 2000 rpm, one might assume that this is a reversible adsorption step and probably only involves one electron. In that case, the charge for monolayer formation would be 0.15 mC cm^{-2}. This means that for the process to be a one-electron, monolayer reaction, the roughness factor would have to be between 25 and 80. Although this is not out of the question, the most that can be said about this process is that it is a reaction of "one or a few" monolayers.

Full sweep voltammograms with and without rotation are shown in Figure 4.22.

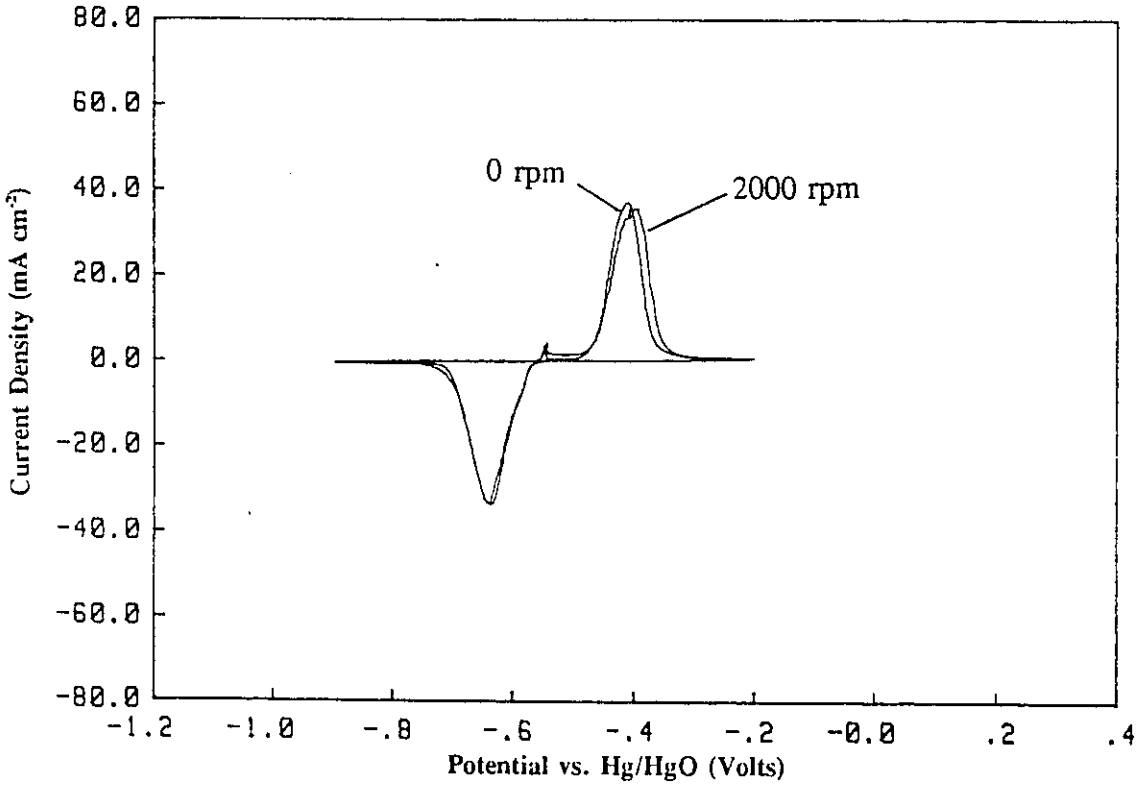

Figure 4.22: The effect of rotation on the full range cyclic voltammetry behaviour of bismuth metal. Voltammograms are shown for no rotation and 2000 rpm rotation.

The ratio of anodic to cathodic charge is slightly less than 1 for no rotation and greater than 1 with rotation at 2000 rpm. This indicates the possible loss of soluble anodic products or intermediates when rotation is applied. If the sweep is reversed part way through the A2-A3 peak, the effect of rotation is more pronounced. This is shown in Figure 4.23 (current scale expanded for clarity). Note also that the bulk of the anodic current arises *after* sweep reversal to the cathodic direction. From these two observations, it is concluded that soluble intermediates play a role in the anodic oxidation of bismuth metal in 9M KOH. If the metal is allowed to fully become fully oxidised but

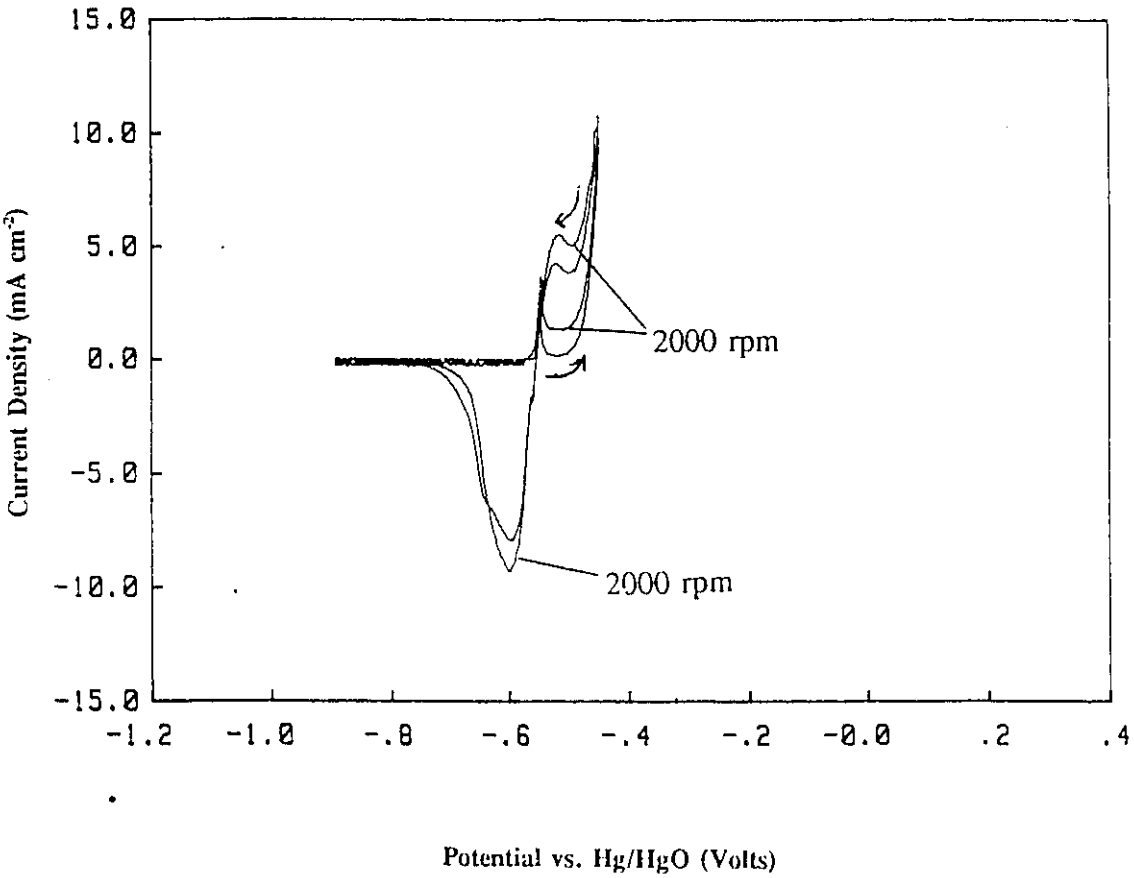

Figure 4.23: The effect of rotation on the cyclic voltammetry behaviour of bismuth metal when the anodic sweep is limited to -0.45V. No rotation and 2000 rpm shown.

the cathodic sweep is reversed during the C2-C3 peak as shown in Figure 4.24, the effectof rotation is not so pronounced. One other interesting observation can be made: the A2 peak becomes more reversible under these partial reduction conditions, being seen to move to a more negative potential away from the A3 peak.

If the sweep rate is slowed by an order of magnitude to 0.5 mV s^{-1} without rotation, the total anodic and cathodic charge are not greatly affected. This indicates that the anodic film that is formed is coherent and effectively passive.

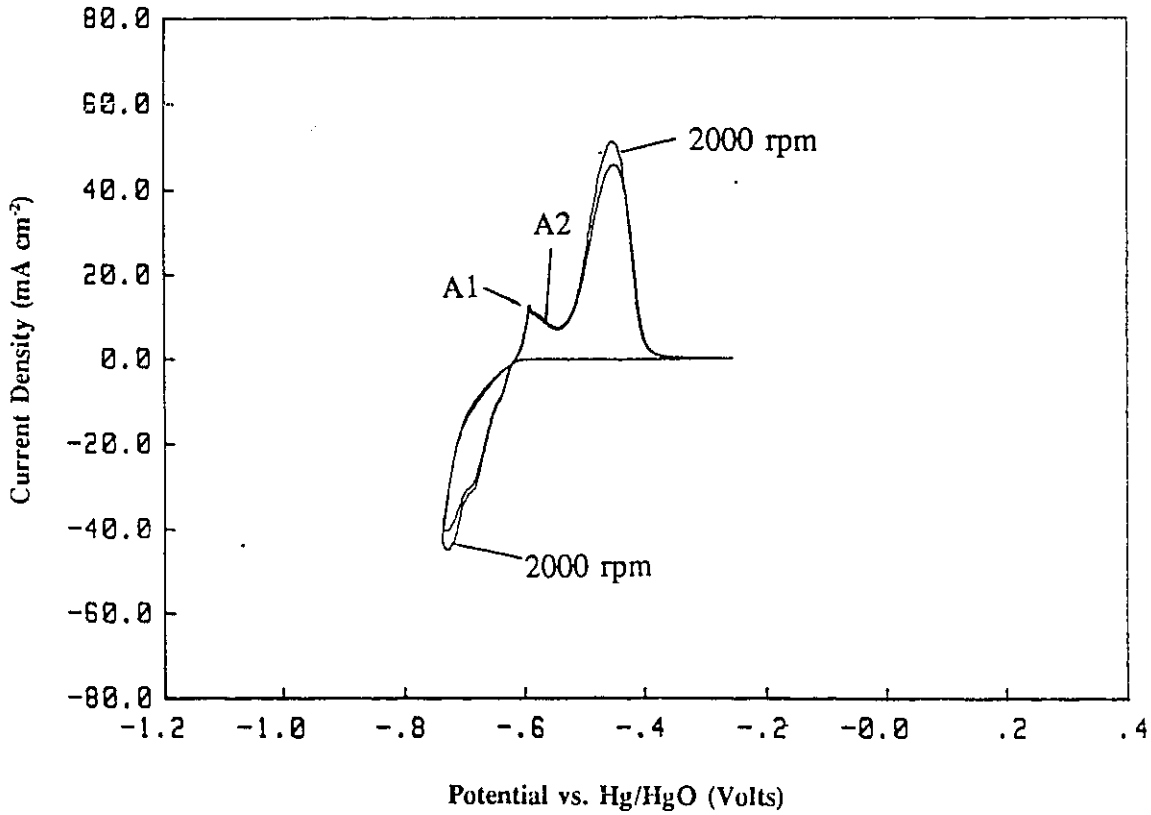

Figure 4.24: The effect of rotation on the cyclic voltammetry behaviour of bismuth metal when the cathodic sweep is limited to -0.69V. No rotation and 2000 rpm shown.

From the above experiments, the following conclusions can be drawn about the cyclic voltammetry of bismuth metal in 9M KOH:

i) That bismuth forms a coherent, passive film when polarised to -0.2V.

ii) The film is formed first by a reaction to produce a layer only one or a few monolayers thick, followed by a thickening process until the layer is several hundred monolayers thick. This thickening proceeds by steps involving soluble intermediates.

iii) The reduction of this film by cathodic polarisation leads to the re-formation of bismuth metal via a reaction pathway that does not appear to involve soluble intermediates.

4.3.8 Rotating-Disk Cyclic Voltammetry Behaviour of Manganese Metal

In order to understand further the processes occurring in deposits of MnO_2, some cyclic voltammetry experiments were conducted with a manganese metal rotating-disk electrode in 9M KOH. The experiments were carried out in the "rotating disk cell" described above.

The voltammograms look remarkably similar to those of deposited MnO_2 with one interesting exception. There is a relatively large anodic peak which arises on the *cathodic* sweep. This peak is assigned the label "AC" in further discussion. All of the peak assignments for this discussion are outlined below and illustrated in Figure 4.25.

A1 -0.15V
A2 -0.05V
A3 +0.05V and tailing to higher potential
AC (Anodic peak on Cathodic Sweep) -0.45 to -0.5V

C1 -0.2V
C2 -0.4V
C3 -0.8V to -1V (broad and sometimes tailing)

Figure 4.25 is for voltammetry of the manganese metal in 9M KOH which is saturated with bismuth. In fact, the C3 peak is only observed on manganese metal in the presence of bismuth. Figure 4.26 shows the effect of rotation at 2000 rpm on the

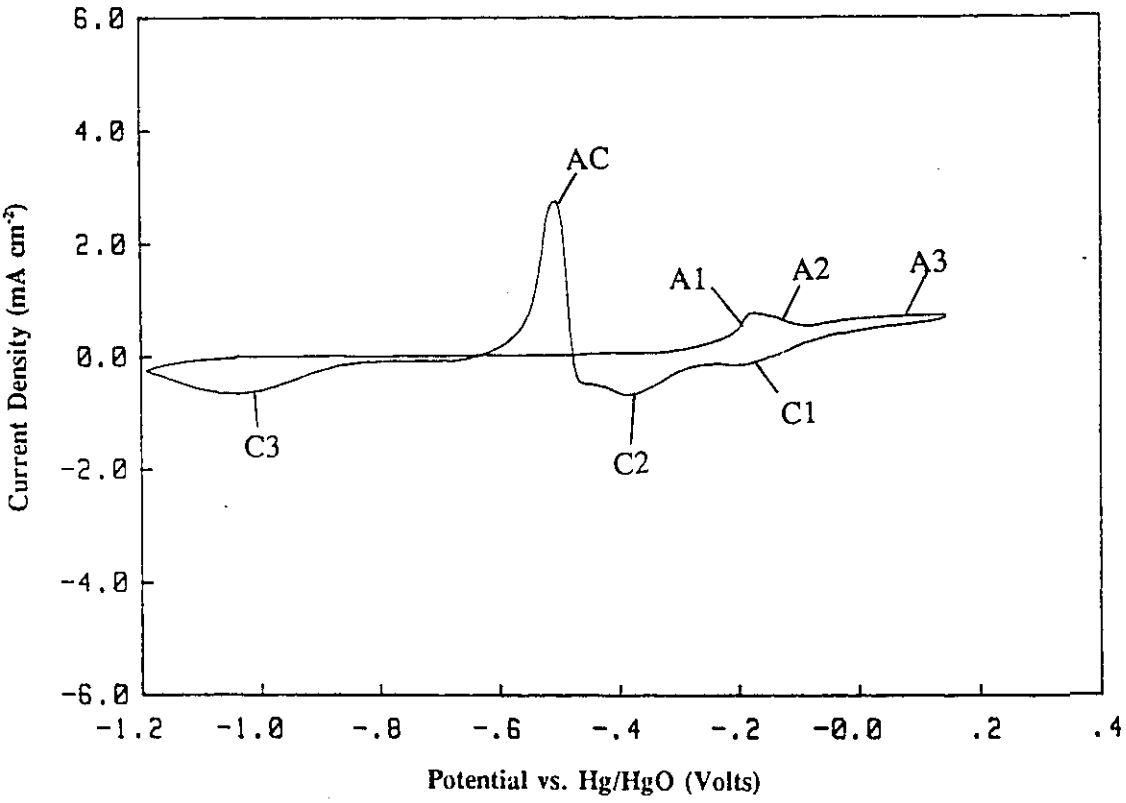

Figure 4.25: Peak assignments for the cyclic voltammetry behaviour of manganese metal in 9M KOH saturated with Bi_2O_3.

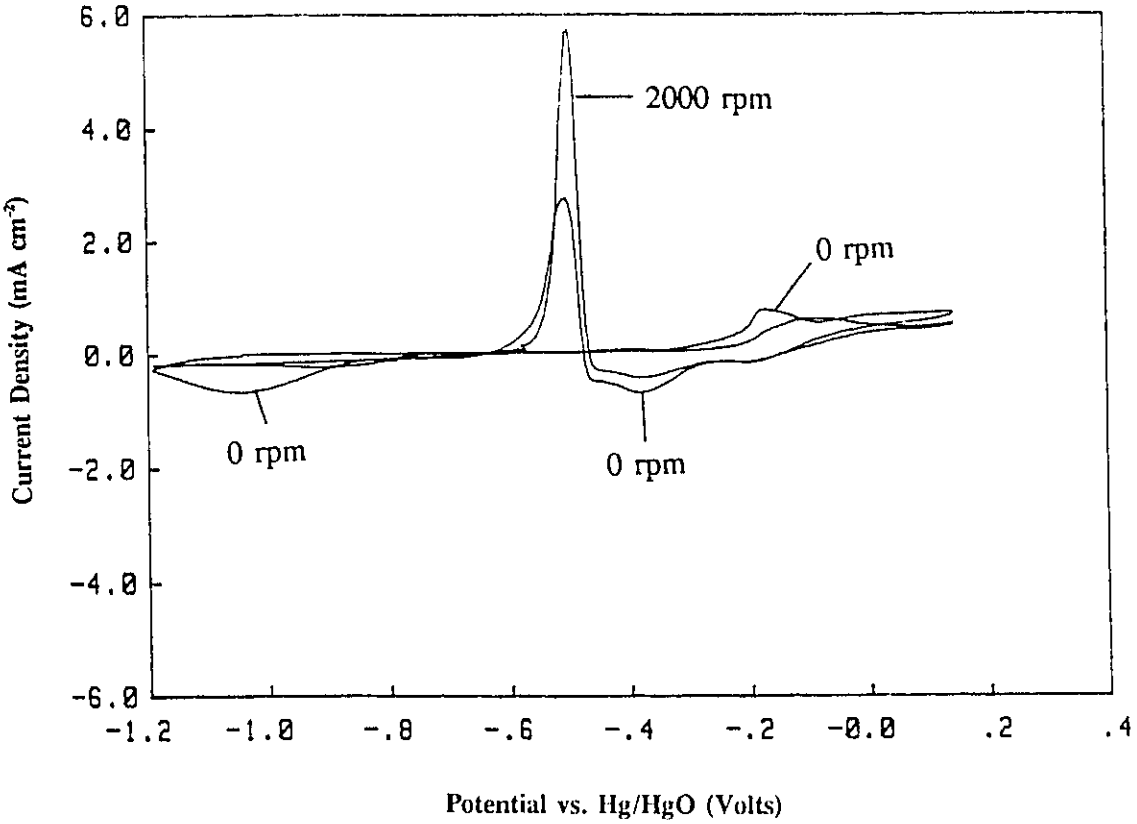

Figure 4.26: The effect of rotation on the cyclic voltammetry behaviour of manganese metal in 9M KOH saturated with Bi_2O_3. No rotation and 2000 rpm shown.

voltammogram. The A1,A3,C2 and C3 peaks are diminished when the electrode is rotated. In these experiments and in other observations, the C3 is observed to be conjugate with at least part of the A3 peak. A more limited sweep reveals that the A1 and C2 peaks are most likely conjugate to each other as they are both affected by rotation.

The AC peak is also affected by rotation but there does not appear to be a conjugate reduction process arising at less positive potentials in the negative-going sweep. Indeed, this peak behaves anomalously and was the subject of further investigation.

Burke and Ahern [56] have reported observation of this peak in a cyclic

voltammetry study of Mn in 1M NaOH. However, they found it only on the first cycle and only if the sweep was started at the anodic end. Although they did not investigate this peak thoroughly, they attributed it to currents associated with " dissolution of Mn metal or some of the oxide layer only when insufficient time had passed to form a thicker compact layer".

It is evident that (cf. Figure 4.27) by no means enough charge is passed in the range -0.4V to -0.25V to relate to the charge manifested in the subsequent cathodic (AC) peak at -0.45V, e.g. through a disproportionation process. Hence, it can be suggested that the reaction occuring at the AC peak involves a species that has been already formed

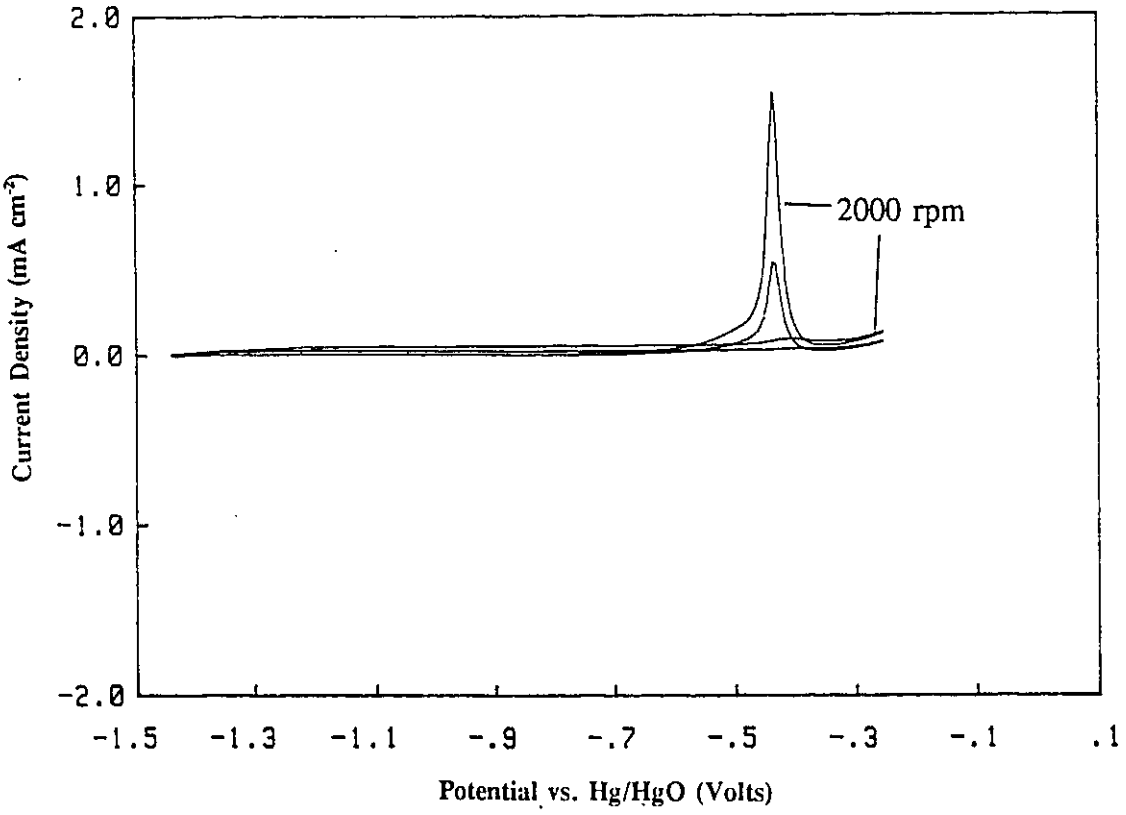

Figure 4.27: The apparent isolation of the "AC" peak by limiting the anodic sweep to -0.15V. Shown with no rotation and at 2000 rpm.

in another region of the potential sweep. If the anodic sweep range is limited to just above the AC peak, as shown in Figure 4.27 (current scale expanded for clarity) the AC peak appears to be the only feature! This would be quite a normal dissolution-passivation process if the peak occurred on the anodic sweep, but *almost all* of the capacity arises on the return *cathodic* sweep. This observation implies that one type of passivity is changed to another near the anodic limit with the "new" passivity breaking down on the return sweep and allowing the anodic dissolution process to proceed.

If the "with rotation" cyclic voltammogram of Figure 4.27 is replotted on a ten times more sensitive current scale (Figure 4.28), the region towards the anodic limit of

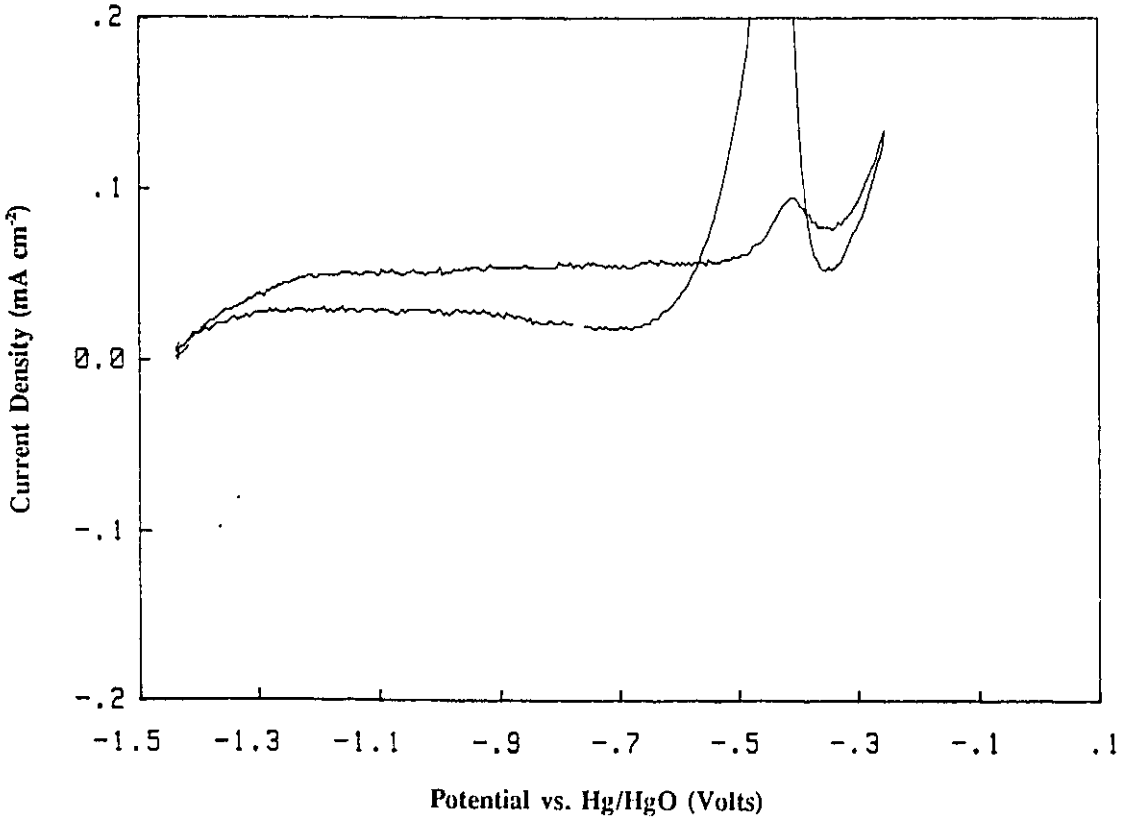

Figure 4.28: Current scale expansion of the voltammogram at 2000 rpm shown in figure 4.27.

the sweep shows that a small anodic charge is actually passed, but only enough to cause an electrochemical reaction involving one or a few monolayers. This is believed to be the reaction that creates the new passive layer.

The rotation dependence of the intensity of the AC peak arises not from an effect on the actual process occurring but from prior effects on the production of the reactants involved in this peak. This was demonstrated by comparing the magnitude of the AC current peak when rotation was stopped at the *beginning* of the peak with the value observed under continuous rotation. The peak height is not then substantially affected. Similarly, rotation only during the passage through the peak gave currents that were not substantially higher than with no rotation at all. This observation tends to rule out manganese metal itself as the reactant of the AC peak as the rotation effect on dissolution of a metal electrode would probably be manifested in the dissolution peak itself.

Potential holding experiments illustrate that there is an effect of both time of holding and the holding potential on the enhancement of the AC peak. The higher the potential of holding, up to the onset of the A1 peak, the more the enhancement. The AC peak is even enhanced by holding at open circuit. Again, this must be an effect of enhancing the prior formation of the reactants involved in the AC peak. It is remarkable that this formation of such reactants has little or no prior measurable net electrochemical charge associated with it and hence must be associated with open-circuit mixed processes.

The following working model is therefore proposed to account for the observations on the AC peak:

i) Manganese spontaneously corrodes to form a layer of Mn^{2+} species,

probably hydrous $Mn(OH)_2$ or some other species coordinated with OH^- groups. The layer is many monolayers thick and is not in electrical contact with the underlying metal. The formation of this layer is diffusion controlled by the diffusion of OH^- through the layer to the electrode interface.

ii) At higher potentials, the spontaneous corrosion is enhanced by increasing the rate of diffusion of OH^- up to and through the layer or the rate of adsorption of OH^- (coverage) on the reacting surface.

iii) If a sufficiently high potential is applied, a passive layer is formed at the electrode surface which is in an oxidation state higher than 2. Upon sweep reversal, this layer is reduced to an Mn^{2+} or Mn^{3+} layer which forms a conductive bridge to the thicker overlayer or the layer at the electrode surface may diffuse into the overlayer imparting some conductivity but not allowing it to depassivate until the potential range of the AC peak is reached. The overlayer may then be oxidised to Mn^{3+} species giving rise to the AC peak on the cathodic sweep.

The intensity of the AC peak has a cycle-life dependence. If the anodic sweep is limited to +0.15V, the AC peak decreases with cycling until it is eventually no longer observable. If the same experiment is conducted with a saturated solution of Bi_2O_3 in 9M KOH as electrolyte, the AC peak remains at a higher charge capacity for more cycles. According to the model presented above, the diminution of the AC peak with cycling might arise for two reasons: impediment of the formation of the reactants for the AC

peak or interference with the formation of the conductive layer that allows current in the AC peak to pass. One impediment to the formation of reactants would be the build up of a thick film of "AC product" with continued cycling. If, as was suggested in Section 3.3.2 (Chapter 3), bismuth forms a soluble complex with Mn^{3+}, then it could reduce the rate of formation of the "AC product" layer by taking it off into solution and slowing down the decline in the AC peak. Another mode of action of bismuth species might be to maintain the reaction involved in the conductive layer formation as proposed above.

As was alluded to earlier, there is another effect of having bismuth species in solution when conducting these experiments. The C3 peak does not arise unless bismuth is present. As was seen with MnO_2 deposits (Section 4.3.3), the C3 peak is conjugate to the A3 peak, although these peaks occur more than 1 volt apart. The interpretation of these peaks is that they arise from processes involving loosely bound layers on the surface and require a large overvoltage to occur. Rotation suppresses the C3 peak which does not arise at all unless bismuth species are present, implying that bismuth may have an effect on the conductivity of the layers near the electrode surface. Without bismuth, the overvoltage may be so large as to push the reaction potential into the potential region of hydrogen evolution.

Lastly, turning attention to the peaks in the redox region for MnO_2, it was pointed out above that the A1 and C2 peaks are affected by rotation and probably correspond to conjugate processes. The diminution of these peaks with rotation implies that soluble reactants are involved. Although we cannot assume that the same reaction steps are involved as those in cycling of MnO_2 on graphite, this is further evidence that soluble

species are involved in that system.

The charge involved in the A1,A2 - C1,C2 redox system does not exceed about 30 mC per apparent cm^2 and generally declines with cycling. No attempt was made to measure the real surface area of the manganese electrode but it could be polished to a smooth mirror finish. If we estimate then a maximum roughness factor of ca.5 for the electrode, then the reaction is limited to about 20 layers at this sweep rate based on the charge of 0.334 mC cm^{-2} for a monolayer of MnO_2 as calculated earlier. The degradation of capacity with cycling parallels the experience with MnO_2 deposits on graphite: with bismuth present, the degradation takes many more cycles. After the cycling experiments, the electrodes are seen to have grown a thick, adherent brown film which is apparently not electroactive. The formation of this film is probably responsible for the decline in electroactivity of the underlying layers of oxide and metal.

In summary, the study of voltammetry of manganese metal has:

i) provided some further evidence for the role of soluble intermediates in the MnO_2 redox system;

ii) shown that bismuth species in solution affect the cycling behaviour;

and iii) provided observation of an interesting new electrochemical phenomenon (regarding the AC peak).

4.3.9 Assignment of Cyclic Voltammetry Peaks to Possible Redox Processes

The electrochemistry of the redox behaviour of MnO_2 is, indeed, very complex. There are at least 4 peaks observable in the reduction regime and at least 3 peaks in oxidation. When bismuth is included in the deposit, there are additionally 2 oxidation and 2 reduction peaks. The MnO_2 deposit used for these experiments was produced from a bath containing 0.5M $MnSO_4$, 0.5M H_2SO_4 and 0.005M Bi galvanostatically deposited at 10 mA cm^{-2} for 5 minutes. The particular electrode used to illustrate the peak assignments was also dip-coated in a 5 wt% solution of Nafion (Aldrich Chemical, Milwaukee,WI) and dried at 65°C for one hour before being placed in the electrochemical cell. The voltammograms of this electrode were chosen because they display the MnA3 and MnC4 peaks prominently.The potential assignments for all of the peaks are shown in Figure 4.29 and are listed below:

MnA1 -0.15V
MnA2 -0.05V
MnA3 +0.05V and tailing to higher potential

MnC1 -0.2V
MnC2 -0.4V
MnC3 -0.5V
MnC4 -0.8V to -1V (broad and sometimes tailing)

BiA1 -0.55V
BiA2 -0.45V

BiC1 -0.65V
BiC2 -0.70V (usually tailing)

These assignments are very similar to those given for the results of the rotating-disk experiments on the respective metal electrodes with a couple of notable exceptions. The AC peak does not arise when cycling MnO_2 deposits (see Section 4.3.8 for

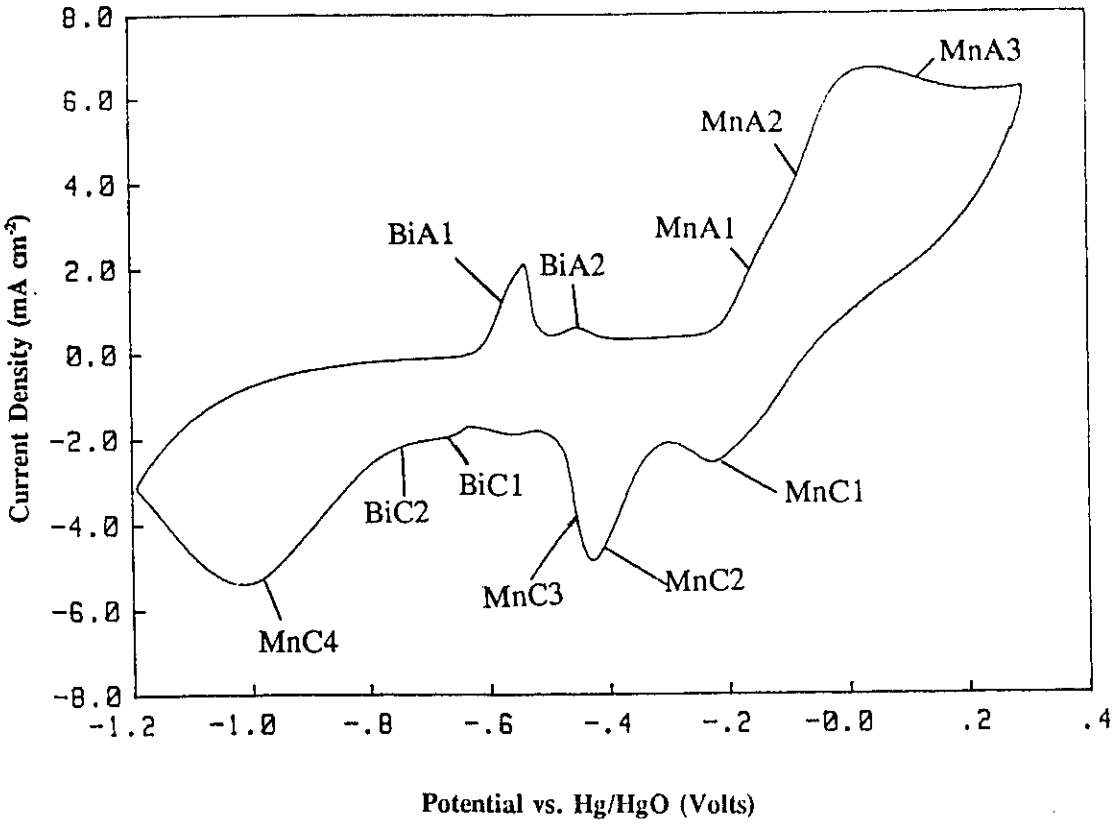

Figure 4.29: Peak assignments for the cyclic voltammetry of MnO_2 deposits containing bismuth species in 9M KOH.

explanation of the AC peak). The MnC3 peak appears at the potential of the AC peak for Mn metal voltammetry. Additionally, the MnC3 peak is not always resolved from the MnC2 peak at the sweep rates used for these experiments.

Concerning the bismuth peaks, the A1 and C1 peaks from the voltammetry on the metal have been omitted from this discussion. These are never seen as distinct peaks when cycling MnO_2 deposits containing Bi.

The sweep limits were varied in order to determine which processes are conjugate to one another. Figure 4.30 shows a comparison of the current profiles for a full range sweep with one where the anodic sweep is cut short from the positive end. From this figure it can be seen that the MnA3 and MnC4 peaks are related.

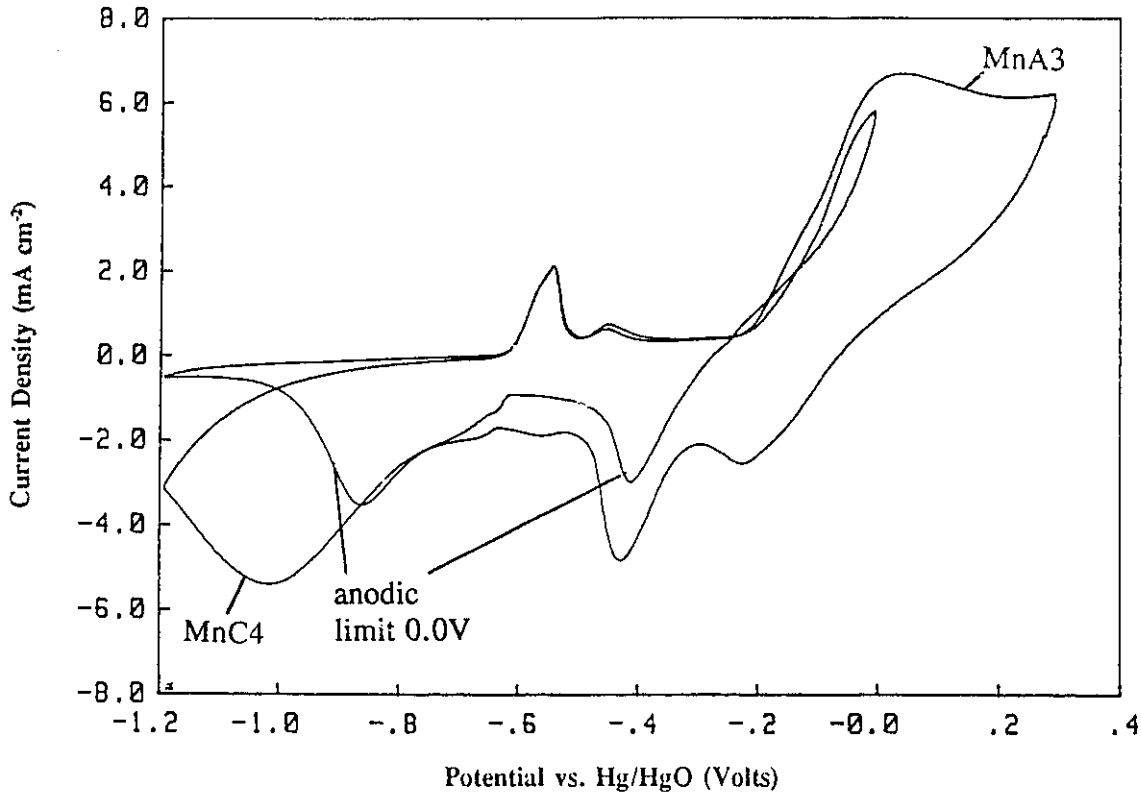

Figure 4.30: The relationship between the MnA3 and MnC4 peaks as shown by limiting the anodic sweep to 0.0V.

If the anodic sweep is cut even shorter as shown in Figure 4.31, a very small conjugate pair of manganese peaks (MnA1 - MnC3) and the bismuth peaks are all that remain. The anodic bismuth peaks do not seem to be affected by this, indicating that the latter processes are quite independent of the manganese oxidation.

If the cathodic sweep is cut short as shown in Figure 4.32, the relationship between MnA3 and MnC4 is confirmed but another interesting observation is as follows: MnA1 and possibly MnA2 are suppressed or shifted to more positive potentials *for the extended sweep range*. Since the MnC1, MnC2 and MnC3 peaks are not affected very much, it is to be concluded that the anodic peaks have been shifted rather than suppressed. Note also that the bismuth peaks disappear entirely under the condition of

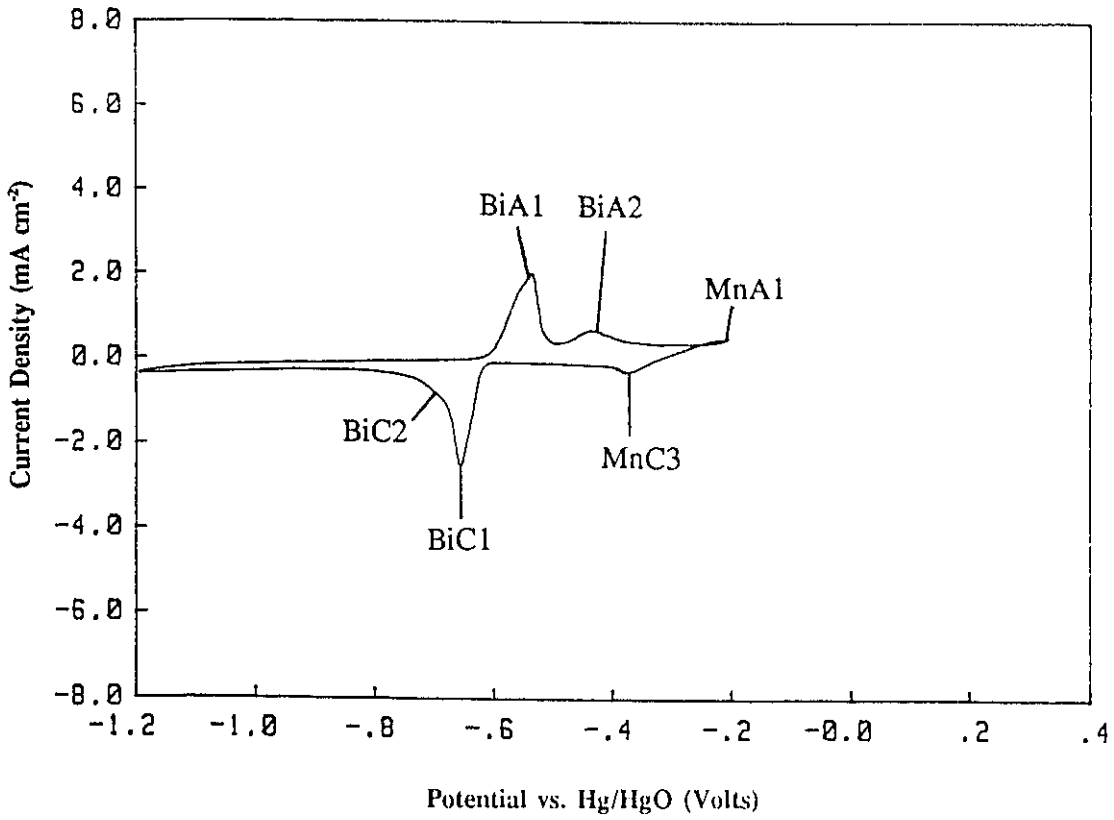

Figure 4.31: Behaviour of the same electrode as that for Figure 4.30 but with the anodic sweep limited to -0.2V.

a shorter sweep range.

Based on the above observations, the product of the MnC4 reduction process is presumed to be $Mn(OH)_2$. The peak is not very reproducible and decreases substantially with cycling. Also, in the Mn rotating-disk experiment, this peak was substantially reduced by rotation and took several cycles to become regenerated after rotation was stopped. For these two reasons, the bulk of MnC4 state is probably the result of the reduction of a loosely bound outer layer of MnO_2. This layer is oxidised directly to MnO_2 at MnA3. It is worth noting that these peaks do not arise, or are very weak when there are no bismuth species in the system. Evidently, bismuth species play an important role in increasing the bulk conductivity of the underlying deposits.

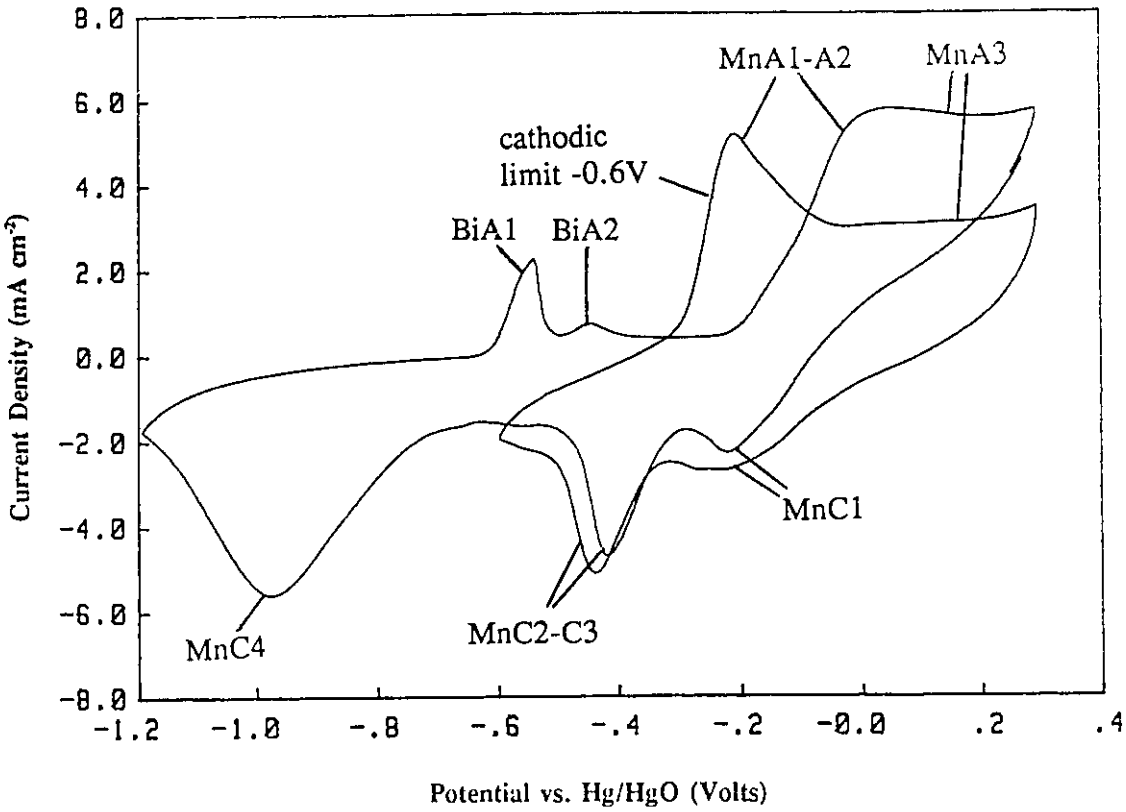

Figure 4.32: The comparison of a full range cyclic voltammogram of the MnO_2 deposit containing bismuth species with one where the cathodic sweep is limited to -0.6V

There are two possible explanations for the shift of the MnA1 and MnA2 peaks to higher potentials when the cathodic sweep goes beyond the MnC4 peak potential. Further reduction of the products of MnC2 and MnC3 could also occur at this potential and change the reaction pathway for re-oxidation, and shift the MnA1 and MnA2 peaks. The other explanation is one of kinetics. If the reduction of the loosely bound outer layer is allowed to proceed, the layer might impede the susequent oxidation of the inner layer, hence shifting the peaks to a more positive potential.

The study by McBreen [30] of the MnO_2 redox system is probably the most comprehensive one to date as was noted earlier. We find that the scheme of McBreen

basically fits our findings but that the presence of bismuth species appears to have some profound effects on the reaction pathway. Referring again to Figure 4.29 we find that if the potential is swept up to +0.3V there is a reduction at -0.2V (MnC1) corresponding to the 1-electron reduction of small amounts of γ-MnO_2 which was shown by McBreen to become reduced at a higher potential on the first sweep of his voltammograms. He proposed that the product, on subsequent oxidation, was δ-MnO_2, a terminology which will be used to describe the present system. The MnC2 and MnC3 reductions correspond to the reduction of δ-MnO_2 to something approximating Mn_3O_4 or possibly $Mn(OH)_2$. The fact that Wroblowa [10,12] and Qu et al [35] have not reported capacities in excess of 85% of the 2-electron charge suggests that the reduction does not proceed all the way to $Mn(OH)_2$ but stops at something approximating to Mn_3O_4. As described in some detail above, the MnC4 peak corresponds to reduction of a loosely bound layer of MnO_2.

The MnA1 and MnA2 peaks are conjugate to the reduction peaks MnC2 and MnC3 and produce an Mn^{3+} oxide which can be approximated as Mn_2O_3. Further oxidation to δ-MnO_2 and direct oxidation of the $Mn(OH)_2$ produced at MnC4 takes place at MnA3. If the sweep rate is fairly high, incomplete reactions may take place giving mixed oxides of intermediate valence state. It is apparent that the final oxidation to MnO_2 is quite slow as the anodic sweep seldom reaches the baseline before the potential of sweep reversal is attained.

4.3.10 Electrochemical Behaviour of Deposited MnO_2 vs. CM MnO_2 Material

In our research group there has been parallel work going on entailing the

production of so called "chemically modified" (CM) MnO_2 material and detailed studies of its electrochemical behaviour. The CM material is produced by co-precipitation of manganese and bismuth hydroxides and subsequent oxidation of the mixture with oxygen. In order to perform cyclic voltammetry on this material, it must be mixed with graphite and formed into a pellet (usually with a Teflon binder) and pressed into a current collecting mesh. Figure 4.33 shows a typical cyclic voltammogram of the CM material at a sweep-rate of 0.5 mV s^{-1}. All of the peaks as described above in Section 4.3.9 are seen in this diagram and at about the same potentials. The MnC4 peak is, however, quite small on this diagram and is often not seen at all in the case of the CM material [57].

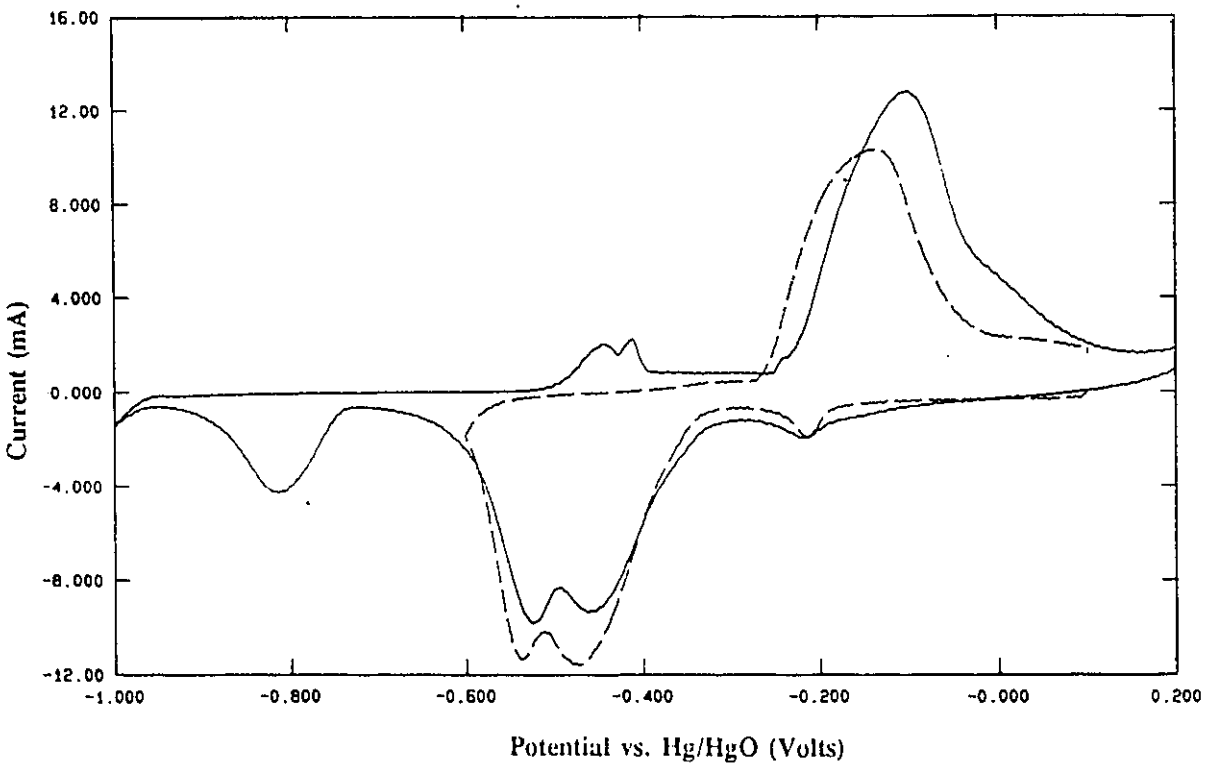

Figure 4.33: Cyclic voltammetry behaviour of "chemically modified" MnO_2 mixed in the ratio 1:10 with Lonza graphite. Sweep rate 0.5 mV s^{-1}. --- full sweep range, ——— anodic limit +0.05V.

However, the commensurate shift of the main anodic peaks to lower potentials when the cathodic sweep is cut short is in accord with the findings in the present work. Figure 4.34 shows results for another CM electrode but for a lower sweep-rate of 0.04 mV s^{-1}. Two cyclic voltammograms are shown, one over the full potential range and the other with an anodic limit of +0.05V. At this sweep-rate, the main anodic features become distinct and the sweep reversal in between these features reduces the main cathodic peak by a commensurate amount. Again, these results fit in well with the proposed peak assignments outlined above.

In addition to this work, considerable effort has been expended to investigate the

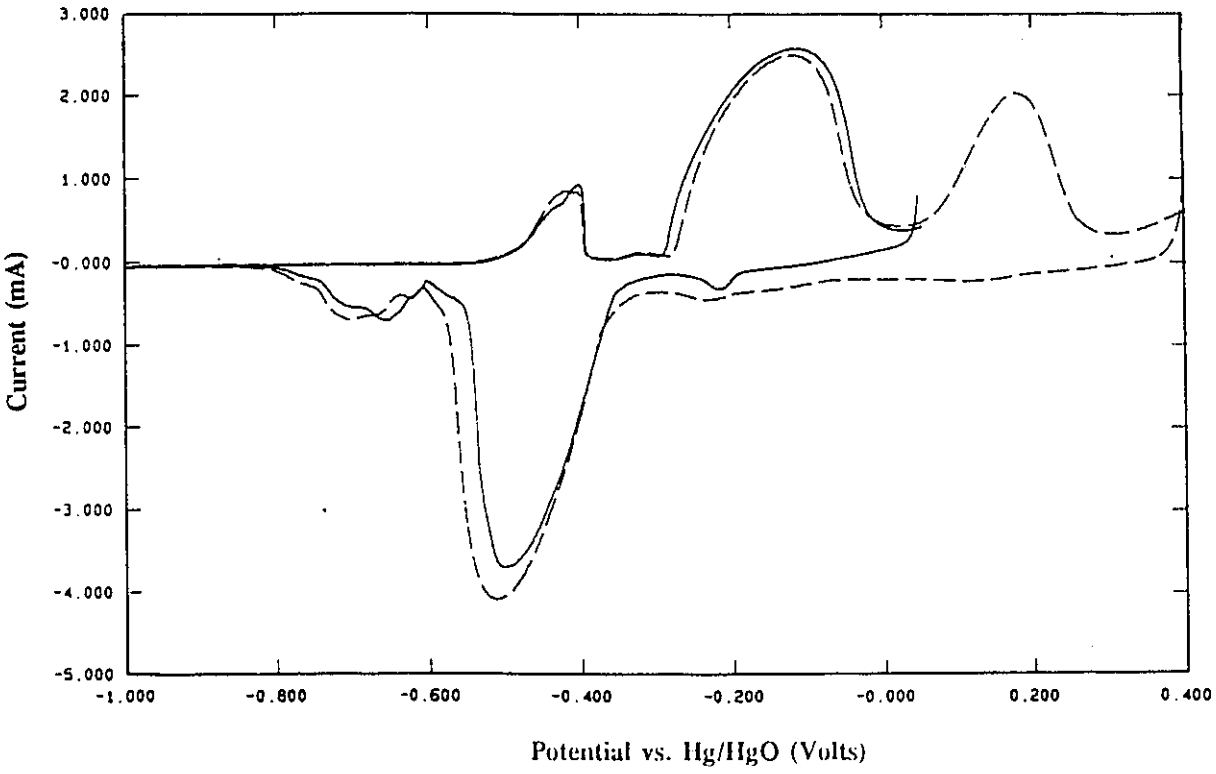

Figure 4.34: Cyclic voltammetry behaviour of CM MnO_2 material at a very slow sweep rate of 0.04 mV s^{-1}. ——— full sweep range, --- anodic limit +0.05V.

role of soluble intermediates in the MnO_2 redox process. The work of Qu et al [35] has shown that soluble Mn^{3+} species are involved in both the cathodic *and* anodic processes for the CM material. Unlike CM MnO_2, the reduction of γ-MnO_2 proceeds via a mechanism that involves soluble species only towards the end of discharge. This difference becomes a moot point on subsequent cycles of γ-MnO_2 due to the change of structure of the material to something resembling blank (bismuth free) CM material after the first cycle (δ-MnO_2 according to McBreen [30]).

The main difference between the results of the present and related work and the findings of McBreen is that, whereas he found that in order for there to be significant anodic charge, the MnO_2 had to be reduced completely to $Mn(OH)_2$, we find that the electrode may be cycled repeatedly from +0.1 to -0.6 volts as shown earlier (section 4.3.2). This implies a different mechanism for the oxidation of the manganese species. Soluble intermediate species have been implicated in the redox mechanism through the results of the experiments on glassy carbon and the Mn rotating-disk work, and the work with CM material has also shown that soluble species (identified optically as Mn^{3+}) play a large part in the redox mechanism of rechargeable MnO_2 material.

Since it is apparent that for further electrochemical activity of a soluble species to occur, it must regain contact with the electrode surface, it can be suggested that a role of the bismuth might be to aid in the nucleation of the soluble intermediate species to the electrode (or as a precipitated solid residing on the electrode) making the intermediate available for further electrochemical reaction.

4.4 CONCLUSIONS

The following conclusions are reached from the work outlined in this chapter:

i) That the inclusion of bismuth species in deposits of MnO_2 from nitrate and perchlorate baths under such experimental conditions is via soaking into the graphite substrate and subsequent precipitation with base. In these deposits, the resultant bismuth inclusion is proportional to its concentration in the acid bath. The mode of inclusion in deposits from sulphuric baths is indirectly electrochemical as described in Chapter 2 and is greater than would be expected from the concentration in the deposition bath itself.

ii) That MnO_2 material with rechargeable characteristics may be produced by anodic deposition from sulphuric acid baths containing bismuth species at a concentration near the saturation limit.

iii) That rechargeable deposits of MnO_2 may also be produced from perchloric and nitric acid baths.

iv) That the addition of Bi_2O_3 to the 9M KOH electrolyte can enhance the rechargeability of MnO_2 cathodes.

v) That soluble intermediates are definitely involved in the redox processes of MnO_2 and that a high surface area substrate such as graphite is necessary for repetitive cycling of MnO_2 to be achievable.

vi) That in the presence of bismuth species, a redox system consisting of a loosely bound layer of $Mn(OH)_2/MnO_2$ may be cycled but with a huge irreversibility.

vii) That the electrochemical behaviour of electrodeposited MnO_2 containing bismuth species, is quite similar to that of CM MnO_2 material.

CHAPTER 5 SUMMARY

The aim of this thesis as outlined in the first chapter was to produce MnO_2 containing bismuth species in a novel way and to study the electrochemical properties of that material.

The production of that material was accomplished by simple anodic deposition of MnO_2 from a bath which contained bismuth species in solution. It was found that good, smooth adherent deposits of MnO_2 could be produced using the accepted conditions of high temperature sulphuric acid baths. The inclusion of bismuth in the baths did not apparently affect the physical properties or appearance of the deposits.

Upon further investigation, it was found that the mode of inclusion of bismuth species into the deposits from sulphuric acid baths was via continuous inclusion whereas from nitric acid and perchloric acid baths it was simply from solution soaking into the graphite substrate. It was proposed that the mode of inclusion of bismuth species in the case of sulphuric acid baths was by precipitation of $Bi_2(SO_4)_3$ or $BiH(SO_4)_2$ due to high local acid strength produced by the deposition reaction to form MnO_2. Some evidence was given for the *anodic* deposition of bismuth species onto a graphite rod from sulphuric acid solution where the reaction at the working-electrode is the oxygen evolution reaction which also produces a high local acid strength.

No matter what the mode of inclusion of bismuth species is, its presence enhances the rechargeability behaviour of the material. This is true of deposits from

sulphuric, nitric and perchloric acids and bismuth species have been shown to have an effect even when they are simply added to the electrolyte during cyclic voltammetry experiments.

Some insights were gained into the mechanism of the redox reactions of MnO_2. Soluble intermediates are definitely implicated. The roles of bismuth in the enhancement of rechargeability have not been entirely elucidated but the most likely effects seem to be associated with the soluble intermediate(s). The bismuth may form a soluble complex with manganese species in solution and in some way discourage side reactions such as the formation of Mn_3O_4. The bismuth may also, in some way enhance the nucleation and growth process that would have to take place in order for the soluble intermediate to react further at the electrode. The involvement of soluble intermediates also means that the rechargeability of a practical battery depends on confining the amount of electrolyte and operating with a high surface area electrode material, including a large area support conductor like Lonza graphite. It appears that the inclusion of bismuth may also enhance the conductivity of the MnO_2 deposit.

From a practical standpoint, the attempts to deposit directly on carbon felt materials were aimed at producing ready-made battery cathodes. Unfortunately these attempts were unsuccessful but the concept is probably a valid one, given the right material. The other considerations which must be addressed for a real battery system, now that it is apparent that bismuth has a real effect on the rechargeability, are those of complications that arise when the MnO_2 electrode is mated with a practical anode. Consideration has to be given to the effects of the soluble species in the battery

including those that may arise from the anode, e.g. ZnO_2^{2-} from Zn. The solubility of the bismuth itself can lead to side reactions at the anode and in a system with a zinc anode, the soluble zinc is known to interfere with the recharging of the MnO_2 electrode. Perhaps these problems will be solved by advanced separator materials for these batteries.

During the course of any investigation, there are observations that are made that do not seem relevant to the problem at hand but are, in themselves, quite interesting. The study of the cyclic voltammetry of bismuth and manganese metals is a case in point, as has been shown in the present work.

The work on bismuth in 9M KOH does not appear to have been done previously. The system shows good, almost-reversible conjugate peaks under the conditions of this study. It might even make a suitable battery electrode system itself although the atomic weight of bismuth and the potential at which the redox processes occur are factors that do not favour such a system, practically.

The other incidental observation was associated with the manganese metal cyclic voltammetry. The so-called AC peak is a rather odd occurrence in that, with the passage of very little anodic current on the forward sweep, an anodic process passing a relatively large charge occurs on the return cathodic sweep. A mechanism for this phenomenon was presented but further study would certainly provide an interesting challenge.

List of References

[1] Handbook of Batteries and Fuel Cells, D.Linden (ed), McGraw-Hill, NY (1984)

[2] Business Opportunities for Portable Batteries, Vol II, Part 2: World Battery Industry and Portable Battery Markets, C.Ward Seitz (Project Leader), SRI International (1988).

[3] C.G.Saxe and R.J.Brodd, Battery Materials Symposium 3, (1987) Honolulu, 89.

[4] W.J.Wruck, B.Reichman, K.R.Bullock and W.H.Kao, J. Electrochem. Soc., 138 (1991) 3560.

[5] Business Opportunities for Portable Batteries, Vol II, Part 1, Global Overview and Portable Battery Technologies, C.Ward Seitz (Project Leader), SRI International (1987).

[6] A.Kozawa, Battery Material Symposium 2 (1985) Graz, 565.

[7] H.S.Wroblowa in: History of Battery Technology Symposium, A..Salkind (ed), Proceedings Vol 87-14, The Electrochemical Society, (1987)74.

[8] R.Huber in: Batteries, Vol 1 Manganese Dioxide, K.V.Kordesch (ed), Marcel Dekker, NY (1974) 229.

[9] K.Kordesch, J.Gsellmann, M.Peri, K.Tomantschger and R.Chemelli, Electrochimica Acta, 26 (1981) 1495.

[10] Y.F.Yao, N.Gupta, H.S.Wroblowa, J. Electroanal. Chem., 223 (1987) 107.

[11] H.S.Wroblowa and N.Gupta, J. Electroanal. Chem., 238 (1987) 93.

[12] M.A.Dzieciuch, N.Gupta and H.S.Wroblowa, J. Electrochem. Soc., 135 (1988) 2415.

[13] H.S.Wroblowa, N.Gupta and Y.F.Yao, Battery Material Symposium 2 (1985) Graz, 203.

[14] M.A.Dzieciuch, H.S.Wroblowa and J.T.Kummer, U.S. Patent #4,451,543 (1984).

[15] Y.Y.Yao, U.S. Patent 4,520,005 (1985).

[16] A.Kozawa and J.F.Yeager, J. Electrochem. Soc., 112 (1965) 959.

[17] A.Kozawa and R.A.Powers, J. Electrochem. Soc., 113 (1966) 870.

[18] A.Kozawa and R.A.Powers, Electrochem. Tech., 5 (1967) 535.

[19] A.Kozawa and R.A.Powers, J. Electrochem. Soc., 115 (1968) 122.

[20] A.Kozawa and J.F.Yeager, J. Electrochem. Soc., 115 (1968) 1003.

[21] A.Kozawa and R.A.Powers, J. Chem. Educ., 49 (1972) 587.

[22] N.C.Cahoon and M.P.Korver, J. Electrochem. Soc., 100 (1959) 745.

[23] G.S.Bell and R.Huber, J. Electrochem. Soc., 111 (1964) 1.

[24] P.Ruetschi, J. Electrochem. Soc., 123 (1976) 495.

[25] A.Era, Z.Takehara and S.Yoshizawa, Electrochimica Acta, 13 (1968) 207.

[26] W.C.Vosburgh and Pao-soong Lou, J. Electrochem. Soc., 108 (1961) 485.

[27] D.Boden, C.J.Venuto, D.Wisler and R.B.Wylie, J. Electrochem. Soc., 114 (1967) 415.

[28] K.J.Vetter, Z. Elektrochem., 66 (1962) 577.

[29] K.J.Vetter, J. Electrochem. Soc., 110 (1963) 597.
[30] J.McBreen, Power Sources, 5 (1975) 525.
[31] J.Fitzpatrick, F.L.Tye, J. Appl. Electrochem., 21 (1991) 130.
[32] C.Mondolini, M.Laborde, J.Rioux, E.Andoni and C.Lévy-Clément, J. Electrochem. Soc., 139 (1992) 954.
[33] R.G.Burns, BMRA Symposium (Brussels 1983) 197.
[34] J.McBreen, Electrochimica Acta, 20 (1975) 221.
[35] D.Y.Qu, B.E.Conway, L.Bai, Y.H.Zhou and W.A.Adams, J. Electrochem. Soc., accepted for publication.
[36] S.Bach, J.P.Pereira-Ramos, N.Baffier and R.Messina, Electrochimica Acta, 36 (1991) 1595.
[37] D.Guyomard and J.M.Tarascon, J. Electrochem. Soc., 139 (1992) 937.
[38] G.D.van Arsdale and C.G.Maier, Trans. Electrochem. Soc., 33 (1918) 109.
[39] G.W.Nichols, Trans. Electrochem. Soc., 62 (1932) 393.
[40] O.W.Storey, E.Steinhoff and E.R.Hoff, Trans. Electrochem. Soc., 86 (1944) 337.
[41] CRC Handbook of Chemistry and Physics, 57th ed., R.C.Weast (ed), CRC Press, Cleveland (1976).
[42] B.E.Conway, Electrochemical Data, Elsevier, London (1952).
[43] D.Y. Qu, unpublished work.
[44] Atlas of Electrochemical Equilibria in Aqueous Solutions, M. Pourbaix , Pergamon Press, London (1966)
[45] F.B.Allan, Am. Chem. Journ., 27 (1902) 284.
[46] S.Skramovsky and O.Vondrasek, Coll. Czech. Chem. Commun., 9 (1937) 329.
[47] D.A.Harrington, PhD Thesis, University of Aukland, (1981) 7.
[48] M.Kh.Karapet'yants and M.L.Karapet'yants, Thermodymanic Constants of Inorganic and Organic Compounds, Ann Arbor-Humphrey Science Publishers (1970).
[49] A.Kozawa, T.Kalnoki-kis and J.F.Yeager, J. Electrochem. Soc., 113 (1966) 405.
[50] K.A.K.Lott and M.C.R.Symons, J. Chem. Soc., (1959) 829.
[51] D.Boden, C.J.Venuto, D.Wisler and R.B.Wylie, J. Electrochem. Soc., 115 (1968) 333.
[52] L.Bai, L.Gao and B.E.Conway, J. Chem. Soc. Faraday. Trans., in the course of publication 89 (1993)
[53] L.Bai, L.Gao and B.E.Conway, (part 2 of ref 52) J. Chem. Soc. Faraday. Trans., in the course of publication 89 (1993).
[54] E.Preisler, Battery Material Symposium 2 (1985) Graz, 247.
[55] D.E.Williams and G.A.Wright, Electrochimica Acta, 21 (1976) 1009.
[56] L.D.Burke and M.J.G.Ahern, J. Electroanal. Chem., 183 (1985) 183.
[57] D.Y.Qu, personal communication.